

School of Science

The Design and Application of Self-assembled Cooperative Catalysts

Bhanumathi Bandi

A thesis submitted in fulfilment
of the requirements for the degree of

Master of Philosophy

Auckland University of Technology

November 2019

Abstract

This thesis describes the application of self-assembly and cooperativity in the design of efficient catalytic systems. In particular, we are looking at chemical reactions which require two or more catalytic units working cooperatively to achieve productive catalysis. In such systems, it is advantageous to bring the catalytic units together into close proximity, and much research has been performed to achieve this using direct covalent linking of catalysts or immobilisation onto solid surfaces. In this thesis, we aim to use the concept of self-assembly to bring catalytic units together, creating more efficient catalytic systems.

In particular, we designed a number of amphiphilic catalysts based on the amino acids L-leucine and L-proline and investigated their catalytic activity in the formation of tetrahydroxanthrones. This reaction involves a reaction between benzaldehyde and cyclohexenone, where each substrate is activated by the two amino acid-based catalysts. While we were able to achieve a rate acceleration with our amphiphilic catalyst system, the amount of acceleration was not sufficiently greater than the control conditions to effectively demonstrate our concept. We also determined the enantiomeric excess of our catalysed reaction to be 30%, which was not high enough to be synthetic useful.

In the second part of this thesis, we investigated a cooperative bimetallic catalyst featuring amphiphiles terminating in 18-crown-6 ethers which bound Ba^{2+} ions. These complexes have been found to act cooperatively in the ethanolysis of esters and anilides. We investigated our amphiphilic system with a number of substrates, including esters, anilides, phosphate esters and activated esters and found that they were effective for the cleavage of the ester *p*-nitrobenzoate. We were able to correlate the onset of catalysis with the onset of structure formation, which were determined by UV and fluorescence spectroscopy, respectively. Further work is still needed to fully demonstrate that cooperative effects are the cause of the rate accelerations observed. The next steps are to visualise and characterise the supramolecular structures formed by our amphiphiles.

In this thesis, we demonstrate that it is possible to create a self-assembled system capable of cooperative catalysis. In the future, we want to use this study as a foundation for the design of cooperative catalytic systems which have synthetic utility. This can decrease the amount of catalyst required for a given chemical reaction and lead to benefits in terms of the cost and sustainability of a chemical process. The dynamic nature of the systems described in this thesis also allows the incorporation of stimuli-responsive units which can lead to the production of smart and intelligent materials.

Table of Contents

Abstract	2
Abbreviations	6
List of Figures:	10
List of Tables.....	13
Attestation of Authorship	14
Acknowledgements	15
CHAPTER ONE: INTRODUCTION	16
1.1 Introduction of catalysis	16
1.2 How can Cooperativity be achieved in Catalysis:	19
1.2.1 Multiple Catalysis	20
1.2.2 Multifunctional catalysis	22
1.2.3 Attachment of Catalysts to a nanoparticle	23
1.2.4 Preliminary Work with Self-Assembled Systems	26
1.2.5 Self-assembled structures	27
1.2.6 Critical Micellar Concentration	29
1.2.7 Hydrophobic interactions.....	31
1.3 Current Project and Key objectives	32
1.3.1 Self-assembled Organocatalysts	32
1.3.2 A Cooperative Bimetallic Catalyst	35
1.3.3 Objectives of this project.....	37
CHAPTER TWO: RESULTS AND DISCUSSION	41
2.1 Synthesis of Tetrahydroxanthone	41
2.1.1 DCC coupling to form N-decylpyrrolidine-2-carboxamide (Cat 2)	41
2.1.2 Leucine based C ₁₀ catalyst (Cat 1).....	48
2.1.3 Synthesis of double-tailed proline-based catalyst (Cat 5)	50
2.1.4 Synthesis of leucine-based catalyst (Cat 4)	56
2.1.5 Formation of tetrahydroxanthone E	60
2.1.6 Investigation of the synthesis of xanthenones using our synthesised catalysts	62
2.1.7 Mosher Ester Analysis	68
2.1.8 Summary.....	72

3.0	Supramolecular catalysis of Ester and Amide cleavage by a Dinuclear Barium (II) complex.....	73
3.1	Synthesis of 1-aza-18-crown-6 (29)	74
3.2	UV-Visible studies for 1-aza-18-crown-6 units.....	74
3.3	Kinetic studies.....	77
3.4	Synthesis of 1-aza-18-crown-6 (29)	78
3.5	Substrate Screening.....	80
3.6	Further Investigations with <i>p</i> -nitrobutyrate.....	81
3.7	Determination of the Critical Assembly Concentration	84
3.8	Summary	88
4.0	CONCLUSIONS and FUTURE WORK	89
CHAPTER THREE: EXPERIMENTAL SECTION.....		92
5.1	General details	92
5.2	Experimental Procedures	94
	2,3,4,4a-Tetrahydro-1H-xanthen-1-one	94
	Decyl 2-((tert-butoxycarbonyl) amino)-3,3-dimethylbutanoate	95
	Benzyl 2-(decylcarbamoyl) pyrrolidine-1-carboxylate.....	96
	<i>N</i> -Decylpyrrolidine-2-carboxamide	97
	Decyl 2-amino-3,3-dimethylbutanoate hydrogen chloride	98
	Didecylamine.....	99
	Benzyl 2-(didecylcarbamoyl) pyrrolidine-1-carboxylate	100
	Benzyl 2-(dodecyl amino) methyl) pyrrolidine-1-carboxylate.....	101
	(<i>N</i> -Decyl- <i>N</i> -pyrrolidin-2-ylmethyl) decan-1-amine	102
	Penta decyl 2-amino-3, 3-dimethylbutanoate.....	103
	2,3,4,4a-Tetrahydro-1H-xanthen-1-ol.....	104
	2,3,4,4a-Tetrahydro-1H-xanthen-1-one	105
	2,3,4,4a-Tetrahydro-1H-xanthen-1-ol.....	106
	2,3,4,4a-Tetrahydro-1H-xanthen-1yl(2 <i>S</i>)-3-fluoro-2-methoxy-3-methyl-2-phenylbutanoate.....	107
	16-Hexadecyl-1,4,7,10,13-pentaoxa-16-azacyclooctadecane	108
	2-((Hexadecyloxy)methyl)-1,4,7,10,13,16-hexaoxacyclooctadecane.....	109
REFERENCES.....		110
Appendices		115

Abbreviations

δ	chemical shift
μ	micro
$^{\circ}\text{C}$	degrees Celsius
ABA	acetoxy benzoic acid
Ac	acetyl
aq.	aqueous
atm	atmosphere(s)
Au NPs	gold nanoparticles
Ba^{2+}	barium (II) ion
Boc	butyloxycarbonyl
br	broad
^{13}C	carbon NMR
Cat	catalyst
Co^{3+}	cobalt (III) ion
CAC	critical aggregation concentration
CMC	critical micellar concentration
C	carbon
ca.	approximately
cat.	catalytic
<i>c</i> -Hex	cyclohexyl
Cr	crown
DCC	dicyclohexylcarbodiimide
d	doublet or day
dd	double of doublet
ddd	double of double of doublet
ddt	double of double of triplet
dq	double of quartet
DMAP	<i>N,N</i> -dimethyl-4-aminopyridine
DMF	<i>N,N</i> -dimethylformamide
DMSO	dimethyl sulfoxide
EtOH	ethanol

EtONa	sodium ethoxide
etc	et cetera
e.e.	enantiomeric excess
EI	electron impact
<i>ent</i>	enantiomer
eq.	equivalent(s)
<i>et al.</i>	<i>et alii</i> (and others)
Et	ethyl
ether	diethyl ether
g	gram(s)
h	hour(s)
¹ H	proton
HBA	hydroxy benzoic acid
HEPES	4-(2-hydroxyethyl)-1-piperazineethanesulfonic acid
HPNP	2-hydroxypropyl <i>p</i> -nitrophenyl phosphate
HRMS	high resolution mass spectroscopy
Hz	hertz
HPNP	2-hydroxypropyl(4-nitrophenyl) phosphate
J	coupling constant
<i>i</i>	<i>iso</i>
<i>i</i> -Pr	isopropyl
IR	infrared
<i>J</i>	coupling constant
L	litre
lit.	literature
mM	millimolar
mg/L	milli gram per litre
M	molar
mol	moles
m	multiplet
m.p.	melting point
<i>m/z</i>	mass to charge ratio
Me	methyl
MHz	megahertz

min	minute(s)
mmHg	millimetres mercury
mmol	millimole(s)
mol	mole(s)
mQ	milli-Q
Me ₄ NOH	tetramethyl ammonium hydroxide
nm	nanometre
<i>n</i>	<i>normal</i>
NMR	nuclear magnetic resonance
Nu	nucleophile
o/n	overnight
OH	hydroxy group
<i>p</i>	<i>para</i>
Pd	palladium
Ph	phenyl
PNB	<i>para</i> -methyl benzoate
PNP	para nitro phenol
ppm	parts per million
py	pyrridine
q	quartet
quant.	quantitative
R	unspecified alkyl group
r.t.	room temperature
RCM	ring closing metathesis
R _f	retention factor
s	singlet
s	second(s)
sat.	saturated
<i>t</i>	<i>tert</i> (tertiary)
t	triplet
TACN	1,4,7-triazacyclononane
TMAH	tetramethyl ammonium hydroxide
<i>t</i> -Bu	<i>tert</i> -butyl
TFA	trifluoroacetic acid

THX	tetrahydroxanthenone
THF	tetrahydrofuran
TIPS	triisopropylsilyl
TLC	thin layer chromatography
TMS	trimethylsilyl or tetramethylsilane
UV-Vis	ultraviolet-visible
v/v	volume to volume ratio
vol	volume
w/w	weight to weight ratio
wt. %	percentage weight
Zn ²⁺	zinc ion
λ	wavelength

List of Figures

- Figure 1** (a) Chemical reaction without catalysis, (b) Conventional synthetic catalysis and (c) Catalysis by enzymes
- Figure 2** A catalytic triad – an example of cooperativity commonly observed in Nature
- Figure 3** Representation of the different kinds of noncovalent interactions
- Figure 4** By combining self-assembly, cooperativity and catalysis, systems can be designed which are stimuli-responsive
- Figure 5** An example of ‘multiple catalysis’, applied to two organocatalysts
- Figure 6** An example of utilising multiple catalysts for a chemical reaction
- Figure 7** Cooperativity by using covalent bond interactions
- Figure 8** Gold nanoparticles used for the hydrolytic kinetic resolution of epoxides by chiral [(salen) Co³⁺] complexes
- Figure 9** Nanozymes created by Manea and co-workers, features properties such as cooperativity and saturation kinetics
- Figure 10a** Gold nanoparticles based upon nano enzymes
- Figure 10b** Investigation of cooperative effects
- Figure 11** Example of using self-assembly as a strategy for the formation of a cooperative catalyst
- Figure 12** Micelles aggregation in polar solvents
- Figure 13** The typical structure of a vesicle
- Figure 14** Formation of micelles and CMC determination
- Figure 15** This structure has shown hydrophobic interactions under dissipative conditions
- Figure 16** Structures of trans Azo-bis (18-crown-6 ethers) and cis-azo bis(18-crown-6-ethers)
- Figure 17** The structures of 4-(2,2,2-trifluoro-N-methylacetamido) benzoate and 4-(2,2-difluoro-N-methylacetamido) benzoate
- Figure 18** Productive catalyst-substrate complex for the basic ethanolysis of esters and anilides
- Figure 19** Proposed self-assembly of the pre-catalysts into micelles or vesicles
- Figure 20** The cleavage of 4-hydroxy benzoic acid (**4-HBA**) by a self-assembled catalytic system composed of 1-aza-18-crown-6 units containing a C16 chain

- Figure 21** The structure of C₁₆ 1-aza-18-crown-6-ethers
- Figure 22** The cleavage of an ester (*p*-nitro butyrate) by a self-assembled catalytic system composed of 18-Crown-6-ethers units containing a C₁₆ chain
- Figure 23** The structure of C₁₆ 18-crown-6-ethers
- Figure 24** ¹H NMR spectra, 400 MHz, of one-tailed catalyst **Cat 2**
- Figure 25** ¹³C NMR spectra, 101 MHz, of one-tailed catalyst **Cat 2**
- Figure 26** ¹H NMR spectra, 400 MHz, of C₁₆ leucine catalyst **Cat 4**
- Figure 27** ¹³C NMR spectra, 400 MHz, of C₁₆ leucine catalyst **Cat 4**
- Figure 28** ¹H NMR spectra, 400 MHz, of Tetrahydro Xanthenone **E**
- Figure 29** ¹³C NMR spectra, 101 MHz and deuterated methanol, of Tetrahydro Xanthenone **E**
- Figure 30** Diastereomers
- Figure 31** ¹H NMR showing the key signals in Mosher ester **30a** from my product
- Figure 32** ¹H NMR showing the key signals in Mosher ester **30b** from TEA
- Figure 33** The conversion of 4-ABA to 4-HBA in the presence of 1-aza-18-crown-6 units
- Figure 34** The structure of 1-aza-18-crown-6 units with C₁₆
- Figure 35** Structures of 4-ABA and 4-HBA
- Figure 36** Absorbance spectra of 4-ABA and 4-HBA, solvent: EtOH/CH₃CN = 85:15, 25 °C.
- Figure 37** Plot of absorbance vs changing time at constant substrate and catalyst concentrations, and in the absence and in the presence of 1-aza-18-crown-6 with barium nitrate. Reaction conditions: solvent (EtOH/CH₃CN: 85:15), catalysts: Ba²⁺ and aza crown C₁₆ (50 μM), Me₄NOH (1 μM) and Substrate: 4-ABA (100 μM), λ = 274 nm, temp 25 °C.
- Figure 38** Plot of absorbance vs changing time at constant substrate and catalyst concentrations, and in the absence and in the presence of 1-aza-18-crown-6 with barium nitrate. Reaction conditions: [Solvent (EtOH/CH₃CN: 85:15), Catalysts: Ba and 1-aza-18-crown-6 C₁₆ (50 μM), NaOEt (500 μM) and substrate: 4-ABA (100 μM), λ = 274 nm, temp 40 °C].
- Figure 39** Structures of HPNPP, BPNP and PNB
- Figure 40** Cooperative catalysis induced by neighbouring C₁₆-18-crown-6-ether with Ba²⁺ complexes upon assembly

- Figure 41** The structure of C₁₆ [18]-Crown-6-Ethers
- Figure 42** Plot of initial rate vs Changing pH values at constant substrate and Catalyst concentrations for the hydrolysis of PNB. The catalysis of PNB cleavage can be achieved by micellar aggregation of amphiphilic ligands containing C₁₆-18-crown-6-ether and Ba²⁺. Reaction conditions: Solvent (mQ Water), Ba(NO₃)₂ [50 μM], C₁₆-18-crown-6-ether **32** [50 μM], PNB [500 μM], pH starting from 5.5 MES to 7.0 HEPES (5000 μM).
- Figure 43** The rate of hydrolysis reaction vs concentration of catalytic ligand in the presence of substrates and barium ions. Reaction conditions: solvent (mQ water), pH at 6.4 (5000 μM), 500 μM of PNB, catalyst C₁₆-18-crown-6-ether (50 μM), Ba(NO₃)₂ and temperature at 40 °C.
- Figure 44** The maximum wavelength measured at different concentrations of C₁₆-18-crown-6-ether **32**. Reaction conditions: [C₁₆-18-crown-6-ether **32**] at various concentrations, [Nile red] = 2 μM, [PNB] = 500 μM, [MES] = 5000 μM, pH at 6.4.
- Figure 45** The fluorescent intensity measured at 635 nm at different concentration of C₁₆-18-crown-6-ether **32** (Reaction conditions: [C₁₆-18-crown-6-ether (**32**)] at various concentrations, [Nile red] = 2 μM, [PNB] = 500 μM, [MES] = 5000 μM, pH 6.4)

List of Tables

- Table 1.** Proposed self-assembly and applied Cat 1 and Cat 2 with C₁₀ carbon chain
- Table 2.** Proposed self-assembly and applied **Cat 2** and **Cat 3** with C₁₀ proline and C₁₆ carbon chain
- Table 3.** Proposed self-assembly, applied **Cat 4** with C₁₆ carbon chain and **Cat 5** with two tailed catalyst
- Table 4.** Fluorescence titration with [18] crown-6-ethers **32** and Ba²⁺, in a constant concentration of Nile red, model PNB and HEPES buffer at pH 6.4

Attestation of Authorship

“I hereby declare that this submission is my own work and that, to the best my of knowledge and belief, it contains no material previously published or written by another person (except where explicitly defined in the acknowledgements), not material which to a substantial extent has been submitted for the award of any other degree or diploma of a university or other institution of higher learning”

B. Bhanumathi

Bhanumathi Bandi

Date: 1st Nov 2019

Acknowledgements

There are many people I would like to thank and acknowledge for their help with completing this thesis and the work that went into it. Without these people this undertaking certainly would not have been possible.

First and foremost, I would like to express my sincere appreciation and gratitude to my supervisor, Dr Jack Li-Yang Chen, AUT. He helped me throughout my studies to develop a deep understanding of the subject, handling the critical situations and in understanding the objective of the work. I am overwhelmed for his supervision, motivation and inspiration throughout my project despite his hectic schedule, who truly remained a driving spirit in my project and helped me in clarifying abstruse concepts, which required knowledge and perception. Thank you for always being there and for devoting many hours on this thesis and encouraging me to study for a Master of Philosophy – without you I would not be able to finish this project. Jack gave me priceless knowledge, wisdom and all the qualities which helped me to understand my project.

Secondly, I express my deepest thanks to Pablo, a PhD member of the group, for giving me excellent training. He has made it a point to be there and show a significant amount of support to me during the experiments. Despite being extraordinarily busy with his own work, he took time out to hear, guide and keep me on the correct path and allowed me to carry out my project. He has truly been a good friend this past year.

Thirdly, thanks to Chloe, for all your help with the UV, endnote and my graphs. I am thankful for the positive attitude you have shown for my work, and for my interactions with you in the lab – I cannot forget that time I have spent with you. I am also thankful to Anau, Giada, Sabeena and Bronte, for extending their friendship towards me and I would like to thank you for being so nice to me and being always around to lend a hand and tell a joke. I would like to acknowledge them for their contributions to my education and research.

To my parents, I would like to thank them for their consistent support and appreciation for my work in my daily life. And finally, this dissertation is dedicated to my husband and my two daughters – without their help and the smiles on their faces this project would not have been possible. I would like to acknowledge them for their contribution to my education and research and thank you so much god for giving me strength and knowledge during my thesis.

CHAPTER ONE: INTRODUCTION

1.1 Introduction to Catalysis

Catalysis shows its importance in numerous aspects of everyday life – for example in the production of medicines, fuel, plastics and fertilizers. In general, a chemical reaction is accelerated in the presence of a catalyst (see **Figure 1b**) as the catalyst decreases the energy required for the chemical process by providing an alternative reaction pathway to the non-catalysed mechanism (see **Figure 1a**).¹ However, despite the enormous advances in this area, synthetic catalysts are in general still much less efficient than enzymes – which are nature’s catalysts. In a typical synthetic process, a single catalyst drives a chemical reaction by activating a single substrate (**Figure 1b**). Enzymes, however, typically utilise multiple catalytic units which work together synergistically to achieve even faster reaction rates. The presence of multiple catalytic units allows both reactant molecules in a chemical reaction to be activated simultaneously (**Figure 1c**). This phenomenon is known as cooperativity and allows enzymes to catalyse reactions with much faster rates compared to synthetic catalysts.² A classic example

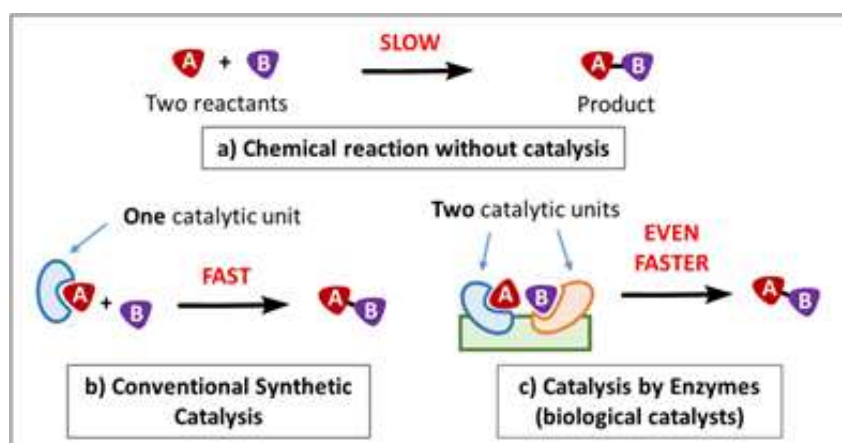


Figure 1. (a) A typical uncatalysed chemical reaction, (b) Traditional synthetic catalysis and (c) Catalysis performed by enzymes (biological catalysts)

of cooperative catalysis is observed in catalytic triads which are common moieties in enzymes (**Figure 2**). In this example, a carboxylic acid (typically from an aspartic acid) activates a base (from histidine), increasing its basicity and its ability to deprotonate the hydroxyl group of a

serine amino acid. Such examples have led us to investigate the development of nature-inspired catalytic systems involving self-assembled systems that are able to cooperate. Such systems are dynamic and modular and should allow for more convenient optimization of a multi-component catalyst.

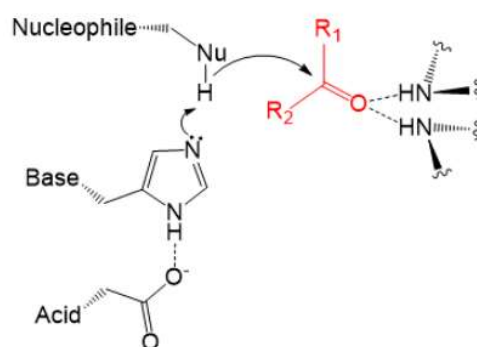


Figure 2. A catalytic triad – an example of cooperativity commonly observed in Nature

In this thesis, we will explore two key concepts in the design of the next generation of catalysts. The first is ‘cooperativity’,³ which occurs when two or more groups work together to give a synergistic effect. Cooperative effects can give rise to what are known as ‘emergent properties’ – where a property or characteristic emerges from the combined action of a collection of individual functional groups, and which cannot be attributed to any of the individual functional groups on its own. These concepts have become hot topics in chemistry research and have implications on the generation of smart materials and stimuli-responsive systems.⁴

The second key concept is ‘self-assembly’, which described the process of forming organised structures from a mixture of disordered components, due to the formation of specific, local interactions between the individual components, rather than by guidance from outside sources.⁵ When the components consist of molecules, this dynamic process is called molecular self-assembly.³ Self-assembly is an area of chemistry which focuses on studying the intermolecular, non-covalent forces between molecules. These bonding interactions include hydrogen bonding, ionic bond interactions, Van der Waals forces, hydrophobic interactions, as well as cation- π interactions and anion- π interactions (see **Figure 3**).⁶ These interactions play a prominent part in biological systems and is receiving more and more attention in the design of new materials.⁷

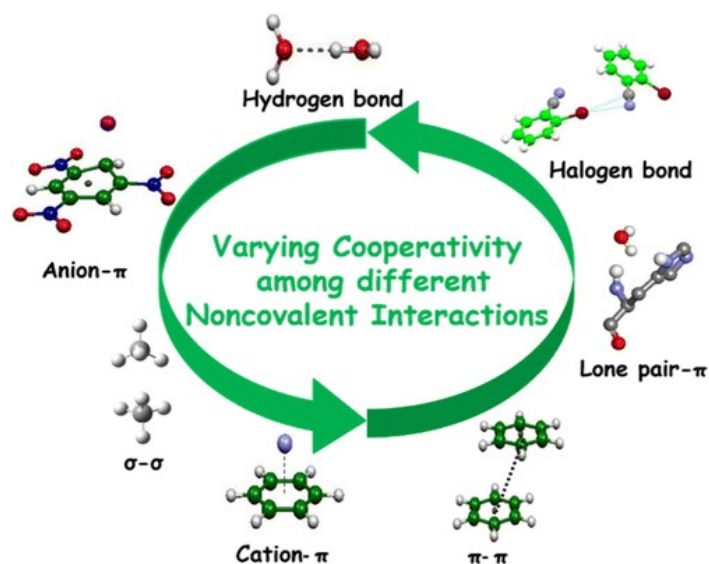


Figure 3. Representation of the different kinds of noncovalent interactions

Compared with traditional covalent bonding within molecules, the weaker and reversible noncovalent interactions are more dynamic and allows the reversible and spontaneous organisation of molecular building blocks into ordered and functional structures (see **Figure 4**).⁸ The reversible nature of these interactions opens the door for systems where specific properties can be reversibly switched on and off.

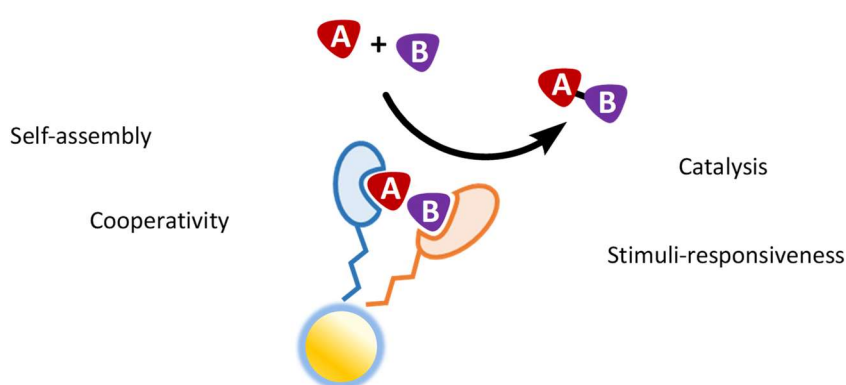


Figure 4. By combining self-assembly, cooperativity and catalysis, systems can be designed which are dynamic and stimuli-responsive.⁹

1.2 How can Cooperativity be achieved in Catalysis:

While there are numerous definitions of cooperativity, in this project, we use ‘cooperativity’ to mean the ability of different catalytic groups to work together in the acceleration of a chemical reaction. Nature commonly uses this concept, and in this thesis, our goal is to utilise cooperativity to design new synthetic catalytic systems. Cooperativity can be an important factor in catalysis when the reaction involves two substrates that can both be activated (**Figure 1**, above), or when a substrate can be activated cooperatively by more than one catalyst. Cooperativity can be achieved by the addition of both catalysts into the solution (multiple catalysis), for example with one catalyst activating substrate **A** and the other catalyst activating substrate **B** (**Figure 5**). However, when catalysts are used, one problem that can be encountered is the low likelihood of one activated substrate (**A**) to collide with and react with a second activated substrate (**B**). Take for example a reaction where there is a 5 mol% of catalyst **1** which activates substrate **A** and 5 mol% of catalyst **2** which activates substrate **B**. In this case, the 5 mol% of activated **A** needs to find a way to collide with the 5 mol% of activated **B**. This may result in low reaction rates, which is commonly observed in reactions catalyzed by organocatalysts, which typically use high catalyst loadings of around 20 mol%.

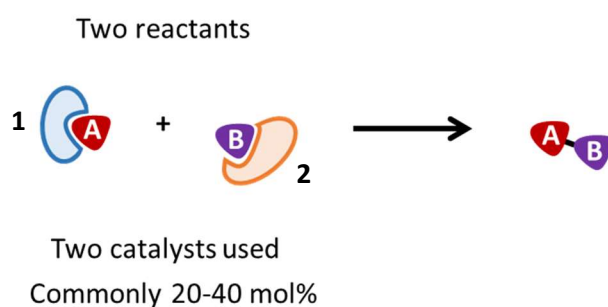


Figure 5. An example of ‘multiple catalysis’, applied to two organocatalysts

One way to increase the productivity of the reaction is to find a way to bring the catalytic units together. This could involve the binding of catalyst **A** and **B** covalently together to form what is called a ‘multifunctional catalyst’. Catalysts can also be brought into close proximity by immobilisation onto a solid surface or onto dendrimers or nanoparticles. Each of these methods have their own advantages and disadvantages which are discussed below. In this project, we

aim to develop a general approach based on the self-assembly of amphiphiles that will bring different catalyst groups into proximity and allow them to react together to give more efficient catalysis.

1.2.1 Multiple Catalysis

Multiple catalysis describes the simultaneous use of two or more catalysts for the acceleration of a chemical reaction. Multiple catalysis can refer to a variety of different mechanisms such as ‘double activation’, ‘cascade reactions’ and ‘synergistic catalysis’. Specifically, double activation refers to cases where two catalysts act simultaneously to activate a single substrate, whereas ‘synergistic catalysis’ refers to when two different catalysts activate two different substrates, which then come together for reaction. Successful demonstrations of multiple catalysis can be found as early as the 1990s and theoretical treatments of these concepts can be traced back to the beginnings of asymmetric catalysis.¹⁰

An example of multiple catalysis (synergistic catalysis) is shown in **Figure 6**, where the Michael addition of an activated cyanide nucleophile is shown. In this example, an erbium complex is used to activate the cyanide donor to make it a better nucleophile and an aluminium complex is used to activate the Michael acceptor, making it more electrophilic. These two catalysts are mixed together in the reaction mixture, and act independently of each other.

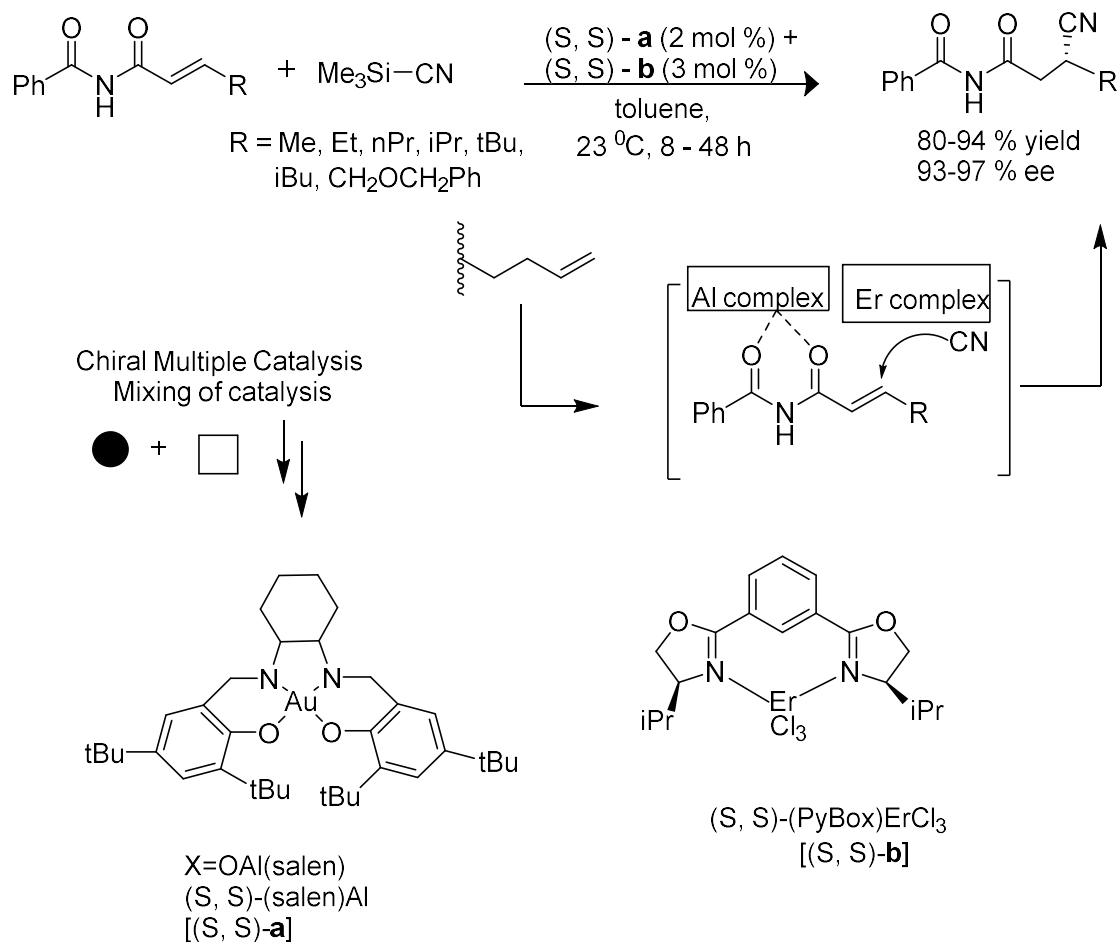


Figure 6. An example of utilising multiple catalysts for a chemical reaction

Probably, the most important advantage of multiple catalysis is that the catalysts used are independent of each other, which allows for easy screening of different catalysts during catalyst optimisation. Using this approach, new catalytic systems can be easily accessed in a combinational way.¹¹ However, one key drawback is that because two catalysts are used, the chance of one activated substrate meeting the other activated substrate can be low. Organocatalysis for example, commonly employs high catalyst loadings. Different methods have therefore been investigated for bringing catalysts together so that they can act cooperatively.

1.2.2 Multifunctional Catalysis

One method of bringing catalysts into close proximity is to join the catalytic units together by direct covalent bonding. This is also known as ‘bifunctional catalysis’. In Figure 6 is shown an example of the reaction between an indanone and a sulfone-based Michael acceptor.¹² For this reaction, a catalyst has been designed that contains functional groups that are able to activate both reagents. One part of the molecule contains a thiourea which can activate the indanone by hydrogen bonding so that it becomes a stronger nucleophile. Another part of this catalyst contains a quinoline ring which is able to promote a deprotonation step in the reaction. The functional groups adjacent to the quinoline group are also able to bind the Michael acceptor by hydrogen bonding, thus effectively bringing the two reagents together. This catalyst is called a multifunctional catalyst and effectively forms a binding pocket for the substrates in the reaction.

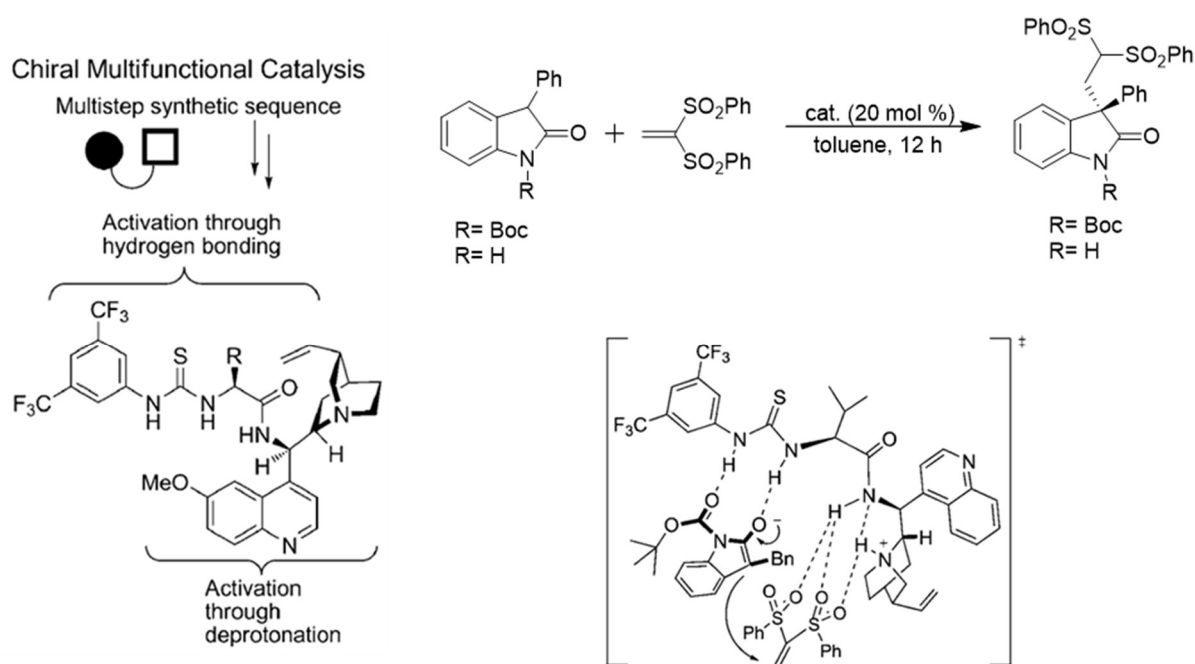


Figure 7. Cooperativity by using covalent bond interactions¹²

The advantage of multifunctional catalysts is that they can be made rigid which gives a greater chance of obtaining high stereoselectivity. Their functional groups that are required for the catalysis are also already in proximity and therefore do not have a low chance of meeting as with ‘multiple catalysis’. However, an important disadvantage of multifunctional catalysis is

that the synthesis of the catalyst is very complex. Looking at the multifunctional catalyst in **Figure 7**, optimisation of this catalyst would be difficult as any desired changes would require a re-synthesis of the entire catalyst. Modifications could not be made in a modular way.

1.2.3 Attachment of Catalysts to a Nanoparticle

Another way to achieve cooperativity is to bind the desired catalysts onto the surface of a nanoparticle.¹³ One early example involved the immobilisation of chiral [(salen)Co³⁺] complexes by Belser and Jacobsen for the hydrolytic kinetic resolution of epoxides (**Figure 8**).¹⁴ This reaction was known to proceed with second order kinetics with respect to the [(salen)Co³⁺] complexes. Belser and Jacobsen therefore theorised that immobilisation of these catalysts onto a nanoparticle will increase their local concentration and results accelerations in reaction rate. They described the functionalisation of gold nanoparticles with salen-terminating thiols by thiol exchange. These functionalized nanoparticles were able to achieve kinetic resolution of racemic epoxyhexane with ten times faster rate than the monomeric catalyst, achieving 99% ee of recovered epoxide within 5 h vs 52 h for the monomeric catalyst. This beneficial effect was deduced to be due to the clustering of catalysts on the monolayer, giving rise to cooperative effects.¹

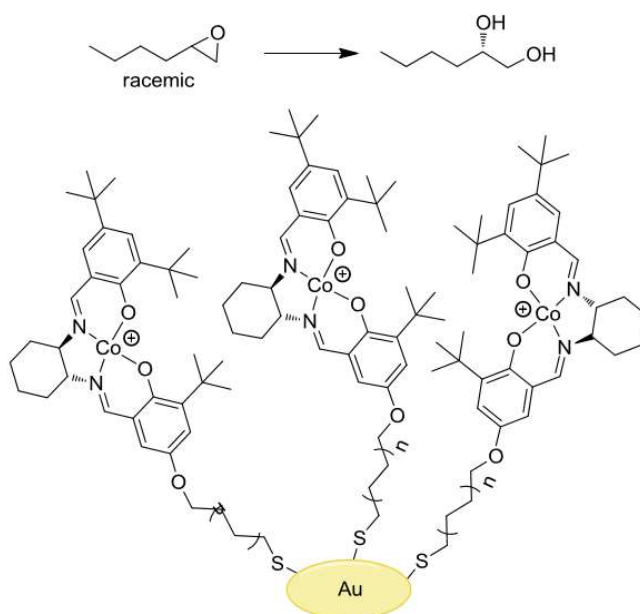


Figure 8. Chiral [(salen)Co³⁺] complexes immobilised onto gold nanoparticles.¹⁵

The clustering of catalytic units on a surface has the potential to be beneficial when more than one catalytic unit is involved in a chemical transformation.¹ This means this concept is beneficial for reactions which are second order with respect to the catalyst, as is the case for Jacobsen's hydrolytic kinetic resolution. Another reaction which is second order with respect to the catalyst is the cleavage of phosphate diesters. Scrimin and co-workers¹⁶ reported the catalysis of a transphosphorylation reaction using a thiol bearing triazacyclononane (TACN)

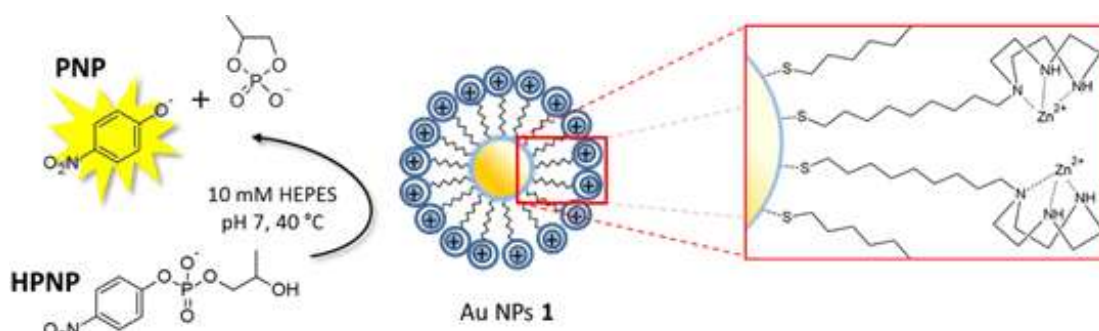


Figure 9. Nanozymes created by Manea and co-workers, featuring properties such as cooperativity and saturation kinetics.¹⁷

attached onto the surface of gold nanoparticles (**Figure 9**). These gold nanoparticles terminate with TACN groups which binds metal ions very strongly, and exhibit many enzyme-like properties such as Michaelis-Menten kinetics and cooperativity.¹⁸ This catalytic system was examined with the substrate 2-hydroxypropyl p-nitrophenylphosphate (HPNP), an activated phosphodiester commonly used as a model substrate of RNA (**Figure 10a**). When HPNP is cleaved, it releases a cyclic phosphate and p-nitrophenol (PNP), which can be easily followed by spectrophotometric methods.

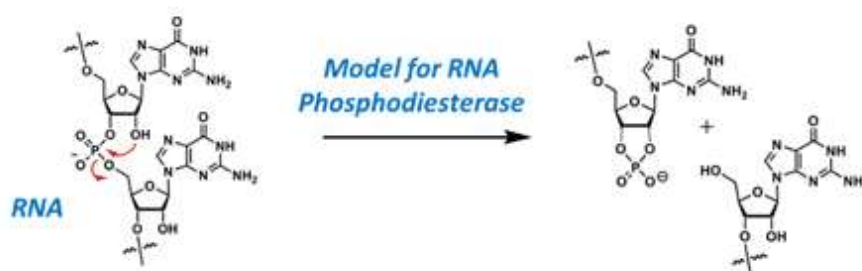


Figure 10 a. Gold nanoparticles based upon nano enzymes

Scrimin and co-workers measured the rate of HPNP hydrolysis with the nanoparticles terminating in Zn^{2+} -binding TACN groups and found it to be three orders of magnitude faster than that rate of the reaction with free TACN in solution. This dramatic increase in catalytic activity was attributed to the close proximity of TACN groups and their ability to act cooperatively. The authors demonstrated this by measuring the rate of the reaction as Zn^{2+} ions are progressively added to a solution of gold nanoparticle with TACN (with no Zn^{2+} initially), up to and surpassing the saturation of the metal-ion binding subunits. At low concentrations, when this is a low concentration of Zn^{2+} on the surface of the nanoparticles, the Zn^{2+} ions are sparsely dispersed so there is a low chance of neighbouring Zn^{2+} , so no cooperativity is occurring. As the concentration of Zn^{2+} increases, the chances of having neighbouring Zn^{2+} increases and there is a rapid increase in reaction rate¹⁹ (**Figure 10b**). At even higher concentrations of Zn^{2+} , most of the TACN units become occupied and the reaction rate reaches a plateau (saturation kinetics). This sigmoidal curve is commonly observed when there is cooperativity in this system.²⁰

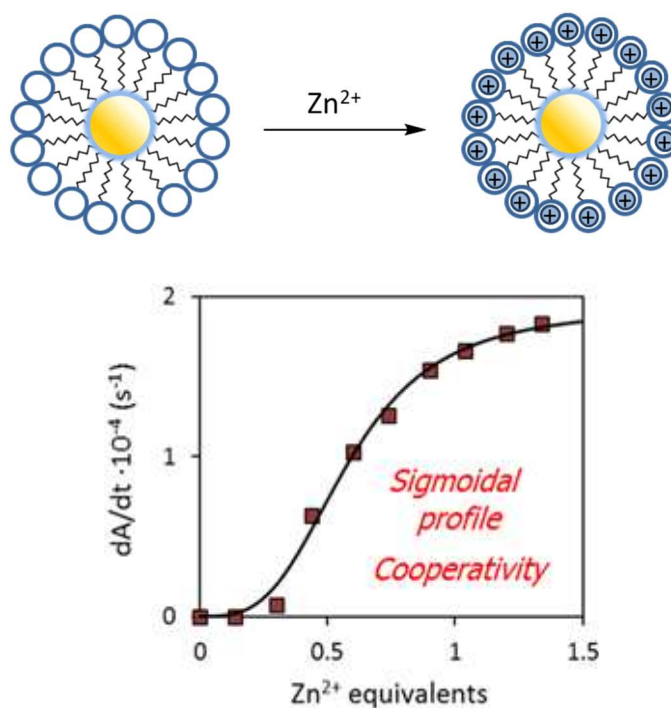


Figure 10b. Investigation of cooperative effects²¹

1.2.4 Preliminary Work with Self-Assembled Systems

Over 15 years ago, Nicholas wrote that ‘groups of molecules, properly assembled, accomplish much more than an equal number of molecules functioning separately’.²² More and more researchers are now taking heed of this statement as evidence is mounting that numerous biological mechanisms occur through multiple simultaneous interactions. These concepts of multivalency, self-assembly and cooperativity are therefore becoming increasingly important in synthetic systems designed for small molecule recognition and catalysis.

Our research group has been focussed on using self-assembly to design catalytic systems that exhibit cooperativity.²³ Inspired by the nanoparticle-based system described by Manea and Scrimin,²⁴ we have shown that $C_{16}TACN-Zn^{2+}$ can self-assemble and exhibit cooperativity without immobilisation onto nanoparticles (see **Figure 11**). $C_{16}TACN-Zn^{2+}$ was shown to form vesicular aggregates driven by hydrophobic interactions in the presence of the substrate HPNP. The formation of vesicular structures relied on stabilisation interactions between the negatively charged **HPNP** and the positively charged Zn^{2+} . Similar counterion interactions have been shown to dramatically decrease the critical assembly concentration (**CAC**) of amphiphiles in solution.

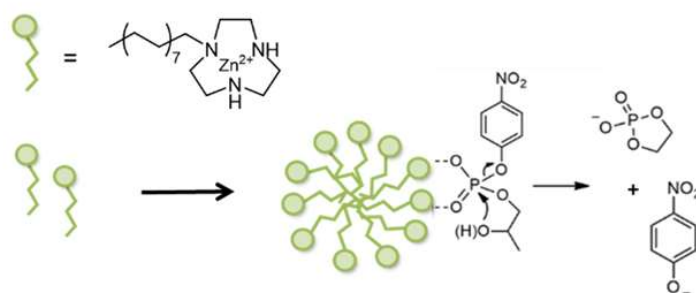


Figure 11. Example of using self-assembly as a strategy for the formation of a cooperative catalyst.

Our reported system is different to traditional micellar catalysis. With conventional micellar catalysis, the rate accelerations often observed are generally to concentration effects in the hydrophobic compartment, or local concentration effects which can affect the local pH value at the surface of the self-assembled structure.²⁵ Our reported system is different because the

catalytic activity is due to the formation of catalytically active pockets on the surface of the structure, which is also stabilised by binding to the substrate. Despite literature suggesting micellar systems to be energetic to allow the formation of cooperative catalytic sites, we show that self-assembled aggregates can be stabilized sufficiently to achieve catalysis by a combination of substrate binding and increased hydrophobicity in the amphiphiles. The vesicular systems that we have formed also appear to have higher stability due to its strong interactions with the substrate.

This self-assembled system provides the advantages of flexibility and modularity when compared to the nanoparticle system above. Because the catalytic units do not need to be immobilised onto a solid surface, they are synthetically much simpler to make, and do not require purification of the catalyst-coated nanoparticle, which is often non-trivial. Because the catalytic units are not directly bonded to each other, this will potentially allow facile optimisation of one catalyst independently of the other, in cases when two different catalytic units are utilised in a chemical reaction.²⁶ Overall, we hope to demonstrate the ease of synthetic access and flexibility/modularity of these self-assembled catalysts for the creation of future complex catalytic and/or functional systems.

1.2.5 Self-assembled structures

In this project, we will utilise a lot the concept of self-assembly. Self-assembly is the description of the spontaneous process by which isolated components orientate into a highly ordered system by non-covalent interactions between molecules themselves, rather than by guidance from outside sources. This aggregation process has its own equilibrium, which is influenced by factors such as the structures of the molecules, pH and solvent temperature etc. Some of the simplest examples of self-assembly include micelles and vesicles.

Surfactants are widely used in various applications such as oil recovery, detergents, colloidal ions, emulsifying agents, wetting agents and foaming agents. Micelles generally consist of a hydrophilic (polar head) and a hydrophobic (non-polar tail) (**Figure 12**).²⁷ The existence of micelles have been known since 1913, when sodium palmitate solution was reported to aggregate and demonstrate abnormal mechanical viscosity but good electrical conductivity,

even though it was originally called a “colloidal ion”. Although preliminary studies were performed by J. W. McBain, these micellar systems were not intensively studied until the 20th century. It is now well accepted that the phenomenon of micellar aggregation is a good example of supramolecular self-assembly, which leads to the orientation of dispersed monomers into a highly ordered micellar system driven by hydrophobic interactions.

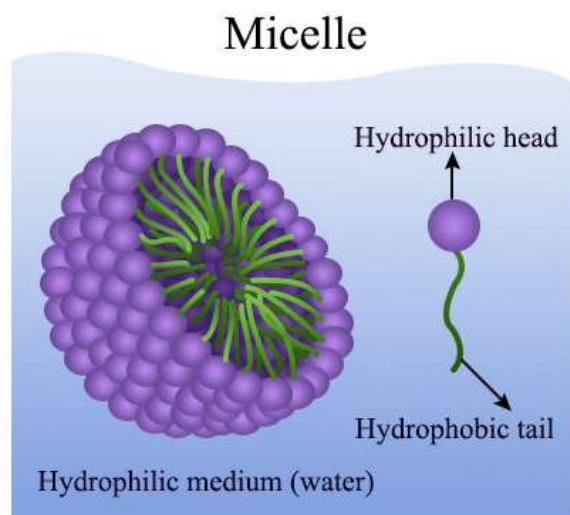


Figure 12. Micelles aggregation in polar solvents²⁸

It is now known that micelles are formed by the self-assembly of amphiphiles in polar solvents.²⁸ Their overall shape is spherical, with the hydrophilic heads on the outside in contact with the polar medium (water) and the hydrophobic tails on the inside away from water.

Another common self-assembled system is a vesicle (**Figure 13**). Self-assembled vesicles are important components of primitive cells, and are of great interest because of their importance as drug delivery vehicles and stimuli responsive substances.²⁹ Consequently, investigation of the properties of vesicular structures has remained important for scientists of numerous disciplines because of its direct resemblance to natural lipid membranes.⁵ Generally, vesicles can be categorised as mono-lamellar, bi-lamellar or multi-lamellar, depending on the number of layers they constitute.

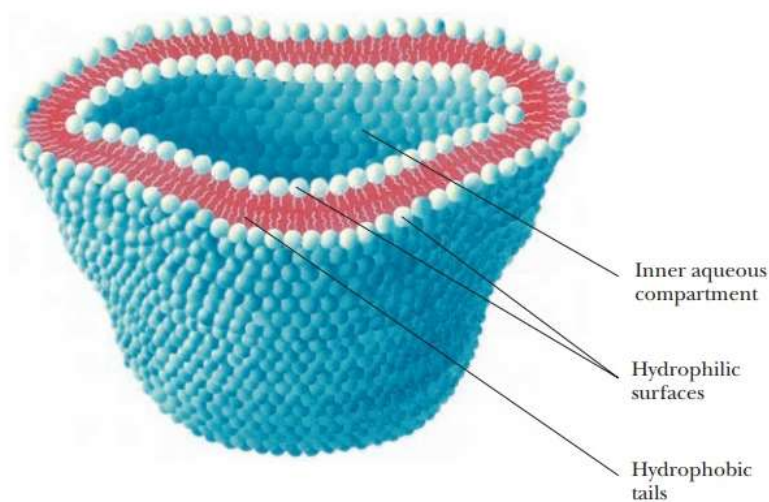


Figure 13. The typical structure of a vesicle.³⁰

1.2.6 Critical Micellar Concentration

The critical micellar concentration (CMC) is one of the key parameters in the study and characterisation of micelles.³¹ It can be determined by a variety of techniques wherein an appropriate property such as osmotic pressure, scattered light intensity or ionic conductance is monitored as a function of concentration. The process of micellar aggregation is shown in **Figure 11**. During the initial addition of surfactant into water phase, the surfactant monomers are favoured to be dispersed at the interface between liquid and air. This reduces the free energy of the system by reducing the contact of hydrophobic ends with water. Consequently, the two phases are gradually saturated with water. After the interface is saturated, surfactants disperse freely much more into the water phase while the concentration is still too low to form micelles (below the CMC, see **Figure 14**). At the CMC, the surfactants aggregate into micelles in solution and the free energy of the whole system decreases due to the decrease of hydrophobic contact with water, since the hydrophobic cores aggregate to expel water molecules from its core.¹⁶ The concentration at which this is reached (CMC) is a specific character of the surfactant and is independent of the properties of the interface.

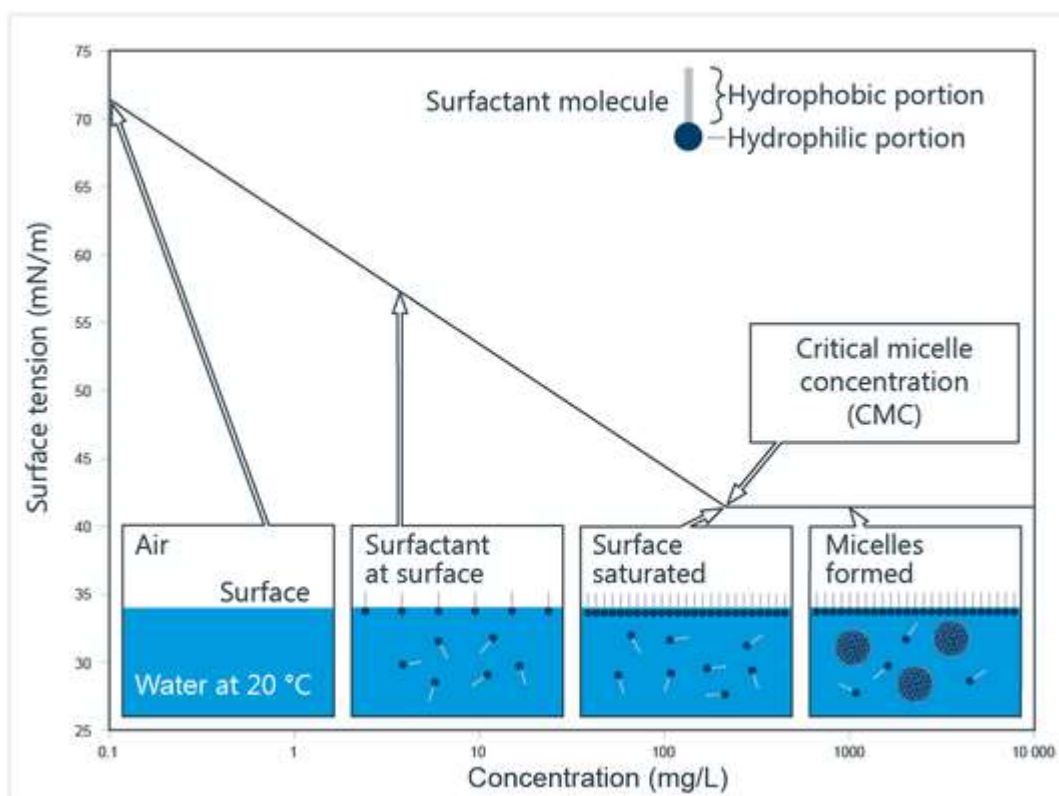


Figure 14. Formation of micelles and CMC determination

Several methods for CMC determination have been published and include light scattering, electrical conductivity, surface tension and spectrophotometric methods.³² Subsequently, electrical conductivity and surface tension those are simplest methods to use in terms of sample preparation but they cannot be used which samples have low CMC values due to low sensitivity. As a result, these can be highly dependent on data analysis procedures. Spectrophotometric methods are advantageous when the micelles interact with, for instance, interfaces or polymers in solution.³³ This is because the method does not rely on diffusive properties, concentration fluctuations, etc. More recently, evidence has been provided for the potential use of spectrophotometric methods as a more accurate method for the CMC determination of low molecular weight surfactants for the solubilization of poorly soluble drugs and for nanoscale delivery systems, with the reason being very high precision and high sensitivity.³⁴ Spectrophotometric methods are suitable even for CMC values below 0.1 mM.

In my project, we determined the CMC of our amphiphiles of interest by using a fluorescent probe. We used Nile red due to its high sensitivity and dramatic change in fluorescence intensity upon the formation of micelles. Nile red does not show strong fluorescence in most

polar solvents but becomes intensely fluorescent in hydrophobic environments.³⁵ Nile red is soluble in numerous solvents and shows a large bathochromic shift in absorbance with increasing solvent polarity.³⁶ This solvatochromic property of Nile red is particularly useful for monitoring micelle formation and the determination of CMC. Moreover, it is often reasonable to neglect the effect of the fluorescent probe on micelle conformation, since the concentration of fluorophores in solution is low compared to the concentration of the substrates.³⁷ The CMC is determined by monitoring the changes in fluorescence intensity during the addition of amphiphiles to a solution in the presence of Nile red. In the present study, what we expect in the experiments is to see the dramatic increase in the intensity of fluorescence upon reaching the CMC. This is because the hydrophobic Nile red probe become solubilised inside the hydrophobic core of the micelles which causes a jump in fluorescence intensity.³⁸ We also monitored the change in the emission maximum, which can also be used to indicate structure formation.

1.2.7 Hydrophobic interactions

The attractive interaction between organic non-polar molecules such as hydrocarbons are unusually strong in water. This hydrophobic interaction is responsible for the very low solubility of hydrophobic molecules in water, which has a role in micelle formation, biological membrane structure, and in determining the conformations of proteins. Micelles are spontaneous aggregates of amphiphilic molecules which have both hydrophobic (oil-like) carbon chains and hydrophilic (water-like) heads (see **Figure 15**).⁵ The hydrophobic tails come close together to shield themselves from water, with hydrophobic interactions as the main driving force. However, it is now recognized that the interactions involve the configurational rearrangement of water molecules within the system. The hydrophilic heads of the amphiphiles orient themselves towards the exterior of the micelle and hydrogen bonds form to achieve solubility in water. Sterically, the hydrophilic head is in general bulkier than that of the hydrophobic tails. Hydrophobic interactions are neutralized when the local structure of water molecules is dominated by their interaction with nearby hydrophilic groups. In addition, its ability for self-aggregation is related to both the structure of the molecule and experimental conditions such as concentration, pH, surface charge, attractive force and temperature.³⁹

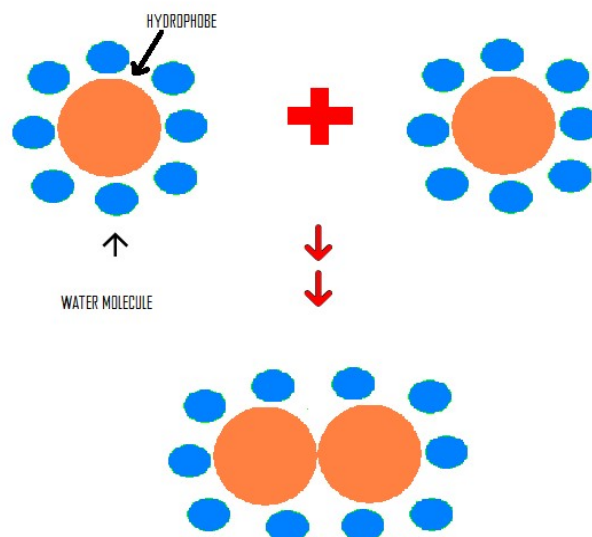


Figure 15: This structure has shown hydrophobic interactions under dissipative conditions.

1.3 Current Project and Key objectives

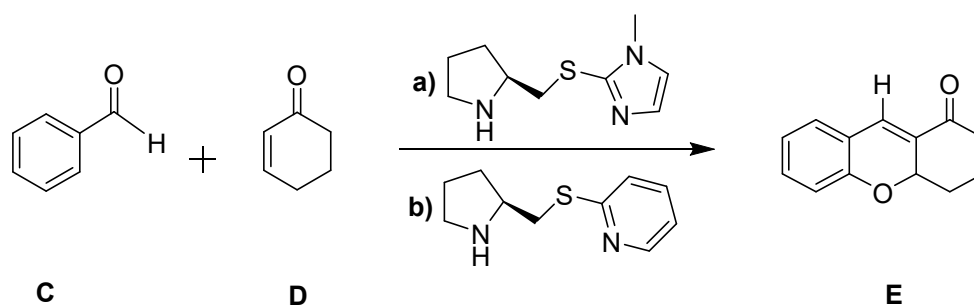
Previously, our research group have shown that we are able to achieve cooperativity in self-assembled vesicular systems. In the current work, we would like to demonstrate that this concept can also be applied to a range of different chemical reactions for organic synthesis. We were inspired by two key reports in the literature, one which involved the self-assembly of two organocatalysts and a second example that described the cooperativity of two metal centres.

1.3.1 Self-assembled Organocatalysts

We were inspired by an example by Xu *et al.*⁴⁰ that described the self-assembly of two organocatalysts by ionic interactions to cooperatively catalyse a reaction to produce xanthenones.²⁶ The unique tricyclic structure of the xanthenes is found in a wide range of natural products with interesting biological activities.⁴¹ They have been recognised as a ‘privileged scaffold’ and are used as synthetic precursors in organic and natural product synthesis. Cordova and co-workers⁴⁰ recently reported the asymmetric conversion of

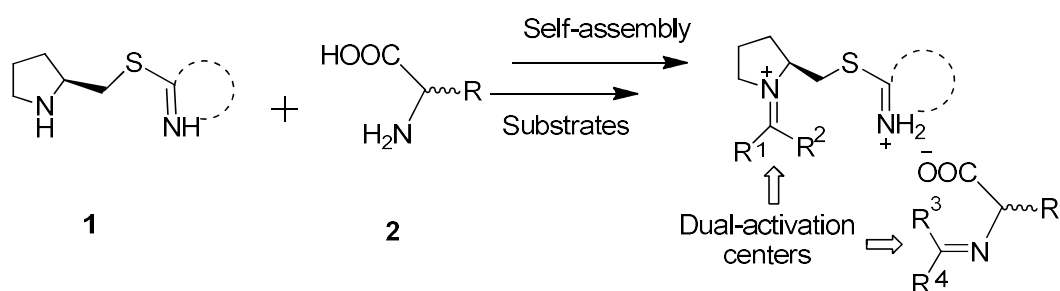
cyclohexanone **C** and salicylic aldehyde **D** to tetrahydroxanthenones **E** by an oxa-Michael-aldol reaction catalysed by a chiral pyrrolidine. Michael addition is one of the most important C-C bonds forming reactions in organic synthesis and many amino acid derivatives have been developed as catalysts for the direct addition of ketones and aldehydes to give xanthenones.

Organocatalysis has made great progress with high activity and enantioselectivity achieved for asymmetric catalysis such as the Michael addition mentioned above. However, organocatalysis is often plagued by the requirement for high catalyst loadings and this can become more of an issue when two or more organocatalysts⁴² are required for a chemical reaction. The synergistic activation of substrates by the self-assembly of two or more organocatalysts has been introduced as a useful strategy for to increase reactivity and/or increase the reactivity of a chemical reaction (see **Scheme 1**).



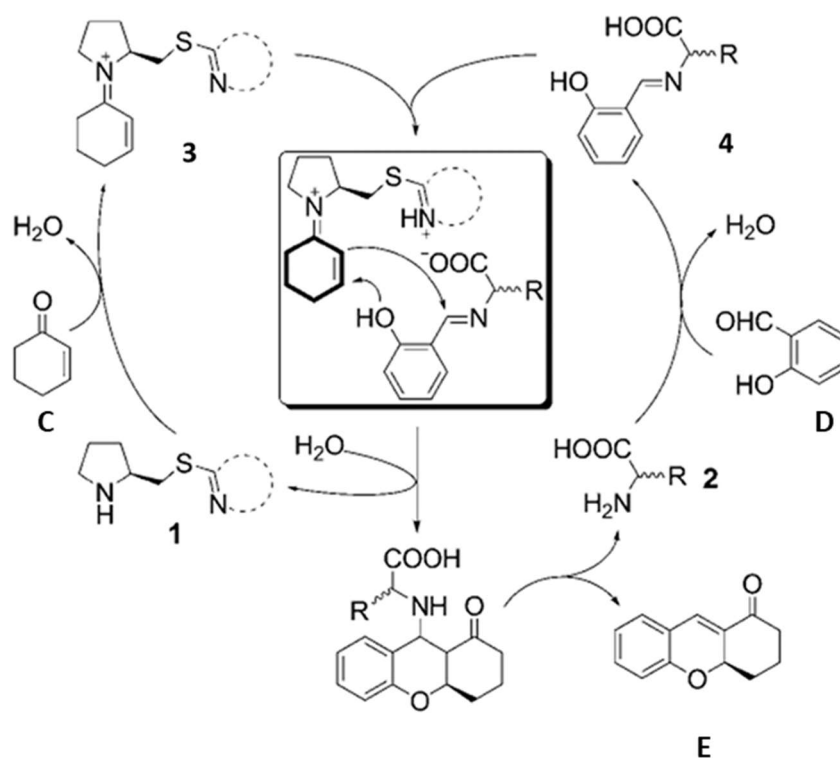
Scheme 1: Formation of Tetrahydroxanthenone by using bifunctional catalyst.

In this example by Xu *et al.*,⁴⁰ the pyrrolidine catalyst exists as a positively charged aromatic amine under the reaction conditions and forms an ion pair with the tert-leucine-based catalyst via the carboxylate (**Scheme 2**). This ion pair can be detected using mass spectrometry. In this example, cooperativity is being achieved by ionic interactions to form a catalytically active complex involving dual-activation centres.



Scheme 2: Self-assembly applied by pre-catalyst modules and the enhanced catalytic activity in the assembled states.

Looking at the mechanism of the reaction more closely, protonation of the aromatic nitrogen in the pyrrolidine-based catalyst **1** by the carboxylic acid in **2** spontaneously leads to ion-pair assemblies. This self-assembled catalyst possesses dual activating centres, and can be likened to catalysis by enzymes, where activation of both the electrophilic and the nucleophilic substrates occur. Specifically, pyrrolidine **1** can activate cyclohex-2-enone **C** forming an iminium ion **3** which makes it more reactive. Salicylic aldehyde **D** can be activated by amino acid **2** forming an imine **4** which is also more reactive and allows it to react with the nucleophilic intermediate (**Scheme 3**). This methodology was elegant in their ability to achieve both high reactivity and high enantioselectivity. We want to examine whether catalysts can be designed with long non-polar chains and whether they would self-assemble by hydrophobic forces to form cooperative catalysts for this reaction. The ability to form cooperative catalysts without having to incorporate positive and negative ions in the catalyst would allow the application of this concept to a greater range of synthetic organic reactions.



Scheme 3: Oxa-Michael-aldol reaction and their transition states for the domino reactions.

1.3.2 A Cooperative Bimetallic Catalyst

We were also inspired by several examples from Cacciapaglia *et al.* that described the cooperativity of Ba²⁺ ions that were held together by 18-crown-6 ethers (**Figure 16**).² Recently they have shown that binuclear alkaline-earth metal ions such as Ba and Sr complexes of bis-crown ether ligands selectively catalyse the basic ethanolysis of esters and anilides (**Figure 17**), which are able to bind to the catalyst via a distal carboxylate (**Figure 18**).

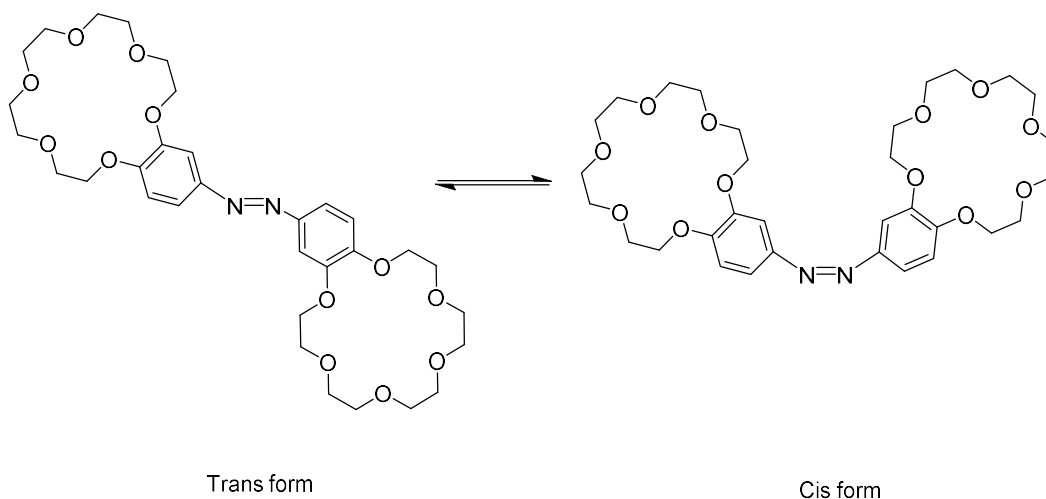


Figure 16. Structures of trans azo-bis (18-crown-6 ethers) and cis-azo bis(18-crown-6-ethers)

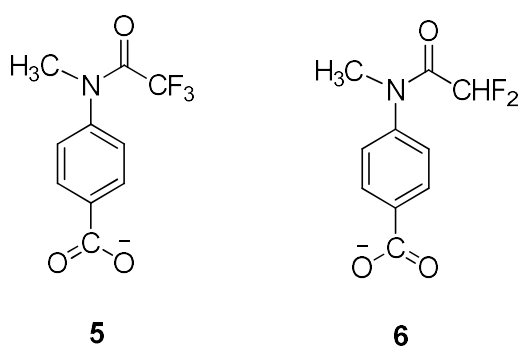


Figure 17. The structures of activated anilides 4-(2,2,2-trifluoro-N-methylacetamido) benzoate and 4-(2,2-difluoro-N-methylacetamido) benzoate

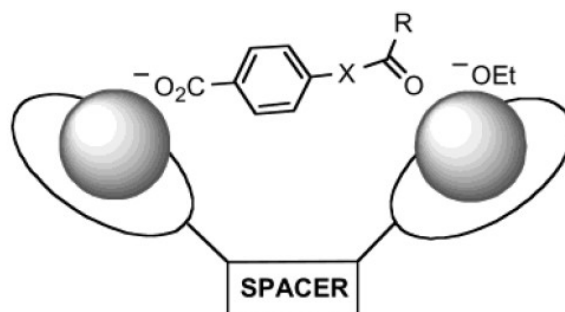


Figure 18. The proposed catalyst-substrate complex for the basic ethanolysis of esters and anilides.

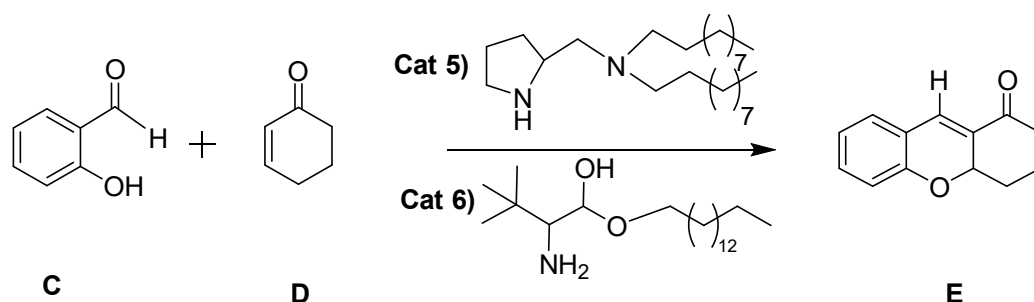
The catalytic efficiency of the bis-barium complex of azo-bis (benzo-18-crown-6) (**Figure 16**) in the basic ethanolysis of anilide derivatives was found to be dependent on the distance between the metal ions. One Ba^{2+} ion binds to the carboxylate group on substrate and the other Ba^{2+} ion activates an ethoxide to attack the carbonyl (see **Figure 18**). This geometry of the productive catalyst-substrate complex is more conducive to catalysis is the concave cis form of the catalyst. Cacciapaglia and co-workers investigated the light-induced changes in molecular geometry of these catalysts and demonstrated that catalysis was much faster when the two Ba^{2+} ions were in close proximity. For example, when crown ether (**Figure 16**) is in the cis form, this complex can catalyse the cleavage of the activated amides **5** and **6**. Crown ether (**Figure 16**) possesses a diazobenzene group which is able to isomerise in response to different wavelengths of light. Irradiation with light in the visible spectrum is thus able to turn the cis form into the trans-form. Cacciapaglia and co-workers demonstrated that the trans-form of crown ether **Figure 16** possessed much lower catalytic rates for the cleavage of amides **5** and **6** due to the increased distance between the Ba^{2+} centres (see **Figure 18**).

Cacciapaglia and co-workers have demonstrated a cooperative system where the two participating active sites are covalently attached to each other. In this project, we want to investigate whether molecules containing these active sites can be programmed to self-assemble into micelles or vesicles, allowing for cooperativity to occur. Demonstrating this concept could also lead to the design of dynamic self-assembling systems that would respond to external stimuli, important for the design of smart and intelligent materials.⁴³

1.3.3 Objectives of this project

The aim of this project is to investigate whether the cooperativity observed in the two systems above can be induced within a self-assembled micellar or vesicular system (see **Figure 19**). In the previous systems, the cooperativity was induced either by ionic interactions or by direct covalent attachment of the two catalytic centres. In this thesis, we want to demonstrate that cooperativity can be induced primarily by hydrophobic interactions. In the first part of the thesis, the objective is to synthesise amphiphilic versions of the proline and leucine-based catalysts used in the reaction of 2-hydroxy benzaldehyde **C** and cyclohexanone **D** to form a

tetrahydroxanthenone **E** (**Scheme 4**). This will involve the synthesis of proline-based and tert-leucine-based catalysts, each containing long chains and investigating their efficiency in the reaction to produce tetrahydroxanthenone.



Scheme 4: Synthesis of tetrahydroxanthenone **E** using newly designed catalysts

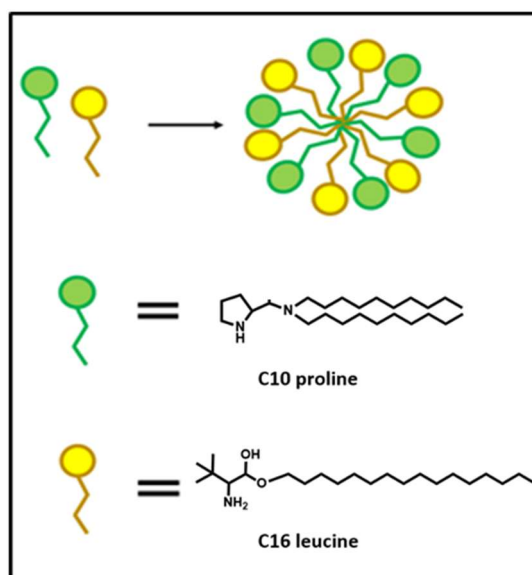


Figure 19. Proposed self-assembly of the pre-catalysts into micelles or vesicles

In the second part of the project, we will synthesise amphiphilic versions of the 18-crown-6 ether containing a 16-carbon hydrophobic chain (e.g. C₁₆-1-aza-18-crown-6-ether, **7**) which will be able to bind to metals such as barium via the 1-aza-18-crown-6 ether **7** and which will be allowed to self-assemble via the long hydrocarbon chain. Similar catalysts have been shown to act cooperatively in the cleavage of esters and activated amides (**Figure 20** and **21**). Our aim is to demonstrate that this cooperativity can also occur within a self-assembled system. As our research group has prior experience with the cooperativity of metal centres for the cleavage phosphodiester, these catalytic systems will also be investigated for several different RNA, DNA and esterase model substrates (**Figures 22** and **23**). Our overall aim is to develop a general

approach that can bring different catalyst groups into proximity and make them to react synergistically using hydrophobic effects. This has the potential to lead to more efficient catalysis meaning lower amounts of catalyst would be needed for a given chemical process, leading to benefits with regards to sustainability and cost.

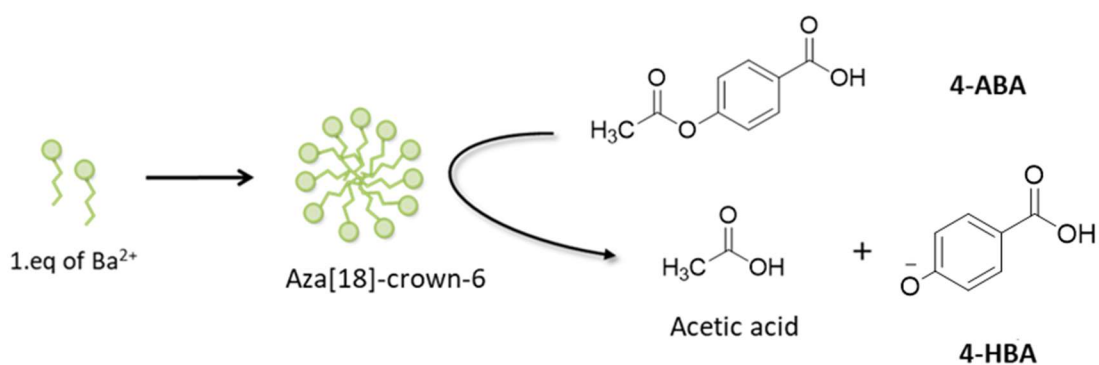


Figure 20. The cleavage of 4-hydroxy benzoic acid (**4-HBA**) by a self-assembled catalytic system composed of 1-aza-18-crown-6 units containing a C16 chain (**7**).

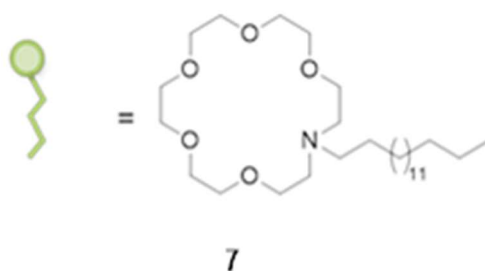


Figure 21. The structure of C₁₆ 1-aza-18-crown-6-ethers

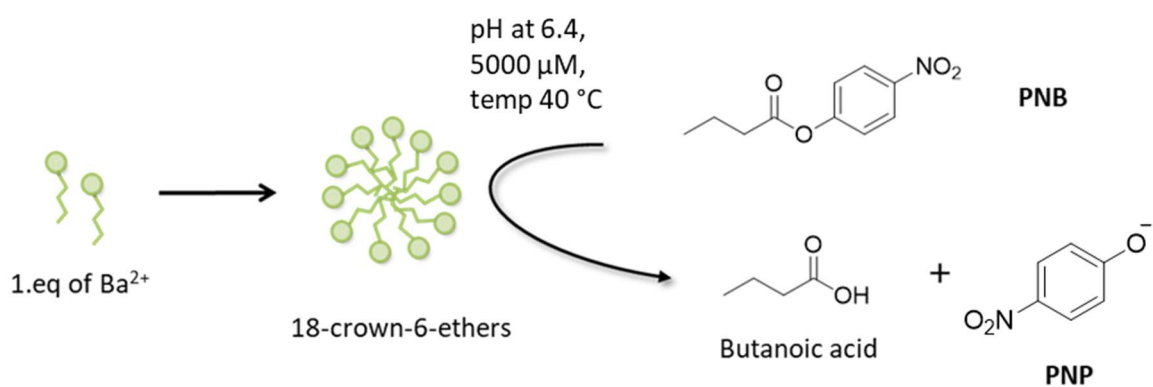


Figure 22: The cleavage of an ester (*p*-nitro butyrate) by a self-assembled catalytic system composed of 18-Crown-6-ethers units containing a C₁₆ chain (**8**).

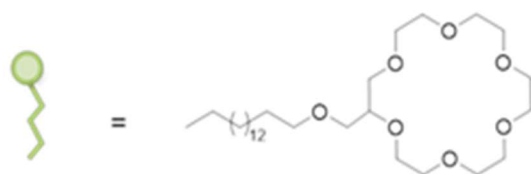


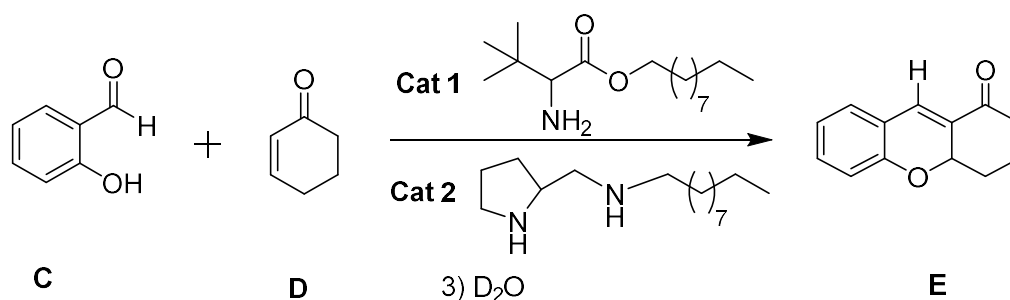
Figure 23. The structure of C₁₆ 18-crown-6-ethers

CHAPTER TWO: RESULTS AND DISCUSSION

Part A

2.1 Synthesis of Tetrahydroxanthenone

The starting point of this project was the design and synthesis of catalysts that have the potential to act cooperatively in the synthesis of tetrahydroxanthenones (**E**). This reaction is a domino oxa-Michael-Mannich reaction, requiring two catalysts in the reaction mechanism. We began by investigating the synthesis of C₁₀-leucine (**Cat 1**) and C₁₀-proline (**Cat 2**). The idea was to use these catalysts to investigate if they can accelerate the reaction between 2-hydroxy benzaldehyde (**C**) and cyclohex-2-enone (**D**). The proline-based organocatalyst is expected to activate cyclohex-2-enone (**D**) while the leucine-derived catalyst should activate 2-hydroxy benzaldehyde (**C**). The addition of the long chains to each of the catalysts is aimed at the formation of micellar or vesicular structures to enable cooperativity to occur (see **Scheme 5**).

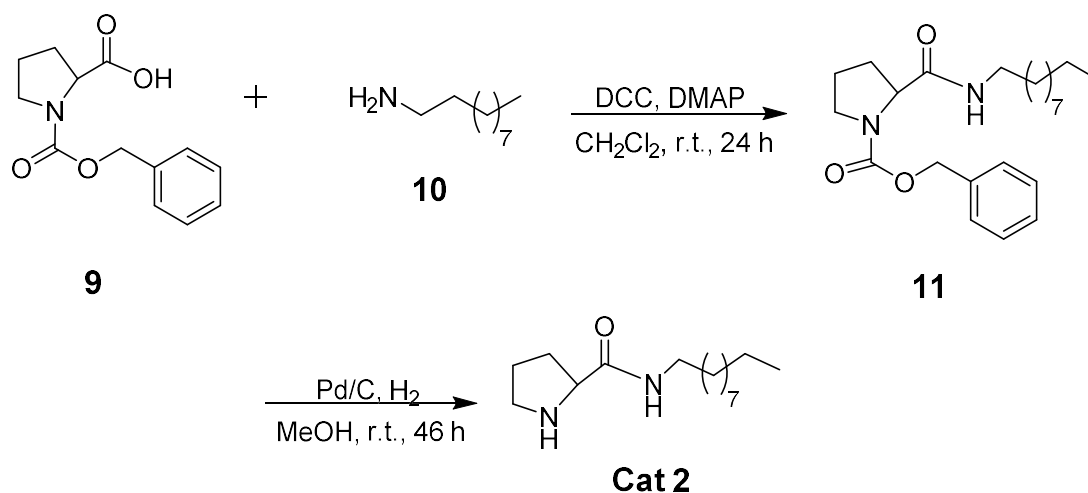


Scheme 5: Formation of tetrahydroxanthenones using **Cat 1** and **Cat 2** in the presence of D₂O

2.1.1 DCC coupling to form N-decylpyrrolidine-2-carboxamide (**Cat 2**)

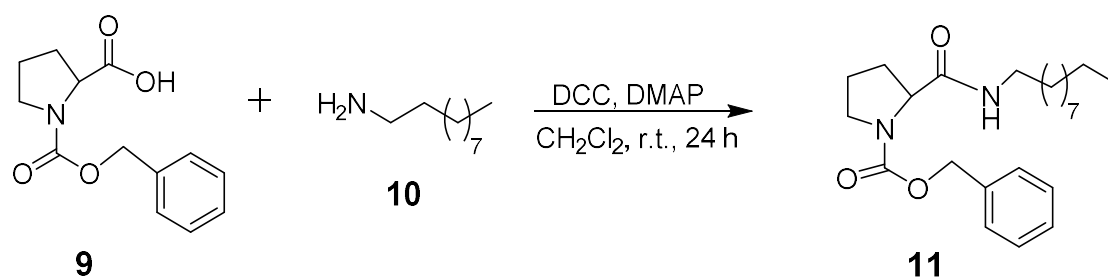
One-tailed proline-based organocatalyst (**Cat 2**) was synthesized over two steps from Z-L-proline (**Scheme 6**). Firstly, benzyl 2-(decylcarbamoyl) pyrrolidine-1-carboxylate **Cat 2** was synthesised from 1-((benzyloxy) carbonyl)pyrrolidine-2-carboxylic acid **9** and decyl amine **10**

in the presence of DCC and DMAP. Finally, removal of the benzyloxycarbonyl protecting group was accomplished in the presence of a catalytic amount of palladium on carbon to yield the desired amine **Cat 2**.



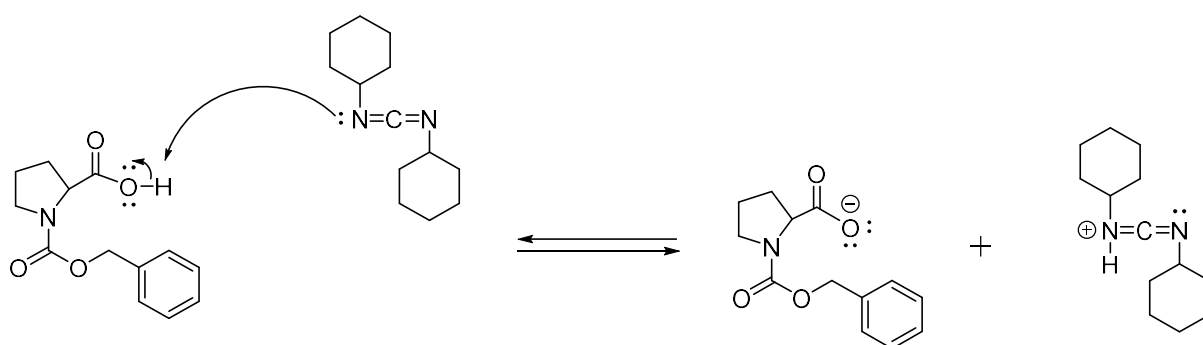
Scheme 6: Mechanism of one-tailed proline organocatalyst (**Cat 2**)

Proline-derived catalyst **Cat 2** was synthesised by the route shown in **Scheme 2**. N-Benzyloxycarbonyl-protected L-proline **9** was coupled with decylamine **10** using dicyclohexylcarbodiimide (DCC) and catalytic amounts of 4-dimethylaminopyridine (DMAP) (**Scheme 7**). The direct conversion of a carboxylic acid to an amide is very difficult due to the basic nature of amines which is able to react with carboxylic acids to form the corresponding carboxylate which is unreactive. In this reaction, the DCC added to the reaction mixture turns the OH group into the carboxylic acid into a good leaving group which can be displaced by an amine by substitution. Initially, this reaction was carried out overnight, but this resulted in the formation of a complex mixture and the desired product was not obtained. The reaction was repeated with carefully monitoring by TLC for the disappearance of the starting materials, which established that the reaction was finished in 24 hours and by product was filtered through the Celite[®] but trace impurities can be difficult to remove. Finally, the solvent was removed in *vacuo* and this crude material was purified by flash chromatography.



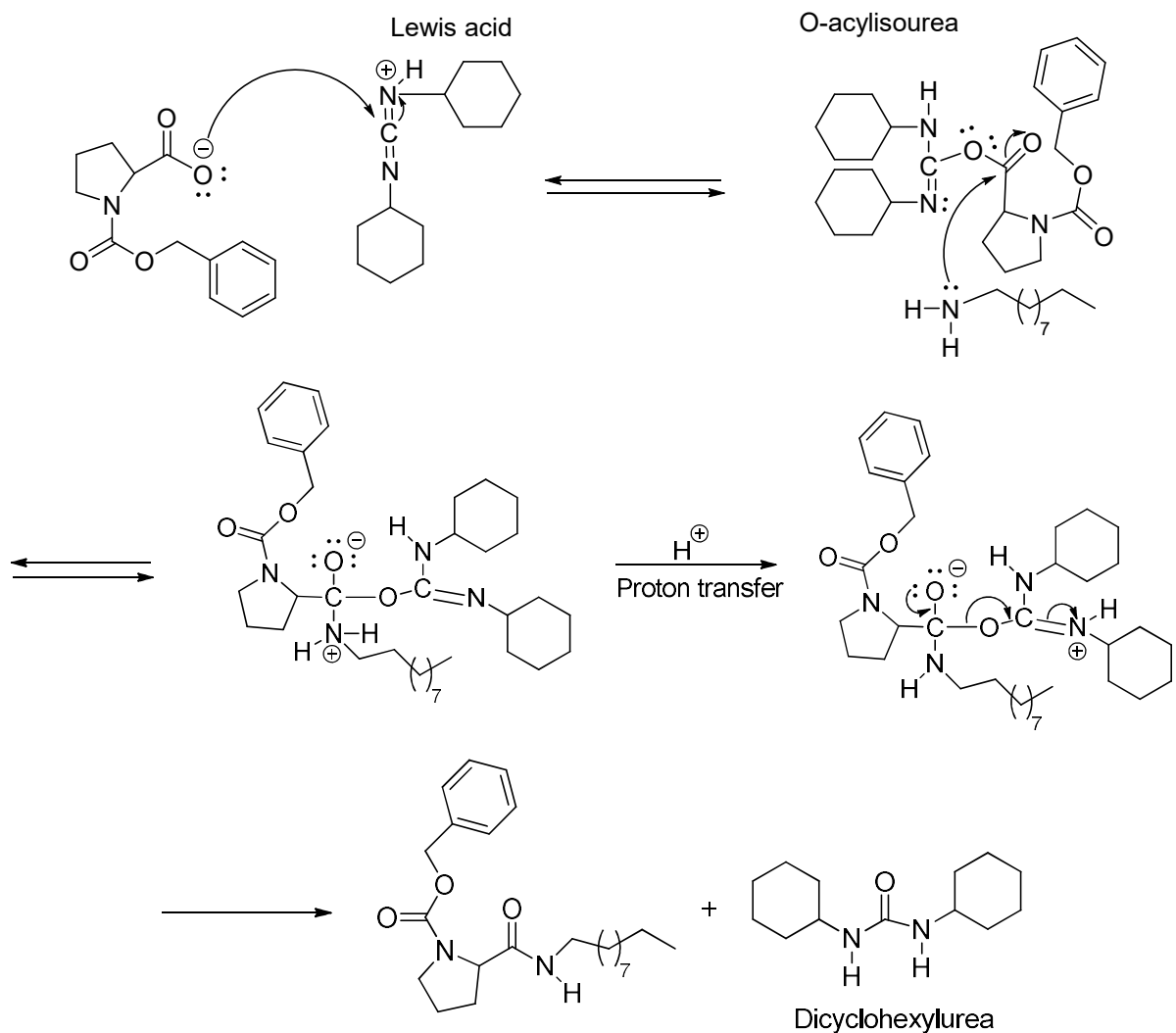
Scheme 7: Formation of N-decylpyrrolidine-2-carboxamide in the presence of DCC/DMAP.

In the following mechanism, DCC acts as a dehydrating agent, which creates a good leaving group and assists in the formation of the amide. In the first step, the carboxylic acid is deprotonated by DCC to form a carboxylate anion (**Scheme 8**).



Scheme 8

In the second step, the carboxylate anion acts as a nucleophile and attacks the protonated DCC to form an O-acylisourea intermediate. The amine is then able to attack the carbonyl group, and this is followed by proton transfer. In the final step elimination reaction occurs as DCC acts as a good leaving group to form dicyclohexylurea as a side product.

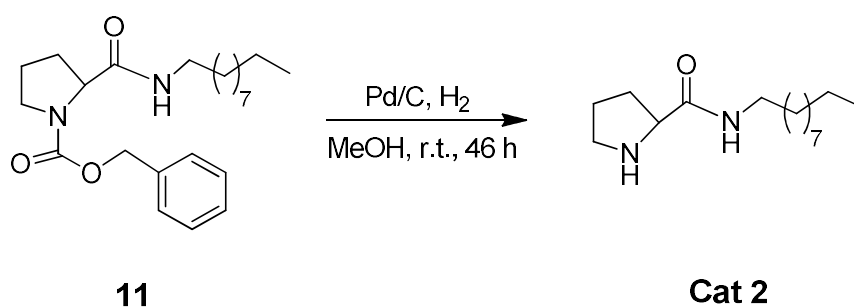


Scheme 9: Preparation and consecutive coupling with amines

In our case, the main undesired reaction pathway involves the rearrangement of the O-acylisourea to the stable side product (**Scheme 9**). After work-up and flash column chromatography, the product was obtained in 32% yield. The formation of the desired product was confirmed by a combination of ^1H NMR, IR and mass analysis. In the ^1H NMR spectrum, the proton signal for 4-H appeared as a triplet at 3.19 ppm and there are 5 protons in aromatic ring in the region 7.22 ppm which confirmed the presence of an aromatic ring.

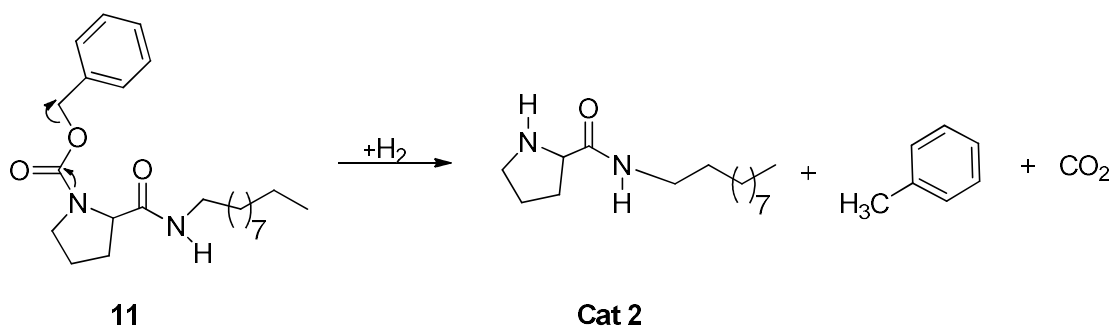
This step involved the conversion of benzyl carbonate **11** to its corresponding pyrrolidine **Cat 2** by a benzyl carbonate deprotection where the atmosphere was changed from nitrogen to hydrogen in the presence of palladium as a catalyst (**Scheme 10**). Here hydrogen acts as a reducing agent, and the by products are carbon dioxide and methyl benzene, which are both

volatile and easily removed. There are various other methods that can be used for this reduction such as sodium borohydride, borane, and lithium aluminium hydride. In this reaction, the presence of nitrogen atoms in the compound can act as a poison to the palladium catalyst. Therefore, subsequent additions of palladium to the reaction mixture was required and the reaction was kept on for a longer period.



Scheme 10: Formation of one-tailed proline catalyst (**Cat 2**)

While this method is commonly used, this reduction mechanism from benzyl carbonate to pyrrolidine derivative remains to be fully understood. The mechanism proposed by Harber *et al.* is the most widely accepted and involves a direct pathway (**Scheme 11**).⁴⁴ The direct pathway undergoes a series of reduction reactions starting with **10** and generates pyrrolidine derivative **Cat 2**. With respect to the experimental operation, it is important to use palladium that is supported on an inert medium due to the high reactivity and potentially safety issues with using palladium. That's why we used palladium that was 5% weight on activated carbon and the reaction mixture was vigorously stirred for 48 hours under hydrogen atmosphere at room temperature. At the end of the reaction, the mixture was filtered through Celite[®] to remove the catalyst and the filtrate was concentrated and the residue purified by flash column chromatography. The successful pyrrolidine derivative **Cat 2** was confirmed by ¹H NMR, which exhibited a new singlet with integration for one proton at 2.0 ppm due to the amino group (see **Figures 24** and **25**).



Scheme 11: Hydrogenation of one-tailed proline catalyst (**Cat 2**)

^1H NMR (400 MHz, CDCl_3)

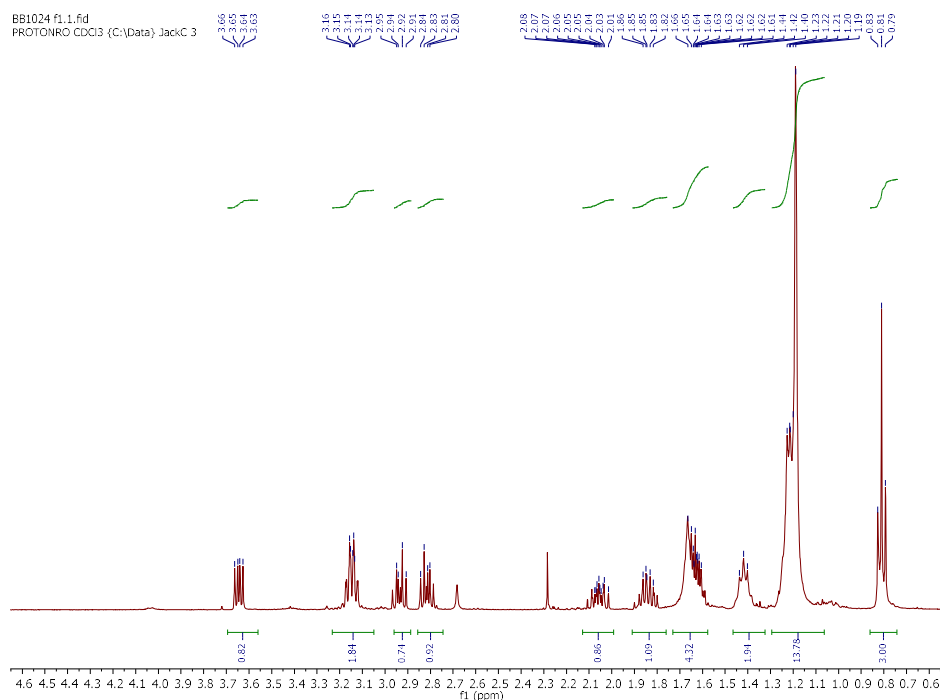


Figure 24. ^1H NMR spectra, 400 MHz, of one-tailed catalyst **Cat 2**

^{13}C NMR (101 MHz, CDCl_3)

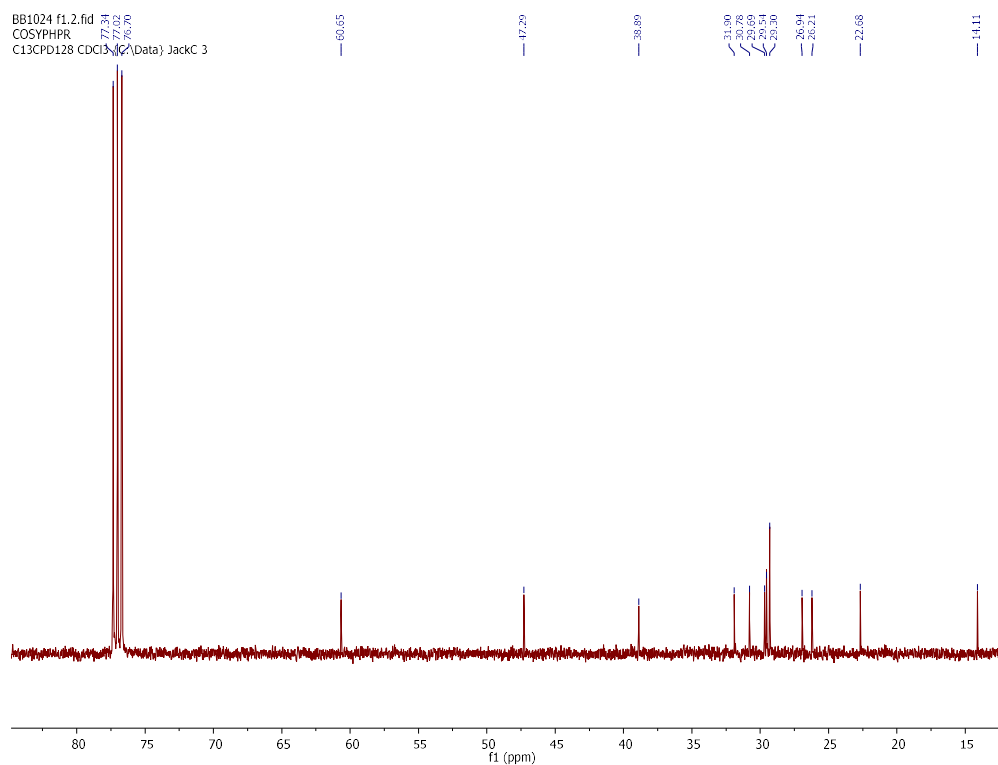
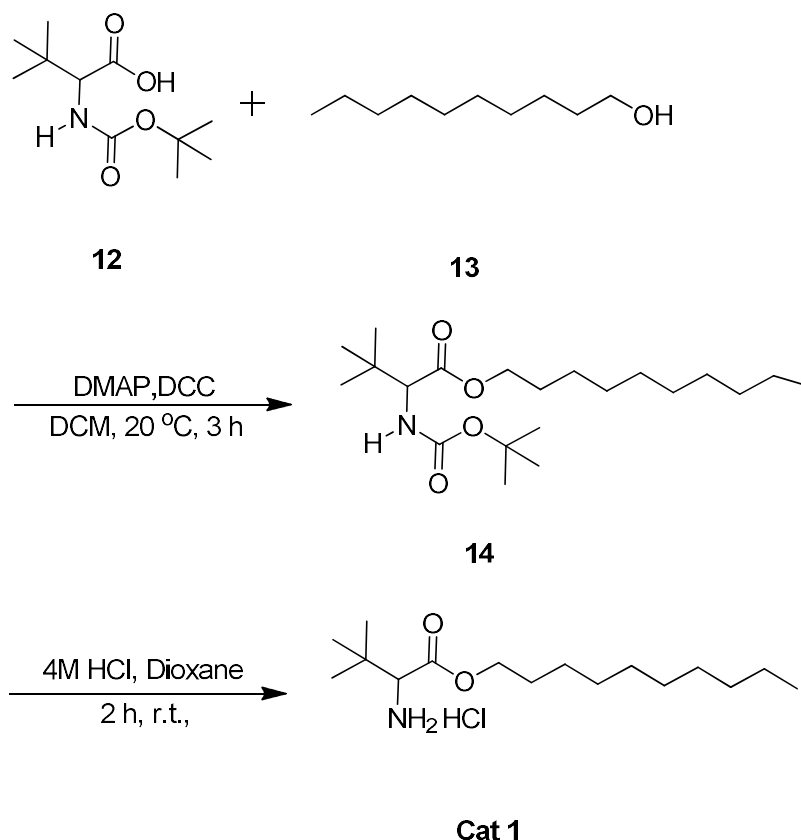


Figure 25. ^{13}C NMR spectra, 101 MHz, of one-tailed catalyst **Cat 2**

2.1.2 Leucine based C₁₀ catalyst (Cat 1)

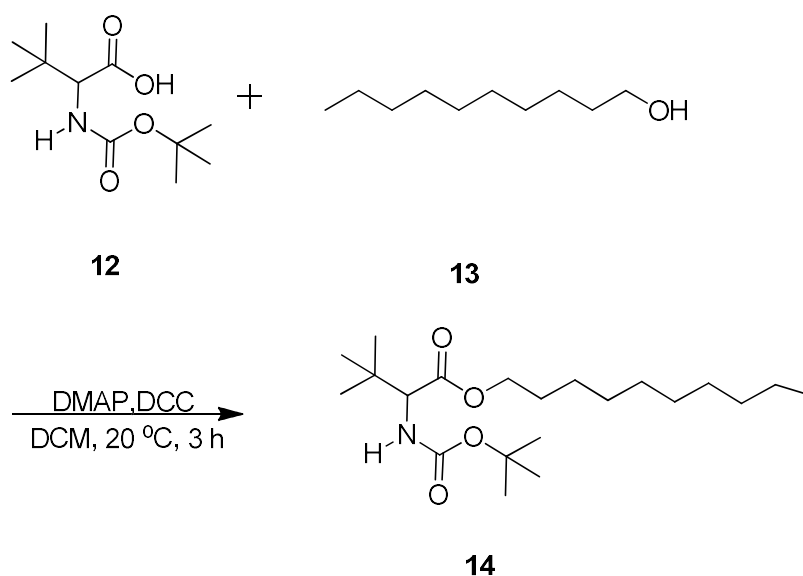
In the next step, to prepare leucine based C₁₀ catalyst (**Cat1**) by using 2-((tert-butoxycarbonyl) amino)-3,3-dimethylbutanoic acid **12** and decanol **13** in the presence of DCC, DMAP at 20 °C. After initial synthesis of **14** was dissolved in hydrochloric acid and dioxane (**Scheme 12**).



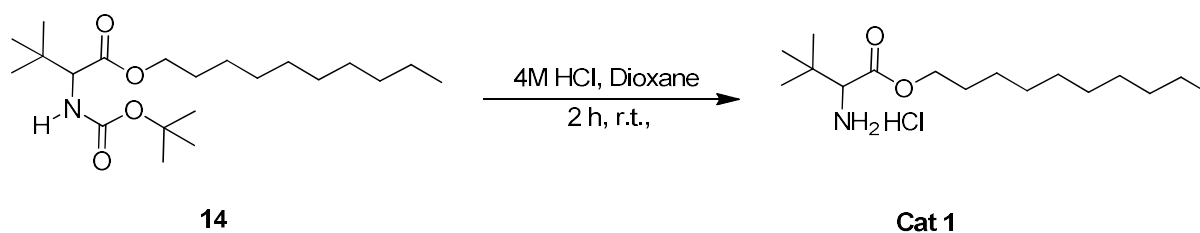
Scheme 12: Preparation of leucine C₁₀ based catalyst (**Cat 1**).

To prepare decyl 2-((tert-butoxycarbonyl) amino)-3,3-dimethylbutanoate **14**, 2-((tert-butoxycarbonyl) amino)-3,3-dimethylbutanoic acid **12** was dissolved in DCM and DCC was added at room temperature under nitrogen gas. Two hours later, decanol **13** was added for the reaction mixture (**Scheme 13**). Initially, this reaction was carried out overnight, but this resulted in the formation of a complex mixture and the desired product was not obtained. The reaction was repeated with carefully monitoring by TLC for the disappearance of the starting materials, which established that the reaction was finished in 24 hours and by product was filtered through the Celite[®] but trace impurities can be difficult to remove. The two different mechanisms

leading to the formation of either leucine C₁₀ based catalyst (**Cat 1**) or leucine C₁₆ based catalyst.



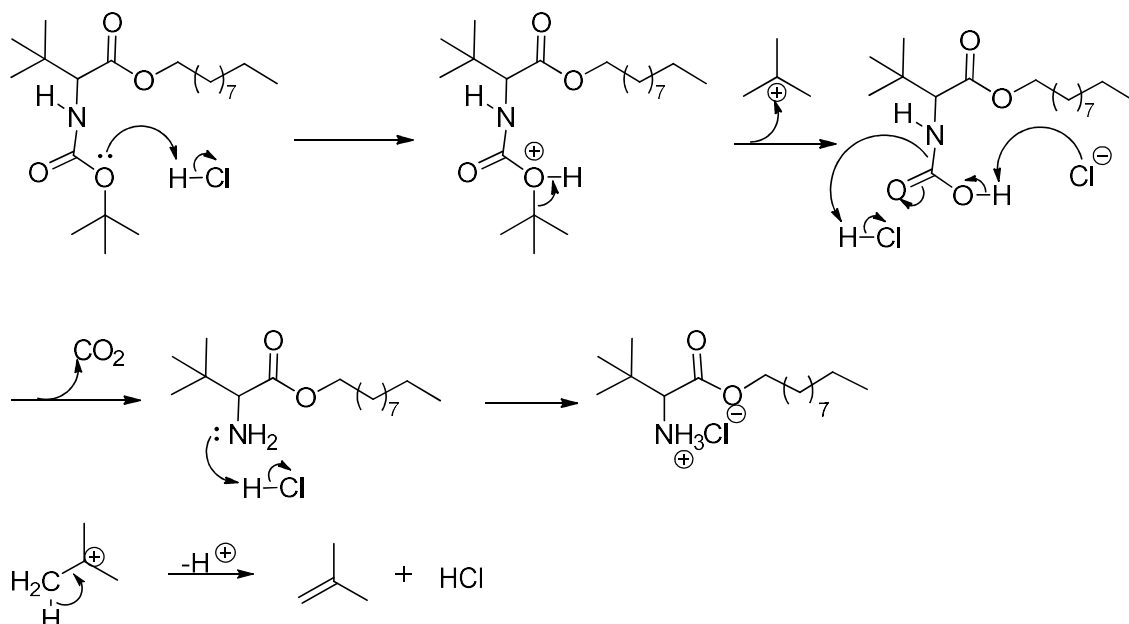
Scheme 13: Synthesis of decyl 2-((tert-butoxycarbonyl) amino)-3,3-dimethylbutanoate



Scheme 14: Synthesis of decyl 2-amino-3,3-dimethylbutanoate hydrogen chloride

The cleavage of the Boc-protecting groups was achieved in strong acid, forming of decyl 2-amino-3,3-dimethylbutanoate hydrogen chloride (**Cat 1**) in 60% yield following concentration under high vacuum and required further purification by flash column chromatography (**Scheme 14**). TLC analysis suggested that the completion of the de-protection when the original spot disappeared together with the formation of a new spot at the bottom of the TLC plate after 12 hours. Because decyl 2-amino-3,3-dimethylbutanoate hydrogen chloride (**Cat 1**) was formed as a salt with a HCl molecule, which has high polarity. This mechanism of the reaction is shown in **Scheme 15** and shows the oxygen in the carbonyl group attacking the hydrochloric acid. The tert-butyl cation falls off due to the rearrangement of electrons which leads to the formation of 2-methyl prop-1-ene (**Scheme 15**). Simultaneously, the lone pairs of nitrogen take a proton and

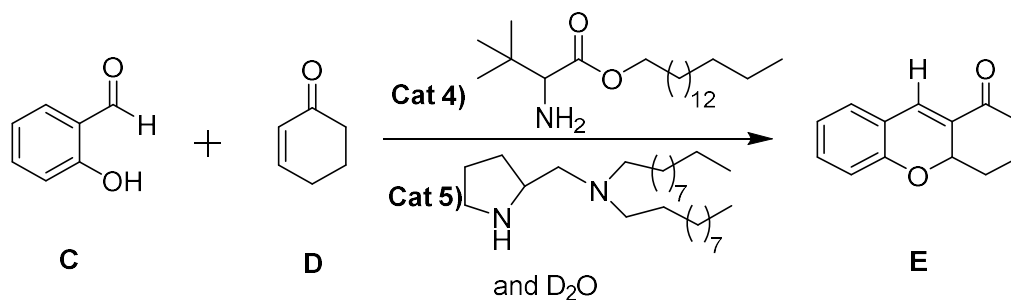
an intramolecular rearrangement occurs to release carbon dioxide. By observing the ^1H NMR, it was clear to see the disappearance of the tert-butyl group integrating for 9 protons. This data, together with low resolution mass spectroscopy confirmed the successful synthesis of our designed decyl 2-amino-3,3-dimethylbutanoate hydrogen chloride.



Scheme 15: Mechanism of designed decyl 2-amino-3,3-dimethylbutanoate hydrogen chloride.

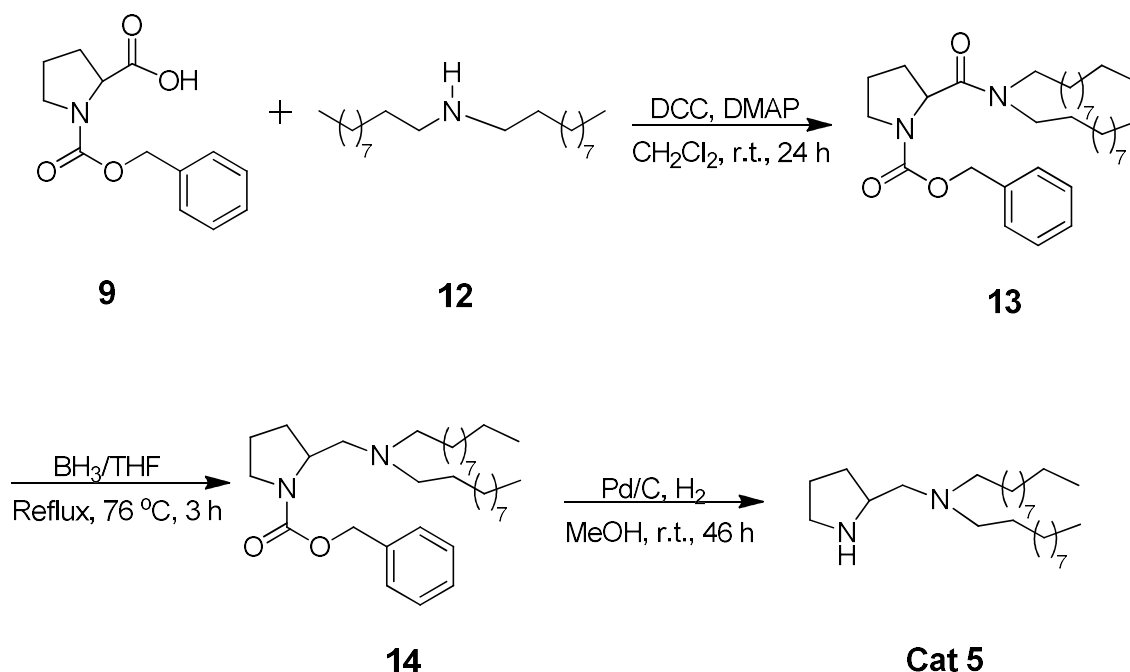
2.1.3 Synthesis of double-tailed proline-based catalyst (Cat 5)

In case the single-chain proline-based catalyst above was not able to form self-assemblies in solution, we decided to also synthesise another proline-based catalyst but featuring two hydrophobic tails (see **Scheme 16**). This molecule is important because Barbas has previously shown that it is able to catalyse reactions in water due to the formation of micellar aggregates. We performed the synthesis of the proline catalyst (**Cat 5**) following a synthetic route modified from Barbas *et al.*

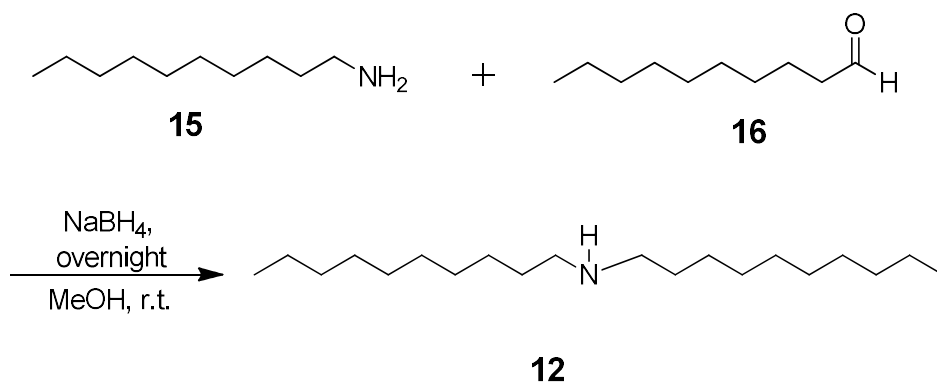


Scheme 16: Formation of Tetrahydroxanthenone by using **Cat 4** and **Cat 5**

The two-tailed proline-based organocatalyst (**Cat 5**) was synthesized over four steps from *Z*-L-proline (**Scheme 17**). Firstly, didecylamine **13** was synthesised from decylamine **15** and decanal **16** in the presence of sodium borohydride in a reductive amination reaction. This was followed by DCC-mediated amide formation between didecylamine **12** and the carboxylic acid of proline. Reduction in the presence of borane-THF was used to remove the amide carbonyl **14** and finally removal of the benzyloxycarbonyl protecting group was accomplished in the presence of a catalytic amount of palladium on carbon to yield the desired amine **Cat 5**.

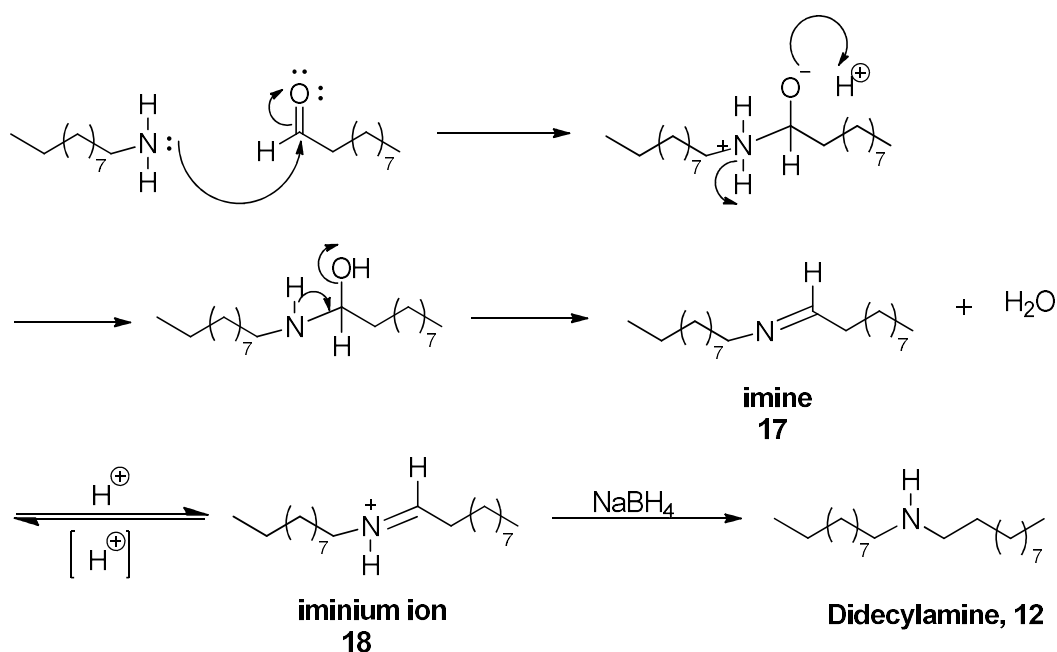


Scheme 17: Formation of the two-tailed proline-based organocatalyst **Cat 5** (two-tailed)



Scheme 18: Formation of didecylamine in the process of reductive amination.

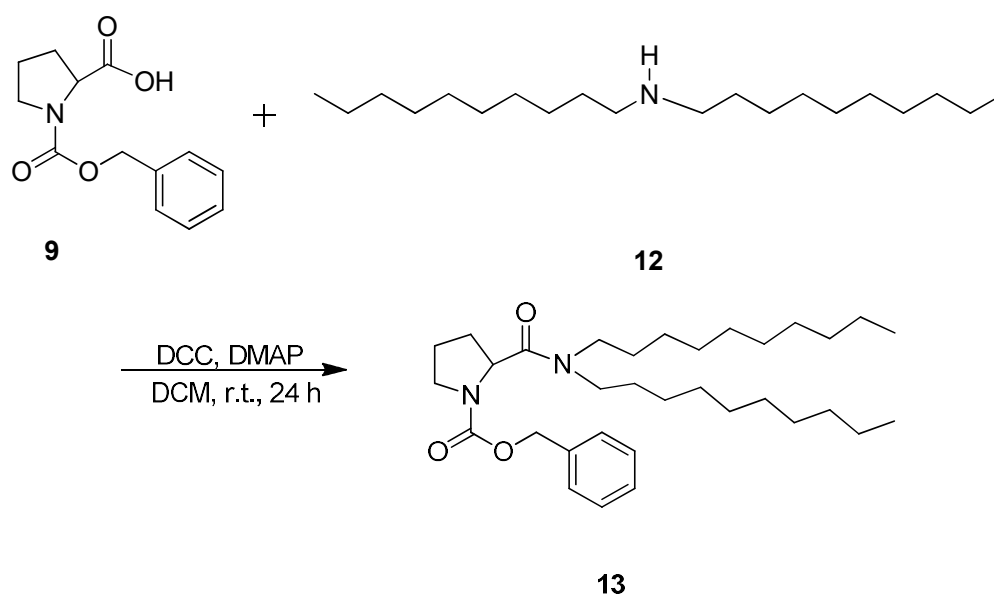
One of the most versatile and reliable ways to form the N-C bond is to use a process called reductive amination. This involves first combining the amine with a carbonyl compound to form an imine and is followed by reduction of the imine to form an amine. In the formation of didecylamine **12**, we can use decylamine **15** as our amine and decanal **16** as the carbonyl compound (**Scheme 18**). The amine attacks the aldehyde group and loss of water gives the imine functional group. This reaction is usually performed under mildly acidic conditions, and under these conditions, the imine **17** would be protonated to give an iminium ion **18** (**Scheme 19**). This charged species is highly electrophilic and reacts with added sodium borohydride in a reduction reaction to give didecylamine **12**.⁴⁵



Scheme 19: Reductive amination

By following the reaction by TLC, we could not see the spot for the starting material decylamine after the reaction mixture was at room temperature for 8 hours, which suggested that this reaction was complete. The successful amine reduction was confirmed by ^1H NMR, which exhibited a new triplet with integration for two protons at 2.56 ppm due to the amino group.

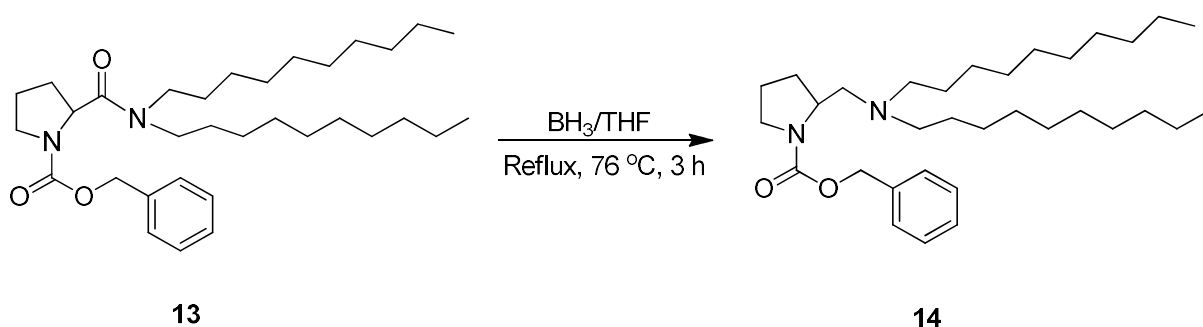
To prepare benzyl 2-(didecylcarbamoyl) pyrrolidine-1-carboxylate **13**, ((benzyloxy) carbonyl) proline **9** was dissolved in DCM and DCC was added at room temperature under nitrogen gas. Two hours later, didecylamine **12** was added for the reaction mixture (see **Scheme 20**). Initially, this reaction was carried out overnight, but the reaction was not completed and the desired product was not obtained. The reaction was repeated with careful monitoring by TLC for the disappearance of the starting materials, which established that the reaction was finished after 24 hours.



Scheme 20: Preparation of the benzyl 2-(didecylcarbamoyl) pyrrolidine-1-carboxylate

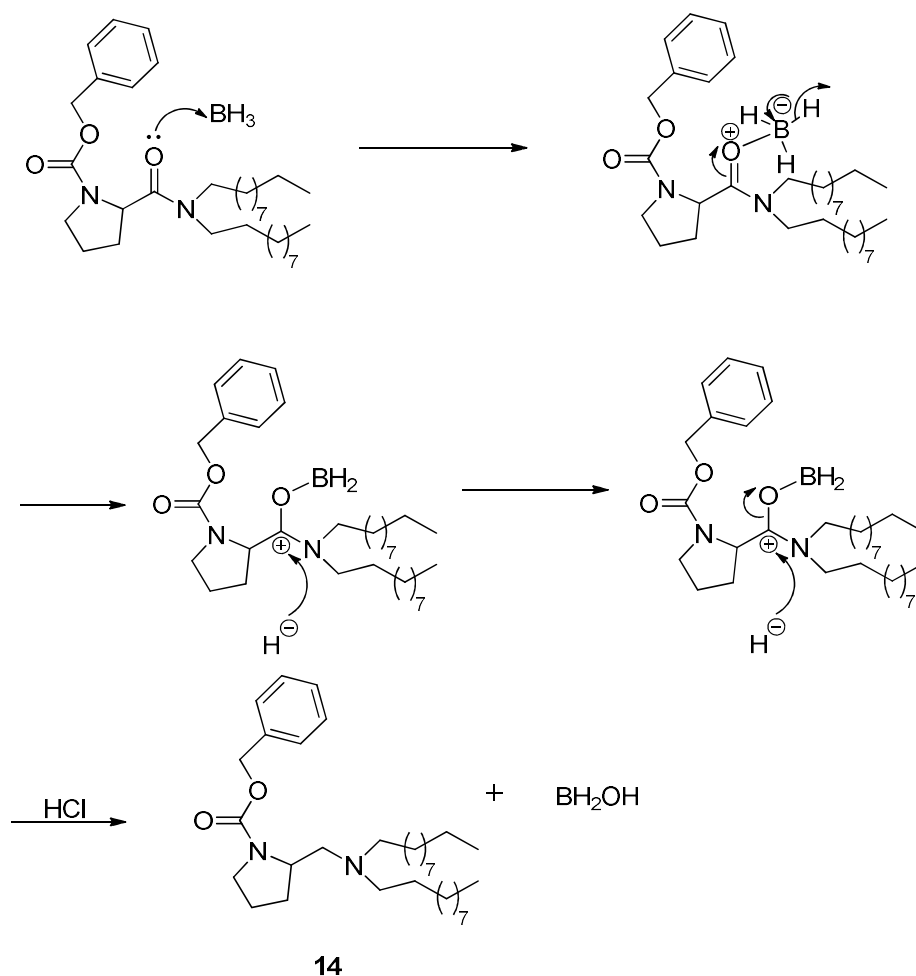
The formation of the desired product was confirmed by a combination of ^1H NMR, IR and mass analysis. In the ^1H NMR spectrum, the proton signal for 4-H appeared as a triplet at 3.19 ppm and there are 5 protons in aromatic ring in the region 7.22 ppm which confirms the presence of aromatic ring (see **Scheme 20**), the product was obtained in 28% yield.

At the start of our investigation, the reduction of benzyl 2-(dodecylcarbamoyl) pyrrolidine-1-carboxylate **13** with borane was performed in the presence of THF and heated for 3 hours at 76 °C under a nitrogen atmosphere (**Scheme 21**). In this reaction, borane does not actually exist as BH_3 *per se*. In this respect, boron has only three electrons in the valence shell, and therefore its compounds are electron deficient and there is a vacant p-orbital on the boron atom. Borane exists as a mixture of $\text{B}_2\text{H}_6/\text{BH}_3$, as dimerization partially alleviates the electron deficiency of the boron. Other boranes can also be used for this reaction, such as disiamylborane, which has one or more of the hydrogens replaced by an alkyl group.



Scheme 21: Formation of benzyl 2-(dodecyl amino) methyl) pyrrolidine-1- carboxylate **14**

The hydroboration reaction is a commonly used procedure first discovered in the 20th Century.⁴⁶ H. C. Brown got the Nobel Prize in 1979 for this and related reactions involving organoboron reagents. The mechanism of the reaction first involves the boron acting as a Lewis acid and binding to the pair of electrons in the $\text{C}=\text{O}$ bond, making it more electrophilic (**Scheme 22**). In the second step, the hydride anion adds to the carbon atom of the $\text{C}=\text{O}$ group, resulting in the formation of an alkoxide bound to boron. A second equivalence of hydride anion then adds to give the alkane. In these reagents, BH_3 is stabilised by Lewis bases such as tetrahydrofuran (THF) and dimethyl sulphide (DMS).

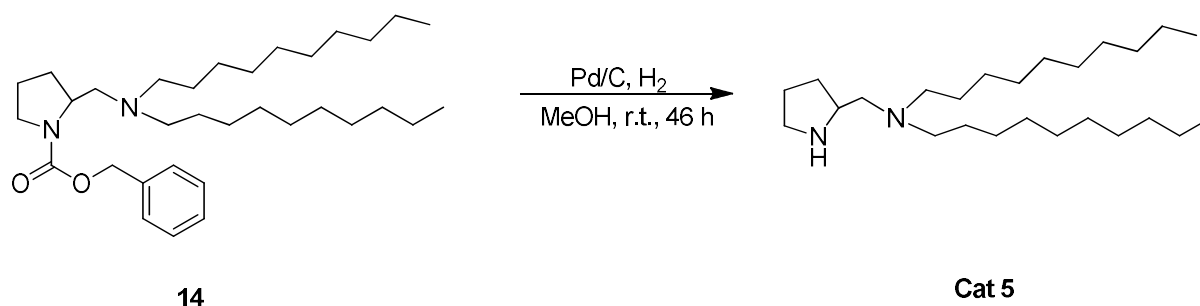


Scheme 22: Mechanism of carbonyl compound using hydroboration

In our case, the reagent used was $\text{BH}_3 \cdot \text{THF}$ and a large equivalent was used because the borane is not a strong reducing agent. After work-up and flash column chromatography, the product was obtained in 7% yield **14**. Unfortunately, the yield is not particularly high, but this compares reasonably well with the hydroboration of similar substrates in the literature. However, our focus was to synthesise a range of structures rather than optimising the reaction yield, so we continued forward with the synthesis.

The formation of alkane **14** was confirmed by ^1H NMR analysis. In the NMR spectrum, the proton signal for 2-H appeared as a multiplet at 3.40 ppm and there are $3 \times \text{CH}_2$ groups attached to nitrogen forming a multiplet.

In the last step of the synthesis, benzyl carbonate **14** was converted to its corresponding pyrrolidine **Cat 5** by a hydrogenation reaction where the atmosphere was changed from nitrogen to hydrogen in the presence of palladium as a catalyst. Palladium on carbon, often referred to as Pd/C, is a form of palladium used as a catalyst (see **Scheme 23**) where the active palladium catalyst is supported on activated carbon to increase its surface area and catalytic activity. It is believed that both hydrogen gas and the carbonyl compounds are adsorbed onto the catalyst and bind to the surface of its crystal lattice. Although this method is commonly used in the chemical laboratory, this mechanism of reduction from benzyl carbonate to the pyrrolidine derivative remains to be fully understood. An advantage of this reaction is that the by-products are carbon dioxide and toluene and so can be removed by vacuum. At the conclusion of the reaction, the mixture was filtered through Celite[®] to remove the catalyst and the filtrate was concentrated and the residue was purified by flash column chromatography. The successful carbonyl reduction was confirmed by ¹H NMR, which exhibited a new singlet with integration for two protons at 3.11 ppm due to the amino group.

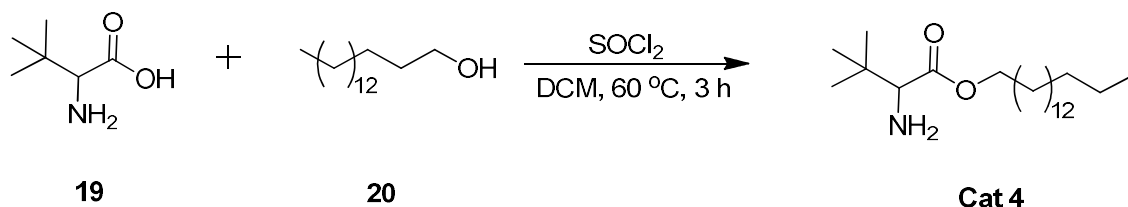


Scheme 23: Hydrogenation of carbonyl compound in the presence of Pd/C (5 wt%)

2.1.4 Synthesis of leucine-based catalyst (Cat 4)

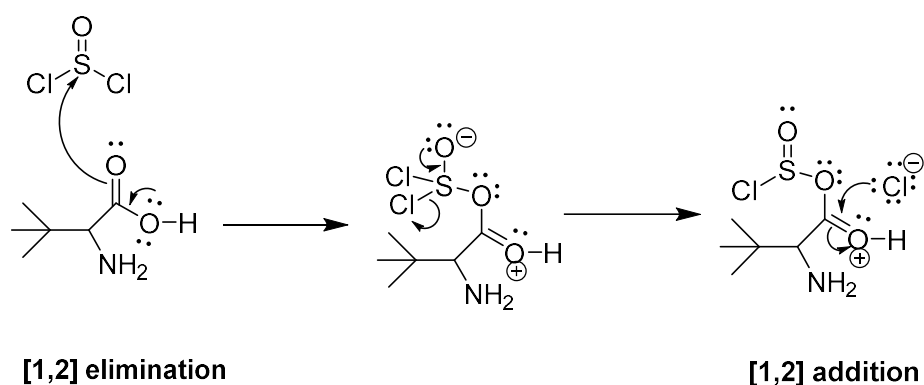
Secondly, we performed the synthesis of the leucine-based catalyst **Cat 4**. The idea was to functionalise both catalysts so that they may self-assemble to form micellar aggregates where the catalysts would be in close proximity and be able to work together. The reaction to form **Cat 4** firstly involved backside attack of the nucleophile on the alkyl halide, with bond formation at carbon and loss of a leaving group (see **Scheme 24**). The reaction proceeded in the presence of thionyl chloride (1.6 eq.) and the reaction was allowed to stir at 60 °C overnight. In this reaction, firstly leucine (**19**, 1.00 eq.) reacts with thionyl chloride to form an acid

chloride and then palmityl alcohol (**20**, 10.0 eq.) was added to get the desired product **Cat 4**. This product was confirmed by crude NMR and then purified by flash column chromatography to get a yield of 75%.

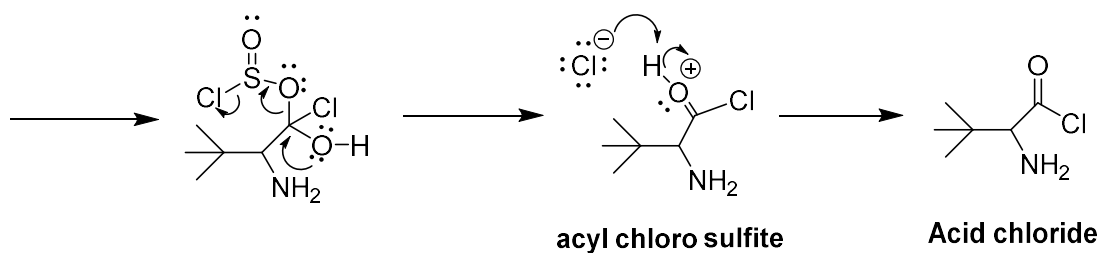


Scheme 24: Formation of hexadecyl 2-amino-3,3-dimethylbutanoate.

The above reaction is called a Fischer esterification and is a commonly used procedure involving the reaction between an acid and an alcohol to obtain an ester. Most carboxylic acids are suitable substrates for the reaction, but the alcohol cannot be a tertiary alcohol. The first step is attack of the oxygen upon the sulfur of thionyl chloride, which results in displacement of chloride ion ([1,2] elimination, loss of a chloride, followed by a [1,2] addition reaction (**Scheme 25**)). This type of reaction is a nucleophilic acyl substitution. To complete the first part of the mechanism, the carboxylic acid is converted into a chlorosulphite which then reacts with chloride to form the acid chloride intermediate (**Scheme 26**).

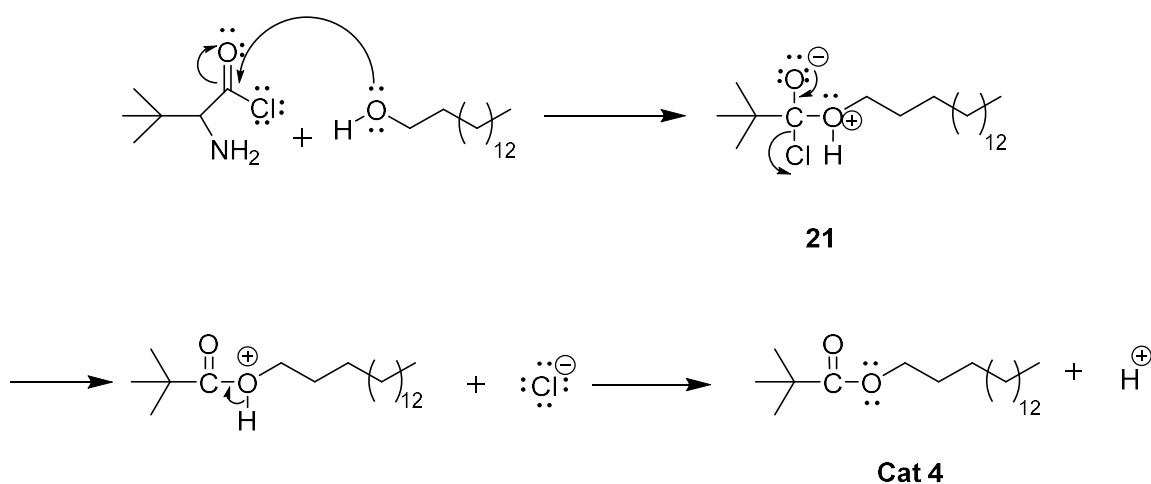


Scheme 25: [1,2]-Elimination followed by [1,2]-addition



Scheme 26: Formation of acid chloride in the presence of thionyl chloride

The next stage involves one of the lone pairs on the oxygen of the alcohol molecule performing a nucleophilic attack on the positive carbon atom of the acid chloride (**Scheme 27**). This is followed by removal of a hydrogen ion by the chloride ion to give hexadecyl 2-amino-3,3-dimethylbutanoate (**Cat 4**). This reaction is exothermic and produces the corresponding ester in high yields with only hydrogen chloride as a by-product.



Scheme 27: Formation of ester with 16 long chain hydrocarbons

^1H NMR (400 MHz, CDCl_3)

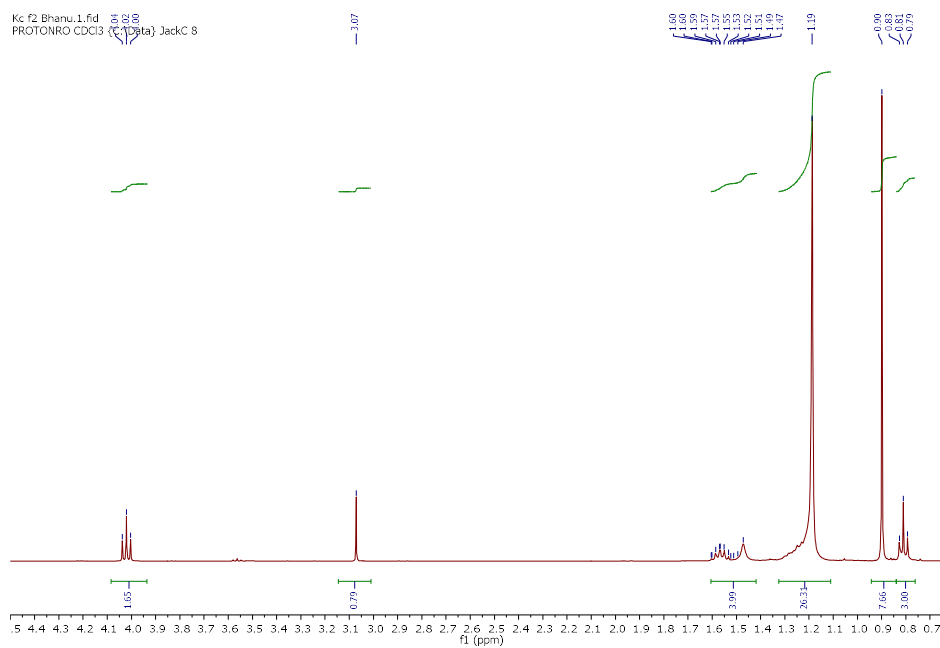


Figure 26. ^1H NMR spectra, 400 MHz, of C_{16} leucine catalyst **Cat 4**

^{13}C NMR (101 MHz, CDCl_3)

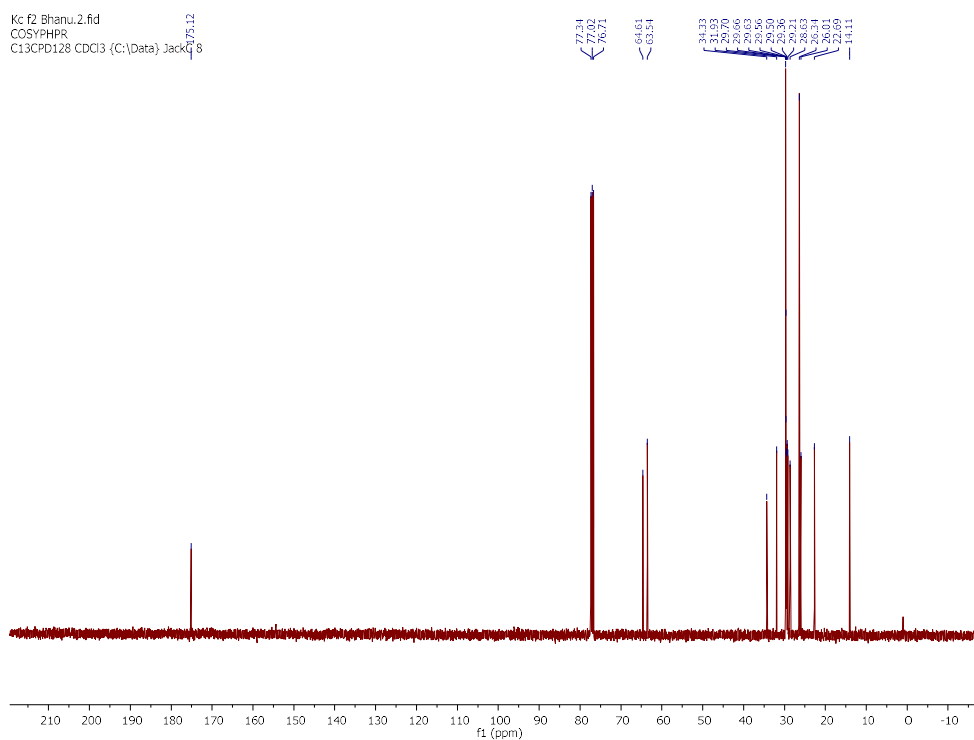
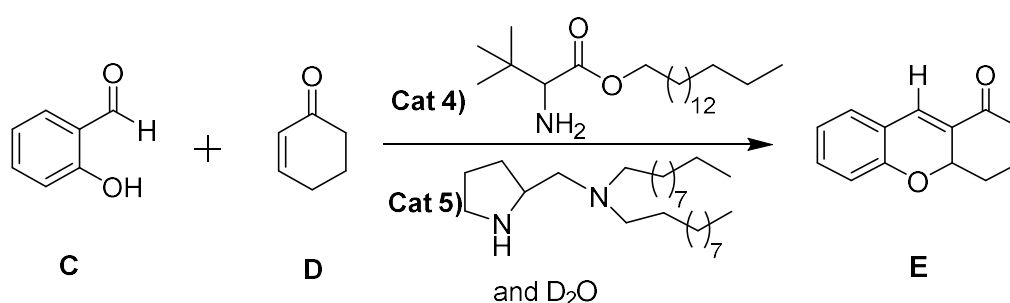


Figure 27. ^{13}C NMR spectra, 400 MHz, of C_{16} leucine catalyst **Cat 4**

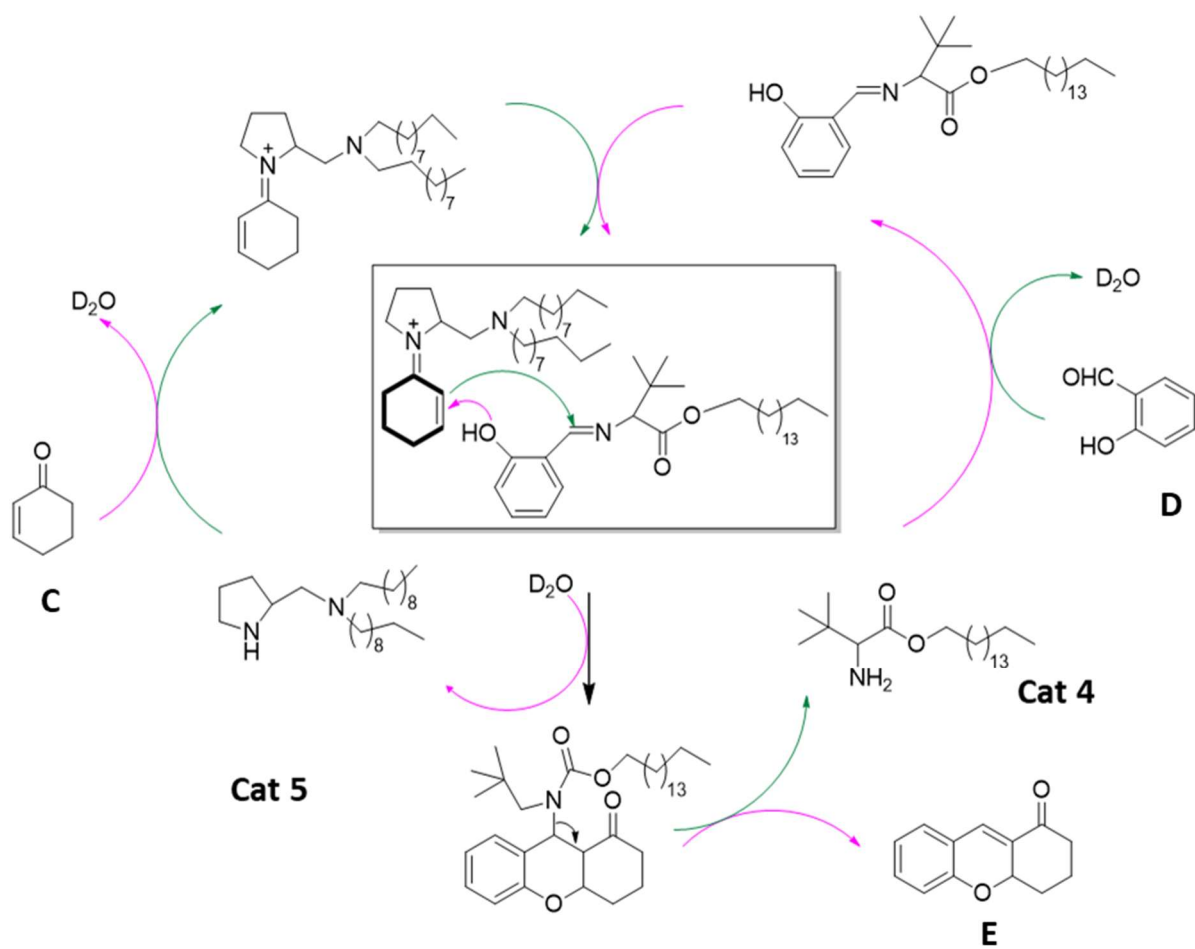
2.1.5 Formation of tetrahydroxanthenone E

With both leucine-based and proline-based catalysts in hand, we proceeded to investigate the use of these two organocatalysts in the formation of tetrahydroxanthenones (**Scheme 28**). We were inspired to apply these catalysts to this reaction because the reaction involves the simultaneous activation of both the salicylaldehyde and cyclohexanone starting materials which implies that cooperativity between the two organocatalysts may be beneficial for the rate of the reaction. This mechanism of this reaction involves sequential iminium and enamine catalysis, which is described below.

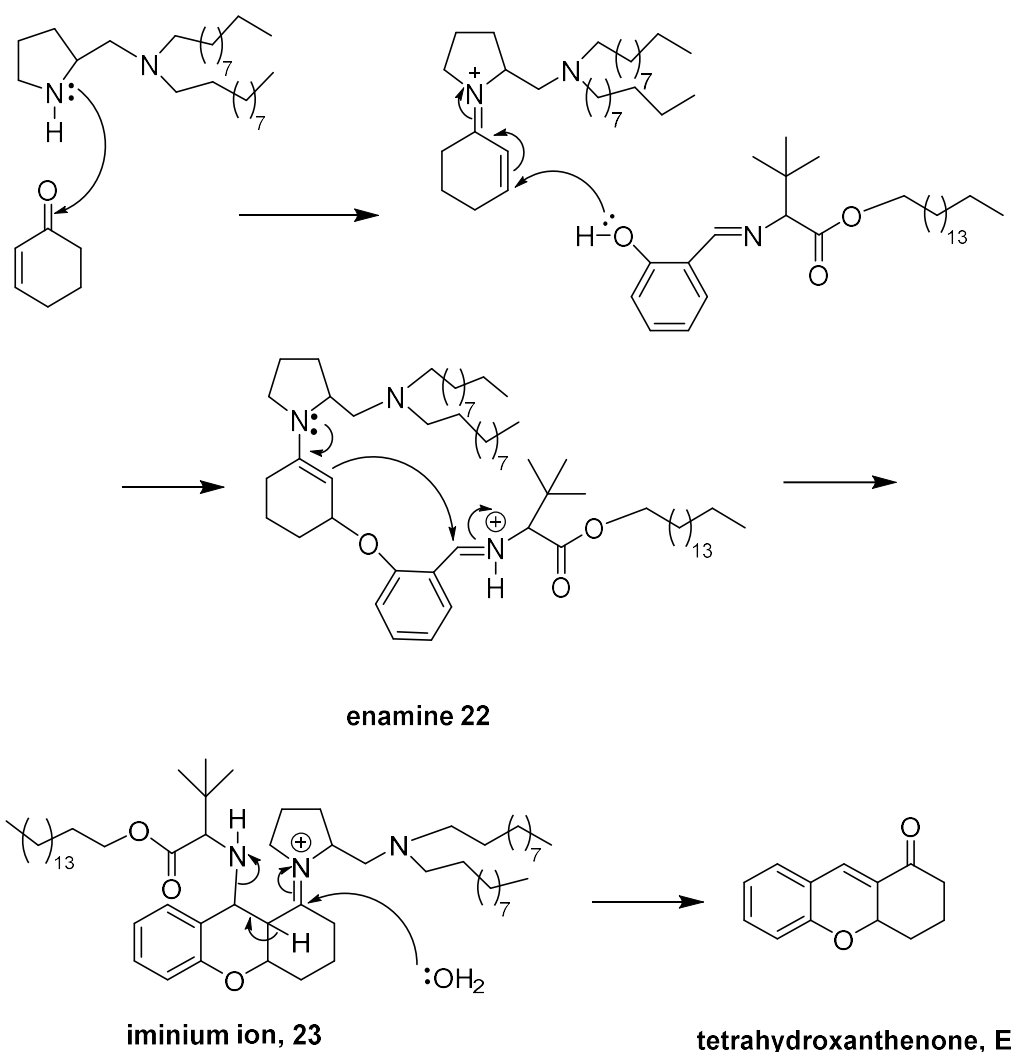


Scheme 28: Formation of tetrahydroxanthenones **E** by using **Cat 4** and **Cat 5**

Enamines have been an important reaction intermediate in organic synthesis since 1954, when Gilbert Stork showed that aldehydes and ketones could be combined with amines to accelerate alkylation and acylation reactions.⁴⁷ The use of organic chiral amines is now a powerful way to produce C-C bonds asymmetrically. Recently, Cordova and co-workers reported the asymmetric synthesis of tetrahydroxanthenones **E** from cyclohex-2-enone **D** and salicylic aldehyde **C** using a chiral pyrrolidine catalyst. The reaction proceeded by an oxa-Michael-aldol reaction via imine/enamine intermediates.⁴⁸ The cyclohex-2-enone (**D**) was activated by the pyrrolidine, forming an iminium ion which makes cyclohex-2-enone **D** a better Michael acceptor (**Scheme 29**). Attack by the hydroxyl group of salicylaldehyde **C** onto this Michael acceptor then generates an intermediate enamine (**Scheme 30**). This enamine **22** is then able to attack the carbonyl group on salicylaldehyde which is activated as an iminium **23** by the leucine-based **Cat 4** organocatalyst. Finally, elimination of the resulting Mannich bases leads to the desired tetrahydroxanthenone **C**, concurrently regenerating the organocatalysts **Cat 5**.



Scheme 29: Proposed catalytic cycle for the synthesis of tetrahydroxanthenones **E**⁴⁸



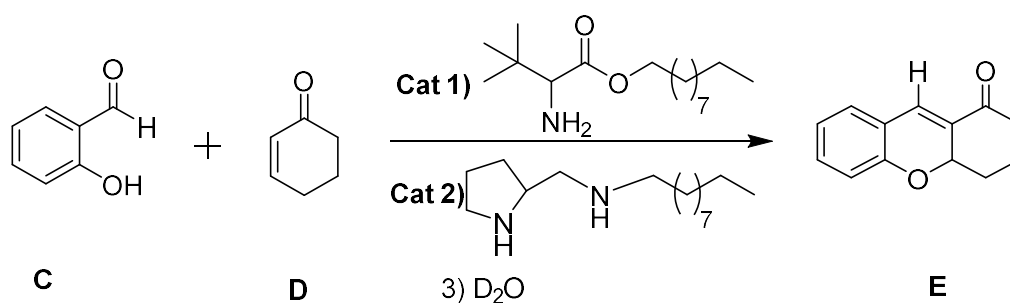
Scheme 30: Formation of tetrahydroxanthenones **E** ⁴⁹

2.1.6 Investigation of the synthesis of xanthenones using our synthesised catalysts

To assess the viability of our new catalysts for the above domino process, we investigated the reaction between salicylic aldehyde and cyclohex-2-enone in the presence of various pre-catalyst modules as shown in the tables below. We began by using 10 mol% of our proline-based catalyst **Cat 2** and 10 mol% of catalyst **Cat 1** at room temperature, with the reaction carried out in D₂O to allow monitoring of the reaction by ¹H NMR. We performed 4 reactions

in parallel: control 1 – which contained no added catalyst, control 2 – containing only the L-tert-leucine-based catalyst **Cat 1**, control 3 – containing only the proline-based catalyst **Cat 2** and the key reaction, which contained both the L-tert-leucine-based catalyst **Cat 1** and the proline-based catalyst **Cat 2**. All four reactions were monitored in parallel. To determine the rate of the reaction, aliquots were taken at specific time intervals and diluted with chloroform-d for NMR analysis. These samples were also analysed by thin layer chromatography.

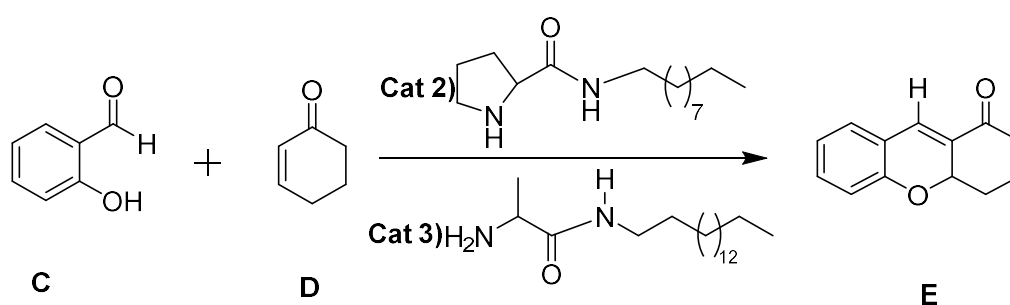
After 1 hour, it was noted that there was the clear appearance of product in the key reaction, but not in controls 1-3. Following stirring at room temperature overnight, the product was still only observable in the key reaction, but the conversion had not proceeded further than 15%. To increase the rate of the reaction, all four samples were heated at 50 °C. After heating at 50 °C for 1 hour, the key reaction proceeded to 20% conversion while control 3 proceeded to 10% conversion. Not product was observed under control conditions 1 and 2. Following stirring overnight the conversion in the key reaction approached 35% while the conversion in control 3 approached 25%. Still not product was observed in controls 1 and 2. Heating the reaction mixtures for another 2 days results in no further progress in the reactions. The progress of these reactions after 3 days is summarised in **Table 1**.



Cat 1	Cat 2	Rate	Conversion (%)
X	X	No reaction	0
✓	X	No reaction	0
X	✓	Moderate reaction	25
✓	✓	Moderate reaction	35

Table 1: Proposed self-assembly and applied Cat 1 and Cat 2 with C₁₀ carbon chain

This initial study was very promising, as it demonstrated a faster rate of reaction in the presence of both catalysts, and indicated a cooperative mechanism was occurring. However, the method was practically limited as the reaction did not progress to completion, resulting in low yields. As the L-tert-leucine-based did not appear to enhance the reaction at all on its own, we deduced that it may not be very reaction under these conditions due to the steric hinderance around the tert-butyl group. We therefore proceeded to investigate another catalyst with less steric hinderance – leucine-based catalyst **Cat 3**, which had been synthesised earlier by another member of the research group.

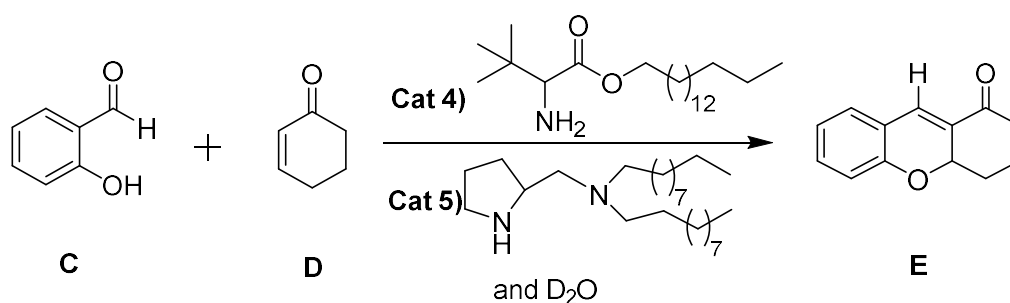


Cat 3	Cat 2	Rate	Conversion (%)
X	X	No reaction	0
✓	X	Very slow reaction	5
X	✓	Moderate reaction	35
✓	✓	Moderate reaction	45

Table 2: Proposed self-assembly and applied **Cat 2** and **Cat 3** with C₁₀ proline and C₁₆ carbon chain.

We again performed 4 reactions in parallel, each with 10 mol% of catalyst: control 1 – which contained no added catalyst, control 2 – now with the leucine-based catalyst **Cat 3**, control 3 – containing only the proline-based catalyst **Cat 2** and the key reaction, which contained both the leucine-based catalyst **Cat 3** and the proline-based catalyst **Cat 2**. With this set of reactions, we began heating at 55 °C from the start of the reaction. After 24 hours at 55 °C, control 1 showed now indication of product, while control 2 containing the leucine-based catalyst **Cat 3**

had small amount of product produced (<5%) while both control 3 (~30%) and the key reaction (~40%) showed decent conversion to product, with the key reaction again exhibiting the fastest reaction. After 2 days however, there was not substantial progress in the reaction with 35% conversion for control 3 and 45% conversion for the key reaction. As the conversion was still not optimum, we decided to trial a catalyst that had previously been used by Barbas to form micellar aggregates. This catalyst was like the proline-based catalyst that we have used earlier, but featured two hydrophobic tails, which we believed would aid self-assembly.



Cat 4	Cat 5	Rate	Conversion (%)
X	X	No reaction	0
✓	X	No reaction	0
X	✓	Fast reaction	60
✓	✓	Fast reaction	70

Table 3: Proposed self-assembly, applied **Cat 4** with C₁₆ carbon chain and **Cat 5** with two tailed catalyst.

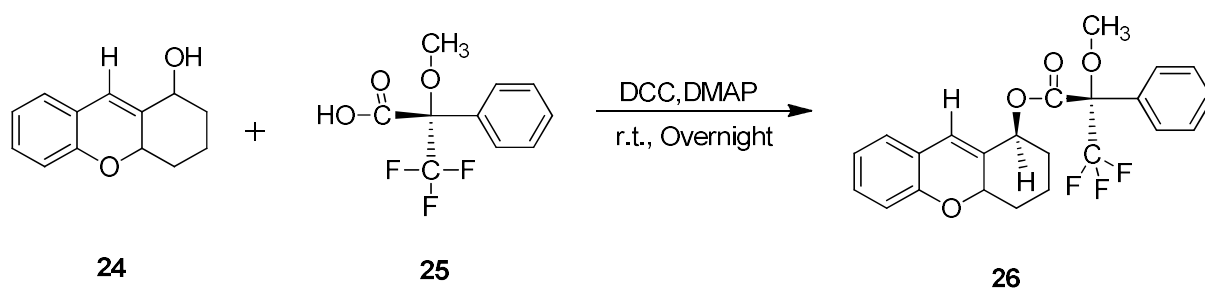
Four reactions were performed in parallel, each with 10 mol% of catalyst: control 1 – which contained no added catalyst, control 2 – now with the tert-leucine-based catalyst **Cat 4**, control 3 – containing only the proline-based two-tailed catalyst **Cat 5** and the key reaction, which contained both the tert-leucine-based catalyst **Cat 4** and the proline-based two-tailed catalyst **Cat 5**. We reverted to using tert-leucine-based catalyst, as the previous set of reactions didn't appear to be a significant improvement to the first set. Bulkier organocatalysts have also been shown to exhibit higher enantioselectivities. With the proline-based two-tailed catalyst **Cat 5**,

it was immediately evident that that the catalytic rate was much faster than previous examples. After 24 hours at 55 °C, control 1 and control 2 both demonstrated no indication of product formation. However, both control 3 and the key reaction exhibited high rates of conversion (60-70%). While encouraging, the lack of difference in conversion rate between control and the key reaction let us to assume that there was not a great deal of cooperativity occurring under these conditions. In other words, proline-based two-tailed organocatalyst **Cat 5** by itself was enough to give decent amounts of conversion.

However, one other reaction result that we needed to investigate was the enantioselectivity of the reaction. Organocatalysts are so powerful because they can induce enantioselectivity in a chemical reaction without the addition of metal ions, which are essential in traditional chiral catalysis. With our above result, even though there did not appear to be a great enhancement of rate in the presence of both organocatalysts, there was the possibility that the presence of both organocatalysts together was essential to provide high enantioselectivity. We therefore proceeded to investigate the enantioselectivity of the above reaction in the presence and absence of certain catalysts.

2.1.7 Mosher Ester Analysis

The enantiopurity of the products that we formed was determined by Mosher ester analysis. The idea here is to attach an enantiopure group onto our molecule and use ^1H NMR analysis to determine the enantioselectivity of our reaction. The phenomenon of NMR non-equivalence of internal or external diastereotopic groups have been carefully reviewed and discussed and are used widely to determine the enantiomeric purity of a chiral alcohol or amine from which these stereoisomers were prepared.⁵⁰ The most commonly used technique employed is use of a Mosher acid (e.g. (S)- α -methoxy- α -(trifluoromethyl)phenylacetic acid), which is commercially available as both the R and S enantiomers in high enantiopurity.



Scheme 31: Formation of the Mosher ester for analysis of stereoselectivity

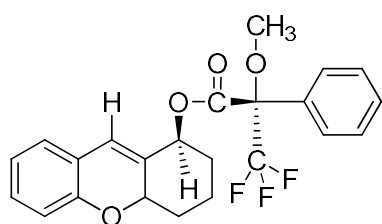


Figure 30a

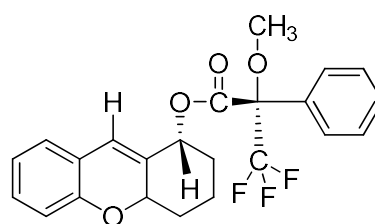
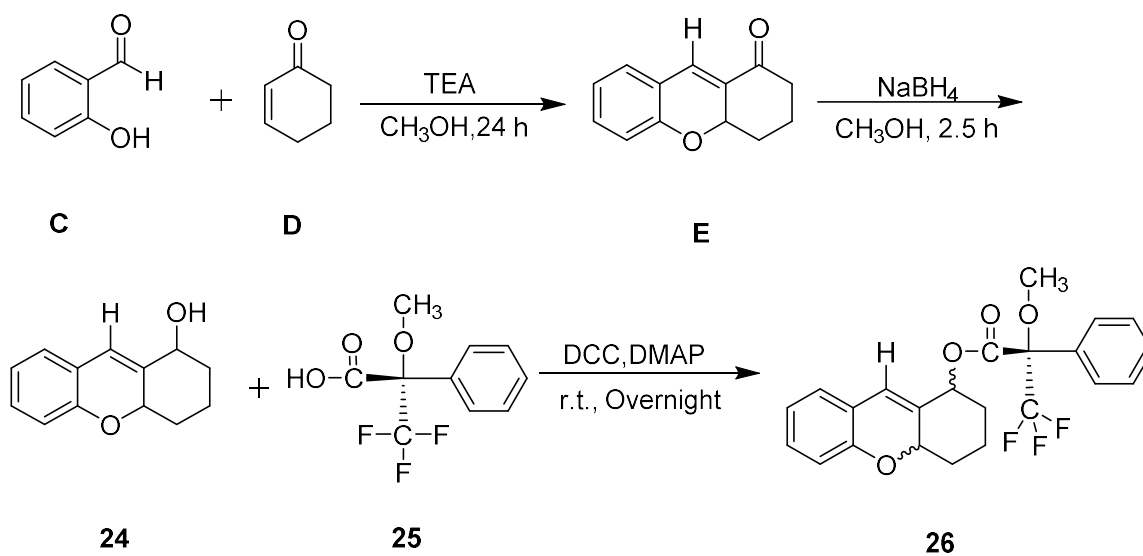


Figure 30b

Figure 30a and 30b: Diastereomers

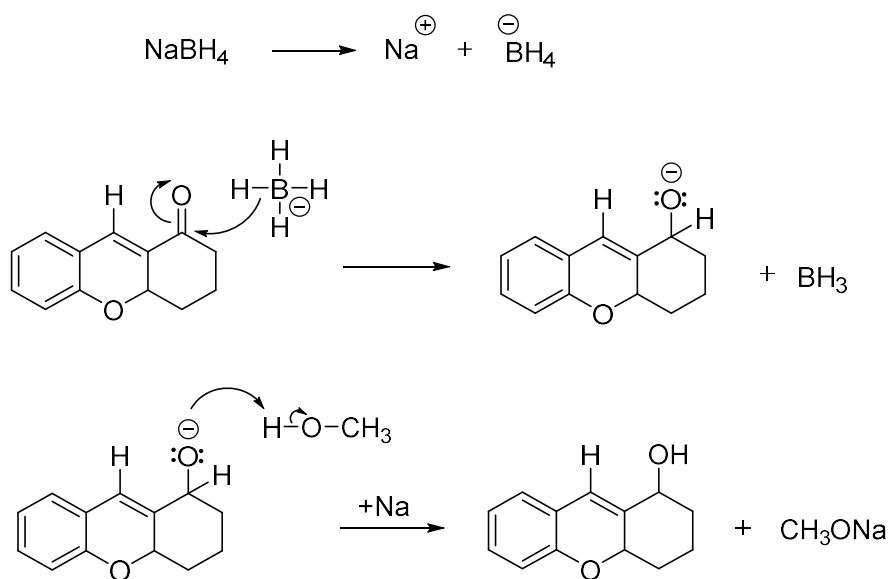
To perform Mosher ester analysis, we first reduced the carbonyl group down to the secondary alcohol with sodium borohydride (**Scheme 31**). The hydroxyl group of the xanthanol was then attached to the Mosher ester via DCC coupling and the enantioselectivity was determined by

looking at the ^1H NMR spectrum and comparing the proton integrations. As a comparison, we first synthesised racemic xanthenone **E** using only achiral catalysts.⁵¹ This was performed by reacting salicylic aldehyde **D** and cyclohex-2-enone **C** together in the presence of triethylamine. The product was then reduced in the presence of NaBH_4 to give the secondary alcohol for attachment of the Mosher ester (**Scheme 32**). The ^1H NMR of the product was then used as a reference point for the enantiomeric reactions.



Scheme 32: Route to formation of the racemic xanthenol and formation of the Mosher ester.

For the reduction of the carbonyl, sodium borohydride was used as the reducing agent (**Scheme 33**). This is one of the weakest hydride donors commonly used in organic synthesis. This can be seen by the fact that other powerful hydride donors such as lithium aluminium hydride (LiAlH_4) reaction violently in water but sodium borohydride can be used in water. Sodium borohydride is able to reduce aldehydes and ketones, but generally not esters and carboxylic acids.



Scheme 33: Mechanism of reduction by sodium borohydride

The ^1H NMR of the Mosher ester **26** derived from the racemic xanthone **C** is shown in **Scheme 31**. The proton next to the secondary alcohol attached to the Mosher ester is observed at 5.67 and 6.01 ppm, with these two protons having equal integrations. The ^1H NMR of the Mosher ester derived from the xanthone **C** formed in the reaction between proline-based catalyst **Cat 5** and tert-Leucine-based catalyst **Cat 4** (as in the last entry of **Table 3**) is shown in **Figure 32**. These same two protons at 5.67 and 6.01 ppm now have non-equal integrations. The enantiomeric excess of the xanthone formation reaction was determined from these integrals to be 32%. While it is promising to see that there is some enantioselectivity, the amount of stereoselection was not enough for the reaction to be synthetically useful.⁵² At this stage, it was decided to change the focus of the project and investigate another catalyst system that had potential for cooperative effects.

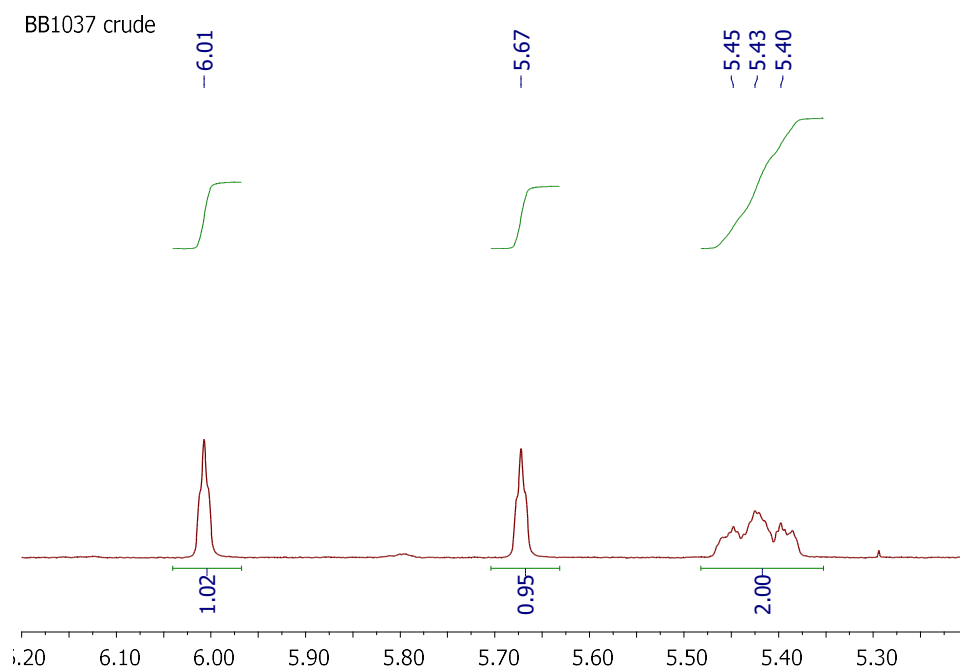


Figure 31: ¹H NMR showing the key signals in Mosher ester **26** (racemic control)

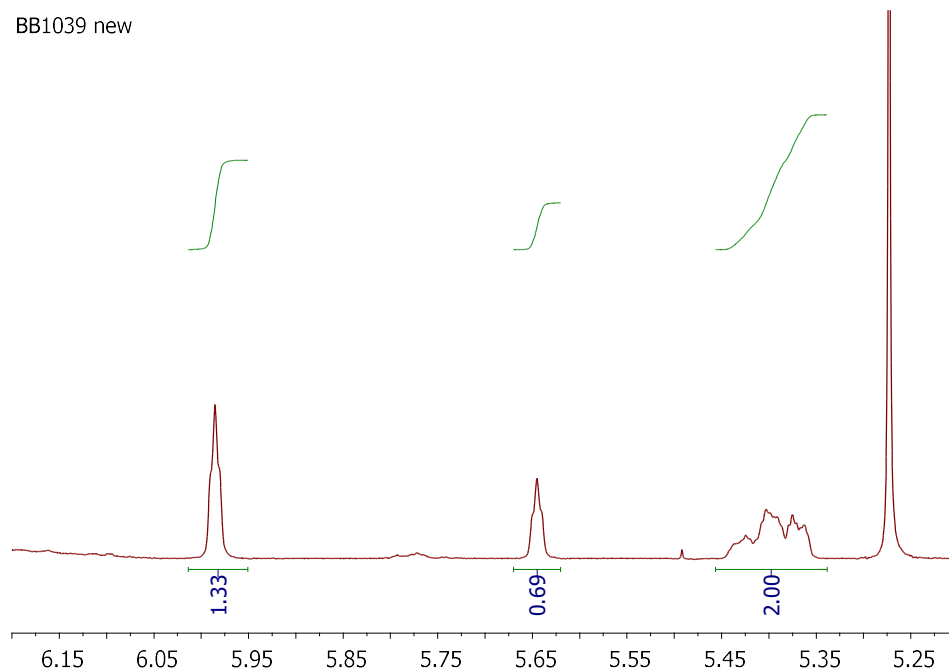


Figure 32: ¹H NMR showing the key signals in Mosher ester of the xanthenone formed in the last entry of **Table 3**.

2.1.8 Summary

We have observed accelerated catalysis in the presence of our synthesised catalysts **Cat 4** and **Cat 5**, but the rate acceleration in the presence of both the proline-based and the leucine-based catalysts did not give greatly accelerated rates compared to the reaction rate just in the presence of the proline-based catalyst (i.e. **Cat 5** only). We found Barbas' proline-based catalyst featuring two hydrophobic tails to be the most efficient for this reaction.⁵³ We also determined the enantiomeric excess of the reaction under our conditions to be 30%, which was decided to be too low to be synthetically useful.

Part B

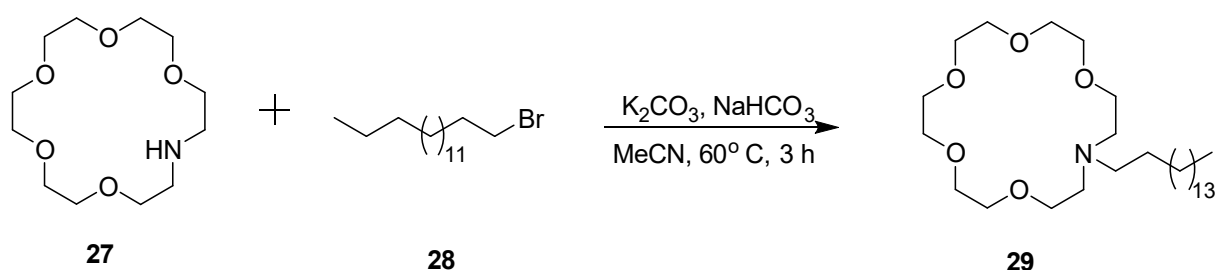
3.0 Supramolecular catalysis of Amide and Ester cleavage by a Dinuclear Barium (II) complex

Following the somewhat disappointing results obtained while investigating the cooperativity between two organocatalysts, we decided to investigate the possibility of an alternative system that bore greater resemblance to our earlier reported system involving cooperative metal centres. Our earlier system involved amphiphilic molecule that had a long hydrophobic tail and a polar head that had 1,4,7-triazacyclononane units which bound zinc. These zinc ions were able to self-assemble into vesicular structures and cooperatively activate the cleavage of the RNA model **HPNPP**.

We were inspired by a system reported by Cacciapaglia *et al.*² which demonstrated cooperativity between Ba²⁺ ions which were able to act cooperatively to cleave activated esters and amides. These Ba²⁺ ions were held together by 1-aza-18-crown-6 (**29**) in a similar way to the 1,4,7-triazacyclononane system described above. The cooperativity demonstrated in this case was in an intramolecular fashion. We wanted to demonstrate that we could design amphiphiles that could exhibit cooperativity in an intermolecular fashion within a self-assembled system.

3.1 Synthesis of 1-aza-18-crown-6 (29)

We began to investigate this idea by synthesising the 1-aza-18-crown-6 **29** (Figure 24). We followed the synthesis by Stefano Di Stefano for the reaction between 16-hexadecyl-1,4,7,10,13-pentaoxa-16-azacyclooctadecane **27** and 1-bromohexadecane **28** (Scheme 34). This reaction was performed for 3 hours at 60 °C in acetonitrile and the product was obtained in 25% yield. Our research efforts are aimed at the development of self-assembled catalysts by means of a modular self-assembly. We believed that in the barium (II) complex of the ligand **29**, would be able to act cooperatively in the cleave of esters such as acetoxybenzoic acid (Figure 33).



Scheme 34: Preparation of 1-aza-18-crown-6 units with a C₁₆ carbon long chain.

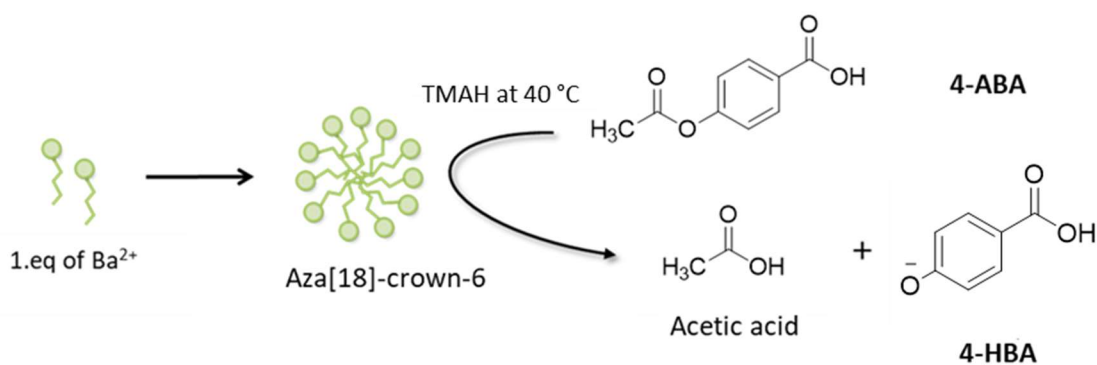


Figure 33. The conversion of 4-ABA to 4-HBA in the presence of 1-aza-18-crown-6 units

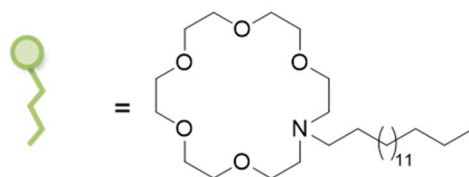


Figure 34. The structure of 1-aza-18-crown-6 units with C₁₆ (29)

3.2 UV-Visible studies for 1-aza-18-crown-6 units

We next investigated the ability of our synthesised amphiphile 1-aza-18-crown-6 (**Figure 34**) to catalyse the ethanolysis of 4-acetoxybenzoic acid into acetic acid and 4-hydroxybenzoic acid (**Figure 35**). We first measured the absorbance of the starting material 4-acetoxybenzoic acid in an 85:15 mixture of ethanol-acetonitrile (which would be the conditions for the hydrolysis) and observed absorbance maximum to be at 230 nm (**Figure 36**). The absorbance of the product 4-hydroxybenzoic acid was observed to have a peak at 274 nm. The progress of this reaction could therefore be monitored by measuring the change in UV absorption at 274 nm over time.



Figure 35. Structures of **4-ABA** and **4-HBA**

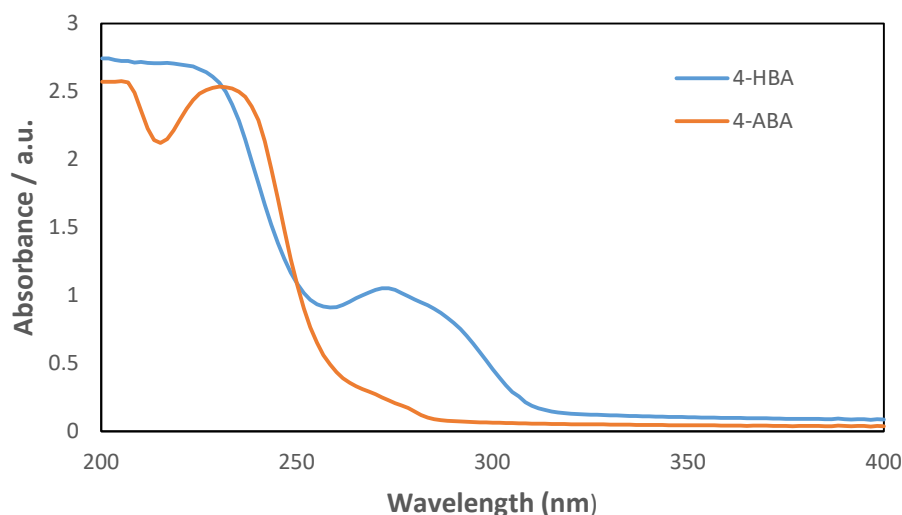


Figure 36. Absorbance spectra of 4-ABA and 4-HBA, solvent: EtOH/CH₃CN = 85:15, 25 °C.

Figure 37 shows the progress of the hydrolysis of 4-ABA to 4-HBA at 25 °C, by measuring the absorbance at 274 nm. The rate of cleavage was measured in the presence of Me₄NOH as the base and in the presence of both the C₁₆-1-aza-18-crown-6 catalyst **29** and Ba²⁺ ions. These rates were compared to the rates in the presence of only Ba²⁺ ions and in the presence of only catalyst **29**, which acted as the two control conditions. In **Figure 37**, it can be seen that there is some catalytic activity in the presence of just the crown ether **29** and significant activity in the presence of Ba²⁺ ions only. Surprisingly, the catalytic activity in the presence of C₁₆-1-aza-18-crown-6 **29** and Ba²⁺ ions was slightly less than the activity in the presence of Ba²⁺ ions only.

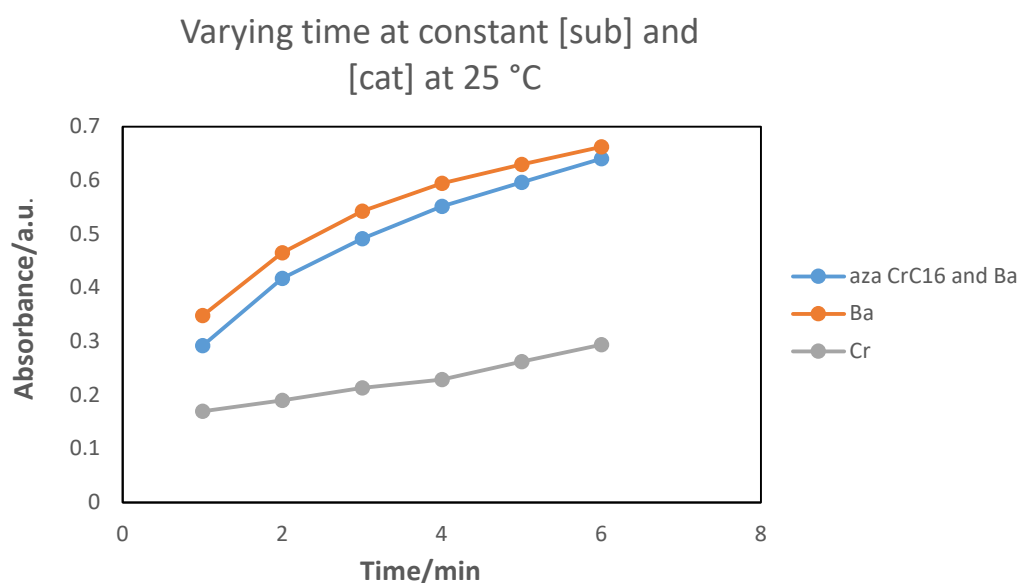


Figure 37. Plot of absorbance vs changing time at constant substrate and catalyst concentrations, and in the absence and in the presence of 1-aza-18-crown-6 with barium nitrate. Reaction conditions: solvent (EtOH/CH₃CN: 85:15), catalysts: Ba²⁺ and C₁₆-1-aza-18-crown-6 (50 μM), Me₄NOH (1 μM) and Substrate: 4-ABA (100 μM), λ = 274 nm, temp 25 °C.

3.3 Further Kinetic studies

We next tried to optimise the reaction conditions by changing the pH of the reaction as well as measuring the kinetics under different temperatures. We also employed sodium ethoxide as the base as it is much stronger than the ammonium hydroxide previously used. Below is a graph showing the kinetics of the cleavage of 4-ABA at 40 °C in the presence of NaOEt (**Figure 38**). Under these conditions, the rate of the catalysis in the presence of crown ether **29** only is slow compared to the rate in the presence of both crown ether **29** and Ba²⁺. The rate with both is also higher than the rate with just Ba²⁺, but the rate in the presence of just Ba²⁺ is still quite high, and under these conditions, the demonstration of our concept is not very effective.

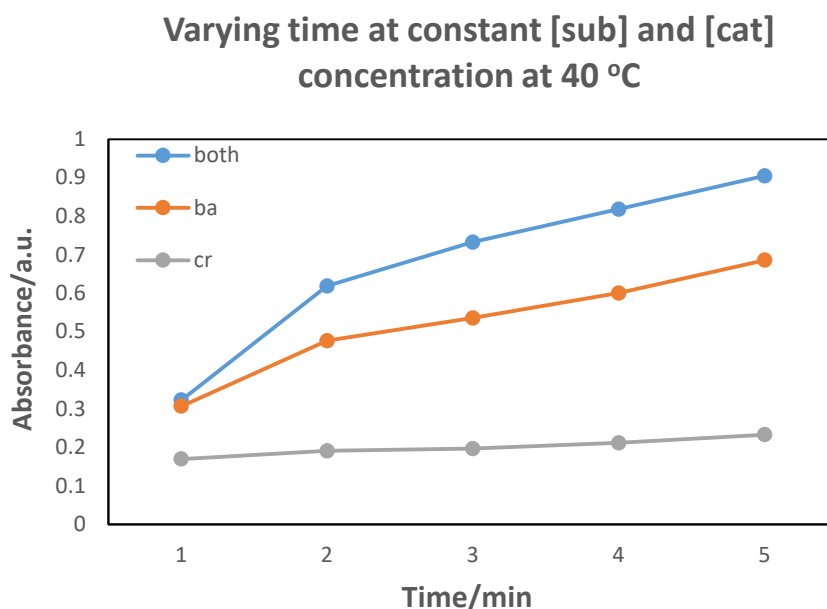


Figure 38. Plot of absorbance vs changing time at constant substrate and catalyst concentrations, and in the absence and in the presence of 1-aza-18-crown-6 with barium nitrate. Reaction conditions: [Solvent (EtOH/CH₃CN: 85:15), Catalysts: Ba and C₁₆-1-aza-18-crown-6 (50 μM), NaOEt (500 μM) and substrate: 4-ABA (100 μM), λ = 274 nm, temp 40 °C].

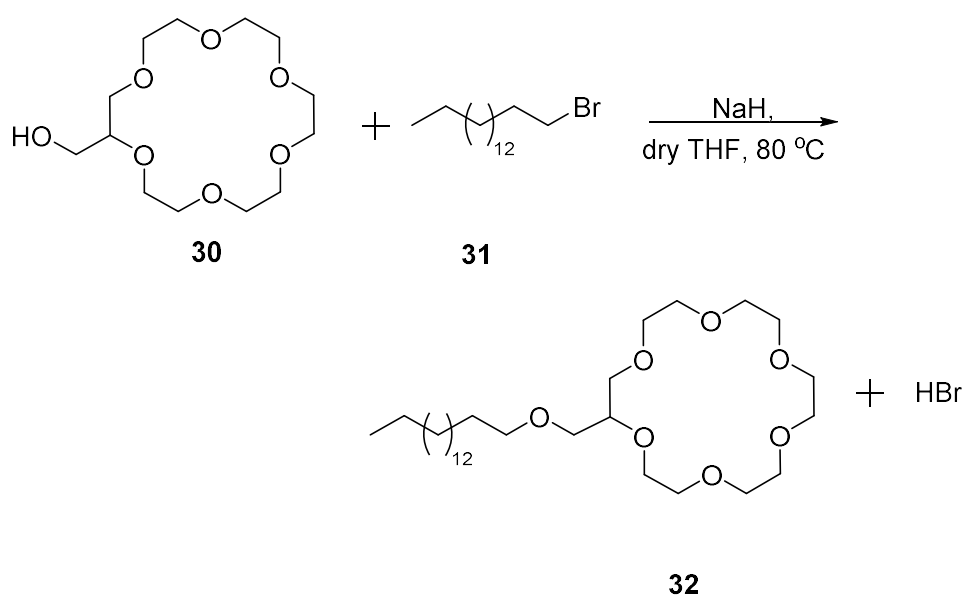
The above reaction conditions to cleave 4-acetoxybenzoic acid required the addition of EtOH in acetonitrile. As acetonitrile is very much less polar than water, we had doubts as to whether

our amphiphiles were forming self-assemblies in acetonitrile. In the absence of self-assembly, there would not be any cooperativity, and therefore no enhancement of catalysis due to cooperative effects. We therefore decided to move into reaction conditions that were more favourable for the self-assembly of amphiphiles – namely aqueous conditions. In aqueous conditions, we would also more easily probe the critical aggregation concentration so that we could ensure we were working at high enough concentrations for aggregation to occur.

3.4 Synthesis of C₁₆-18-crown-6-ether (32)

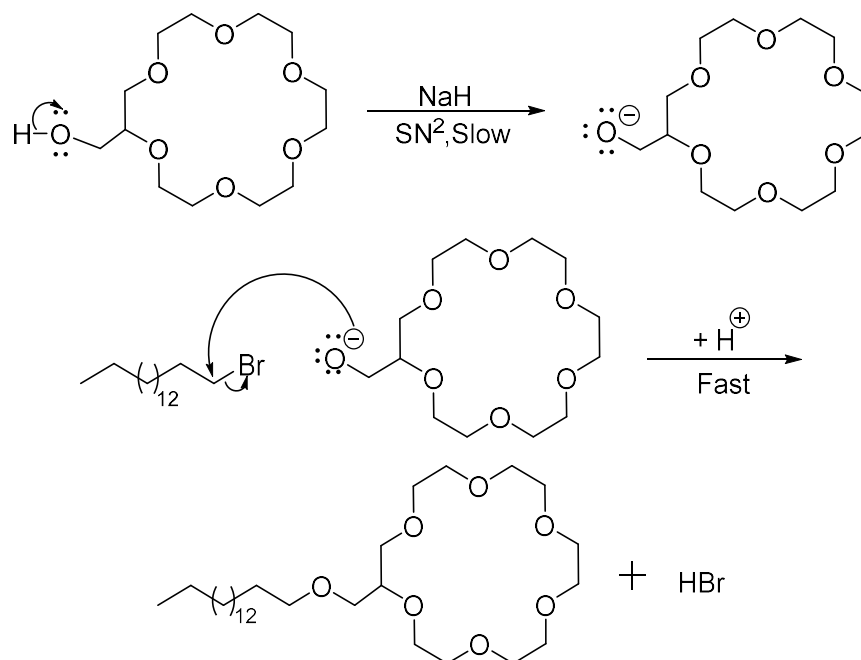
At the same time, we decided to change the amphiphile that we were using, to a standard C₁₆-18-crown-6-ether units, so that we could be sure that there would be no unexpected effects from the nitrogen present in the crown ether.

We therefore began to investigate the following reaction sequence involving the Williamson² ether synthesis of (1,4,7,10,13,16-hexaoxacyclooctadecan-2-yl) methanol and 1-bromohexadecane (**Scheme 35**). Both reagents were dissolved in dry THF and heated overnight at 80 °C under a nitrogen atmosphere. In this reaction, sodium hydride acts as a base and dry THF acts as a solvent.



Scheme 35: Formation of C₁₆-18-crown-6-ether (**32**) in the presence of sodium hydride.

The Williamson synthesis is a commonly used procedure first reported in 1850. This reaction proceeds via a S_N2 mechanism.⁵⁴ In this particular case, the mechanism begins with deprotonation of the alcohol by NaH, which is a very strong base (**Scheme 36**). This generates an alkoxide, which is a very strong nucleophile and attacks the alkyl halide via backside attack to form the ether product.



Scheme 36: Mechanism of formation of C₁₆-18-crown-6-ether

3.5 Substrate Screening

With the new catalyst in hand, we screened several different substrates that had the potential to be cleaved in aqueous buffer. This was because 4-acetoxybenzoic acid would no longer be able to be cleaved under these conditions due to the need for ethoxide as a reagent. The new substrates that we screened included the RNA-model **HPNPP**, the DNA-model **BPNP** and the esterase model para-nitrobutyrate (**PNB**) (see **Figure 39**).

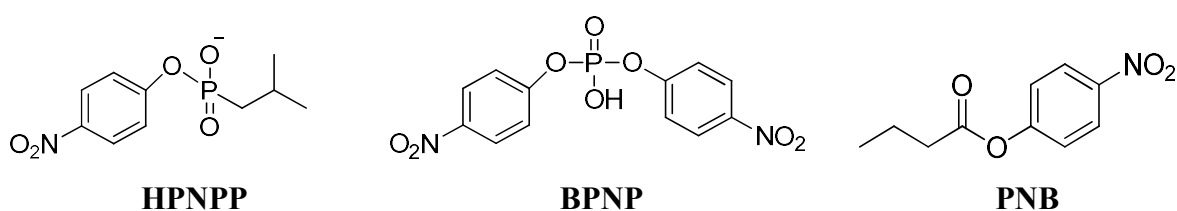


Figure 39. Structures of HPNPP, BPNP and PNB

These three substrates were initially screened in pH 7 HEPES buffer and 500 μ M with monitoring of the formation of para-nitrophenol (**PNP**) which could be observed at 410 nm with the UV spectrophotometer. No cleavage was observed with **HPNPP** and **BPNP** after 1 hour, but a reaction was observed with **PNB** (**Figure 40**).

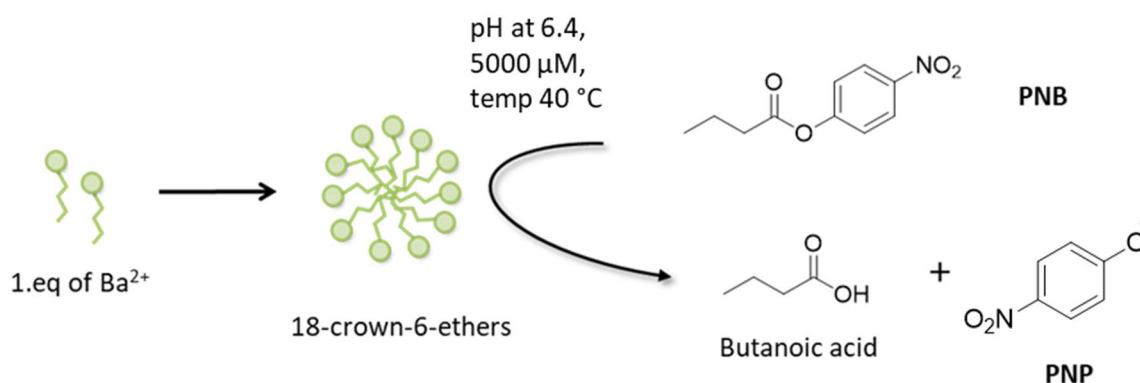


Figure 40. Cooperative catalysis induced by neighbouring C₁₆-18-crown-6-ether with Ba²⁺ complexes upon assembly.

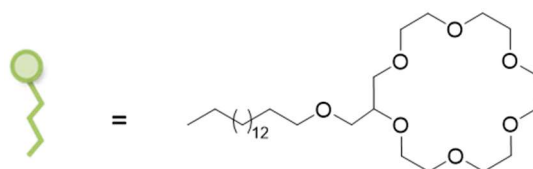


Figure 41. The structure of C₁₆-18-crown-6-ether **32**

3.6 Further Investigations with *p*-nitrobutyrate

As these reactions are often pH-dependent, we studied the reaction at varying pH's at constant catalyst and substrate concentrations. The reaction kinetics of the catalyst (C₁₆-18-crown-6-ether **32**-Ba²⁺) were performed alongside control reactions where either only Ba²⁺ was present (without the crown ether amphiphile) or only the crown ether amphiphile was present (in the absence of Ba²⁺; **Figure 42**). As can be seen in Figure 43, at pH 5.5, the rate of the reaction in the presence of both the catalyst and Ba²⁺ is essentially the sum of the rate of the reaction in the presence of Ba²⁺ only and the rate in the presence of the crown ether **32** only. At pH 6, the rate in the presence of both crown ether **32** and Ba²⁺ is lower than the rate with crown ether **32** only. This is an interesting data point which we currently do not have a good explanation for. The rate of the reaction at pH 6.4 is roughly double the rate of reaction at pH 6 placed at constant catalyst and substrate concentration, and we felt that this was a fast-enough rate to continue with further investigations. The rate of the reaction in the presence of both catalyst

Figure 44 and Ba^{2+} is still only the sum of the rate of the reaction in the presence of Ba^{2+} but at this point, we rationalised that we were potentially working at conditions that were below the CAC of catalyst **32**. The rate of the reaction at pH 7 in the presence of both catalyst **Figure 42** and Ba^{2+} is actually lower than the sum of the rate of the reaction in the presence of Ba^{2+} and the reaction in the presence of catalyst **32** only, so we decided to perform further studies at pH 6.4.

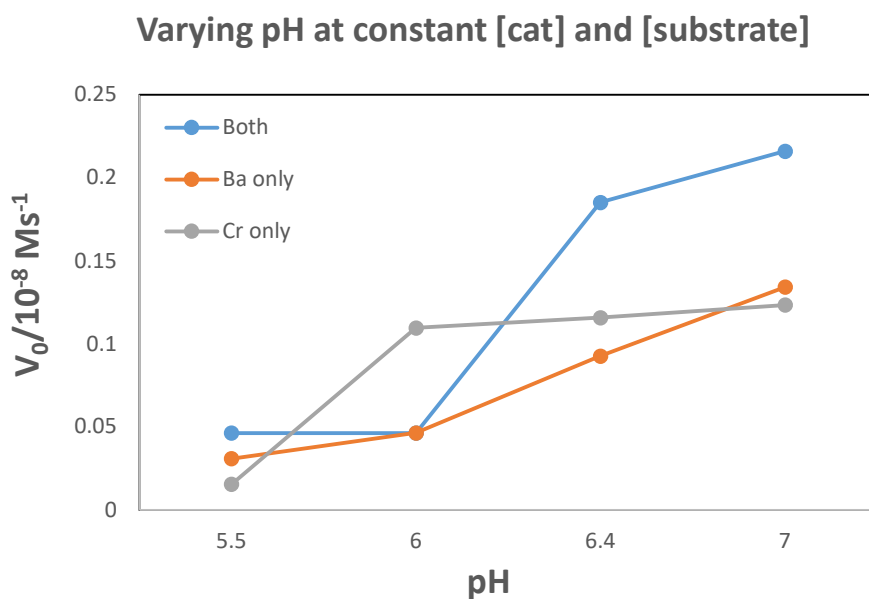


Figure 42: Plot of initial rate vs Changing pH values at constant substrate and Catalyst concentrations for the hydrolysis of **PNB**. The catalysis of **PNB** cleavage can be achieved by micellar aggregation of amphiphilic ligands containing C_{16-18} -crown-6-ether and Ba^{2+} . Reaction conditions: Solvent (mQ water), $\text{Ba}(\text{NO}_3)_2$ [50 μM], C_{16-18} -crown-6-ether **32** [50 μM], **PNB** [500 μM], pH starting from 5.5 MES to 7.0 HEPES (5000 μM).

We next performed kinetic studies with increasing concentrations of catalyst **32**. **Figure 43** shows a plot of the initial rates of reaction with varying concentrations of catalyst **32**· Ba^{2+} in the presence of **PNB** (500 μM) in aqueous buffer ($[\text{MES}] = 5000 \mu\text{M}$, pH 6.4). At low concentrations of catalyst **32**· Ba^{2+} (0-30 μM), low reaction rates are observed, comparable to the rate in the presence of catalyst **32** only or Ba^{2+} only. We reason that this could be because at these concentrations, the CAC has not yet been reached so there are low number of catalytic pockets formed by neighbouring Ba^{2+} complexes. At higher catalyst **32**

concentrations, the rate increases significantly (especially around 50 μM) and becomes significantly faster than the reaction rate under the two control conditions. At higher concentrations, it appears that a plateau is reached, which may be due to not having enough substrate to bind with the catalyst present. The sudden jump in catalytic rate at 50 μM however, is very promising as suggests aggregate formation and cooperativity.

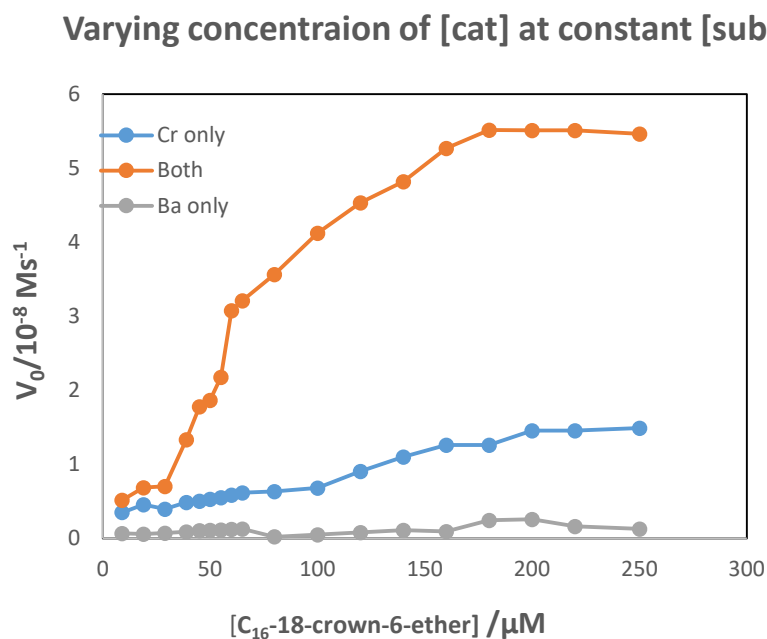


Figure 43. The rate of hydrolysis reaction vs concentration of catalytic ligand in the presence of substrates and barium ions. Reaction conditions: solvent (mQ water), pH at 6.4 (5000 μM), 500 μM of **PNB**, catalyst C₁₆-18-crown-6-ether **32** (50 μM), Ba(NO₃)₂ and temperature at 40 °C.

3.7 Determination of the Critical Assembly Concentration

To confirm that the increase in catalytic activity was due to structure formation and cooperative effects, we determined the CAC of catalyst **32** using Nile red as a fluorescent probe. Nile red is a hydrophobic fluorescent probe and can be used to determine the CAC of amphiphilic molecules because it exhibits strong solvchromic effects. In other words, the fluorescence intensity and emission maximum will change according to the polarity of the environment in which it is in. In more non-polar environments, the fluorescence intensity is greater due to it being able to more effectively solubilise the Nile red. Therefore, when amphiphiles shift from concentrations below the CAC to concentrations above the CAC, a noticeable change in the fluorescence behaviour of Nile red is observed.

We had reason to believe that **PNB 33** would be able to act as an efficient counterion and to have a significant effect on the assembly behaviour of C₁₆-18-crown-6-ether **32** with Ba²⁺. An experiment was therefore performed where increasing amounts of catalyst **32** was added to a solution of Ba²⁺, substrate **PNB (33)** and Nile red (5 μM, λ_{ex} = 570 nm, λ_{em} = 643 nm) in MES buffer at pH 6.4. **Figure 44** shows the change in the fluorescence maximum as increasing C₁₆-18-crown-6-ether **32** and Ba²⁺ is added. The emission was observed to shift dramatically from 658 nm before any catalyst **32** was added, to 637 nm after 25 μM of catalyst **32** was added. At higher concentrations, this solvchromic shift was less dramatic, with the emission maximum settling at 625 nm. By using the linear parts of the graph before and after the inflexion point in the curve, we can extrapolate these lines both forwards and backwards to find the intersection between these two lines. This method is commonly used to determine the CAC of surfactant molecules and from the intersection seen in **Figure 44**, we can determine that the CAC of C₁₆-18-crown-6-ether **32** to be approximately 33 μM.⁵⁵

Table 4: Fluorescence titration with C₁₆-18-crown-6-ether **32** and Ba²⁺, in a constant concentration of Nile red, model **PNB** and MES buffer at pH 6.4.

[32 + Ba ²⁺] (μ M)	Maximum Wavelength (nm)	Maximum intensity	Intensity at 635 (nm)
0	655	56.5	34.2
2.99	655.6	64.8	44.7
5.98	652.3	69	53.1
8.95	649.4	71	62.3
11.92	646.9	80.4	74.5
17.83	641.7	96.7	93.1
23.33	636.9	113.2	108.3
33.43	633.9	144.8	145.1
43.05	631.6	176.9	178.1
52.58	630.5	206.9	206.3
71.35	628.9	253.5	253.5
116.76	628.5	343	336
125.58	628.5	399.5	392
134.32	628.4	423.6	412.3
142.98	627.7	433.6	423
147.29	627.4	442	435
151.57	627.4	452	446
155.83	627.9	466.7	458
164.29	626.9	475.3	466.4
180.99	626.4	502.9	493.1
197.38	626.3	522.5	512.7
213.48	626.3	567.5	546
252.51	626.0	602.7	589

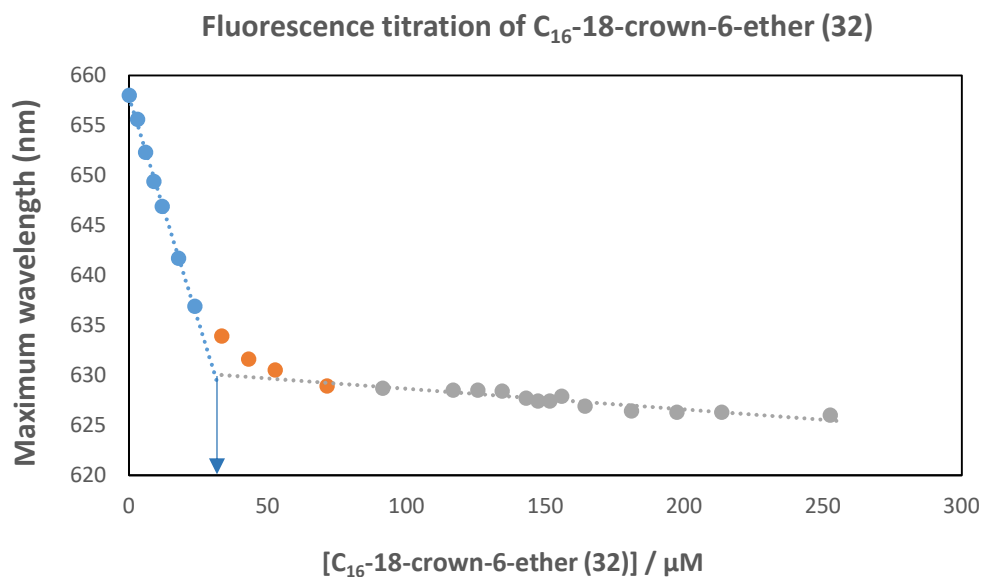


Figure 44. The maximum wavelength measured at different concentrations of C₁₆-18-crown-6-ether **32**. Reaction conditions: [C₁₆-18-crown-6-ether **32**] at various concentrations, [Nile red] = 2 μM, [PNB] = 500 μM, [MES] = 5000 μM, pH at 6.4. At 29 μM of C₁₆-18-crown-6-ether **32**, we begin to see a less rapid decrease in the rate of fluorescence intensity.

Figure 45 below shows the fluorescence *intensity* at 635 nm with increasing concentrations of C₁₆-18-crown-6-ether **32** and Ba²⁺. We can see that up to 9 μM of C₁₆-18-crown-6-ether **32**, there are negligible increases in the fluorescence intensity. However, after the addition of 29 μM of C₁₆-18-crown-6-ether **32**, we can see a jump of fluorescence which corresponds to the beginning of Nile red molecules trapped inside the hydrophobic part of micelles. After this point, we see a steady increase in the fluorescence intensity. At higher concentrations above 29 μM of C₁₆-18-crown-6-ether **32**, we begin to see a less rapid increase in the rate of fluorescence intensity. This is potentially due to self-quenching of fluorescence or may be due to the formation of supramolecular structures other than micelles. The rapid increase in fluorescence around 30 μM reaffirms the formation of supramolecular structures at this concentration.

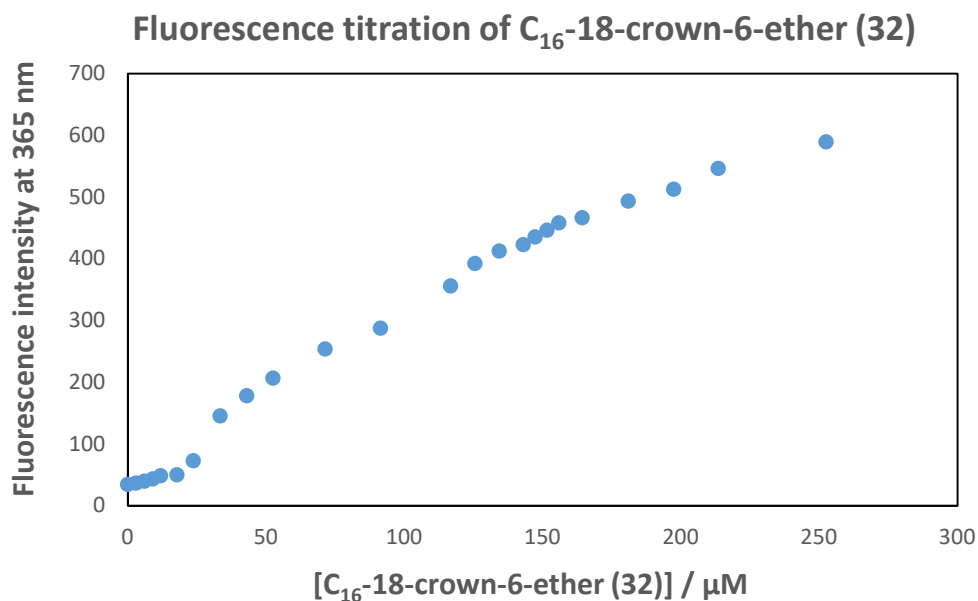


Figure 45. The fluorescent intensity measured at 635 nm at different concentration of C₁₆-18-crown-6-ether **32** (Reaction conditions: [C₁₆-18-crown-6-ether (**32**)] at various concentrations, [Nile red] = 2 μM, [PNB] = 500 μM, [MES] = 5000 μM, pH 6.4)

Pleasingly, the calculated CAC of catalyst **32** using fluorescence measurements matches with the concentration at which catalytic activity is observed to dramatically increase, as shown previously in **Figure 43**. This suggests that the increase in catalytic activity is indeed related to structure formation and cooperative effects, although further work still needs to be done to confirm the validity of these assumptions. This observation of cooperative catalysis by amphiphilic assemblies was not an obvious result. In fact, it has been previously shown that related amphiphilic molecules had very low catalytic activity due to the highly dynamic nature of the presumed micellar assemblies.¹⁷

3.8 Summary

In this section, our objective was to design and synthesise an amphiphilic molecule containing a crown ether, which was able to self-assemble and catalyse a reaction cooperatively. We synthesised two crown-ether-containing amphiphiles (catalysts **29** and **32**) and investigated them for the catalysis of a range of substrates including activated phosphates and activated anilides. In the end, we were able to show that catalyst **32** was efficient for the catalysis of the cleavage of the activated ester p-nitrobutyrate (**PNB**). Following demonstration of the catalytic activity, we investigated the capability of the molecule to assemble into supramolecular assemblies by using fluorescence spectroscopy. We were able to confirm that the CAC of these molecules in the reaction conditions was approximately 30 μM , which matched with the concentration at which we observed a rapid increase in the catalysis rate. Future work in this topic will involve the determination of the actual aggregates formed (e.g. micelles or vesicles) and further investigation of the kinetics of the reaction.

4.0 CONCLUSIONS and FUTURE WORK

In this thesis, we have investigated the catalytic activity of organocatalysts based on proline and leucine for formation of tetrahydroxanthenones. The proline and leucine-based catalysts had been designed with long hydrophobic chains to induce self-assembly and the formation of supramolecular structures. The catalytic activities of these catalyst combinations were compared to control conditions containing ‘only C₁₆-proline’ and ‘only C₁₆-leucine’. While some of the new catalyst combinations provided accelerated rates of reaction, we found that the control condition of ‘only C₁₆-proline’ also had substantial rate accelerations, such that using our catalyst combination did not provide as large of a benefit in rate acceleration as we had hoped for. This is due to the possibility that the two-tailed proline catalyst **Cat 5** was also known to form micelles and provide rate acceleration on its own. Further work still needs to be done to determine the presence of supramolecular structures such as micelles or vesicles.

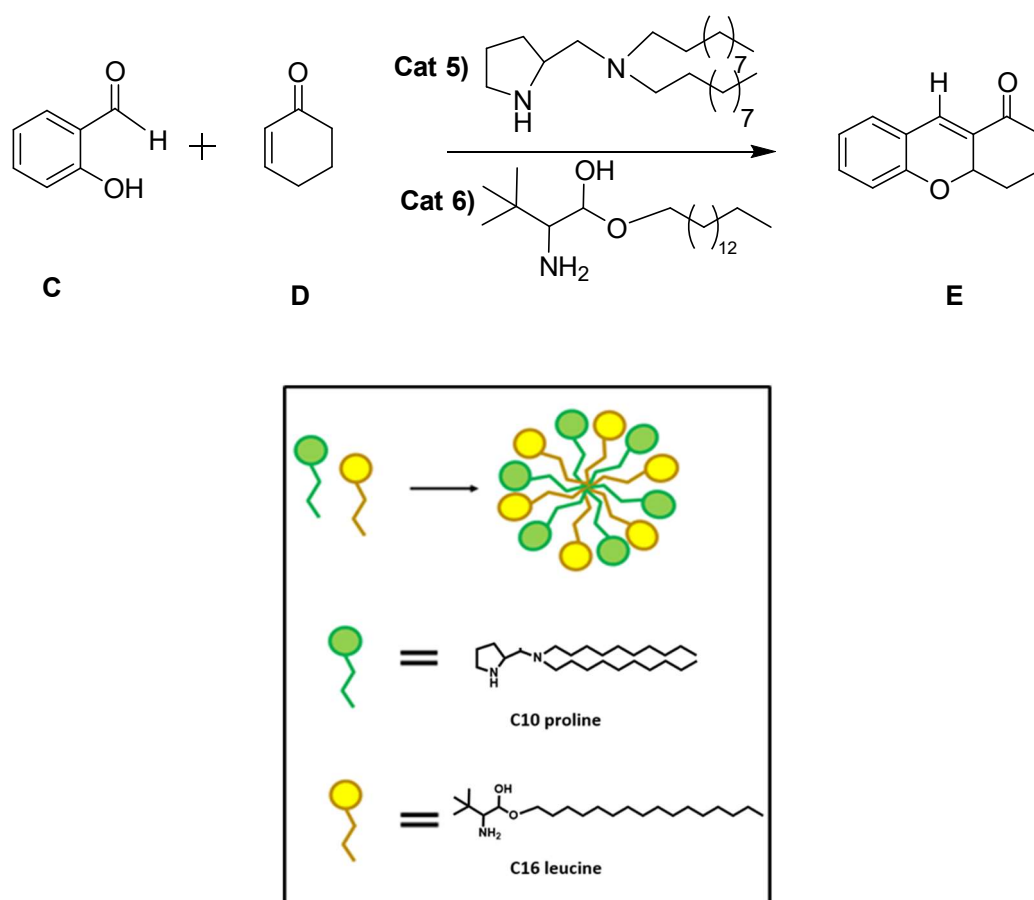


Figure 46. Proposed self-assembly of the pre-catalysts into micelles or vesicles

We also investigated the enantioselectivity of the tetrahydroxanthenone **E** formation, which is a crucial measurement of success in reactions which produce chiral centres. Following transformation of the product ketone to a secondary alcohol and formation of a Mosher ester, we determined the enantioselectivity of the reaction using ^1H NMR analysis of the diastereomers formed. We were able to determine that the enantioselectivity of the tetrahydroxanthenone **E** formation was 30% (Using **Cat 4** and **Cat 5**). While it is interesting that we were able to induce enantioselectivity, the value is still low and would likely not be synthetically useful. Future work in this area would be to screen several other catalysts to see if the enantioselectivity of the reaction can be improved.

In the second part of the thesis, we demonstrated the successful synthesis of C_{16} -18-crown-6-ether- Ba^{2+} catalyst **32** and investigated its catalytic activity in a few different chemical reactions. We investigated this catalyst in the cleavage of activated amides and esters as well as the cleavage of phosphodiesters related to RNA and DNA. We demonstrated that catalyst **32** was able to catalyse the cleavage of the activated ester *p*-nitrobutyrate **PNB**, which we monitored using UV spectrometry. We were able to show that the onset of catalysis coincided with the onset of structure formation, as determined by fluorescence spectroscopy. This was an exciting result, as this type of Ba^{2+} -based catalyst had not been previously demonstrated to be able to cleave esters. We were also able to achieve our goal of demonstrating that cooperative effects induced by self-assembly of amphiphiles can achieve catalyst which is not seen in the non-assembled state.

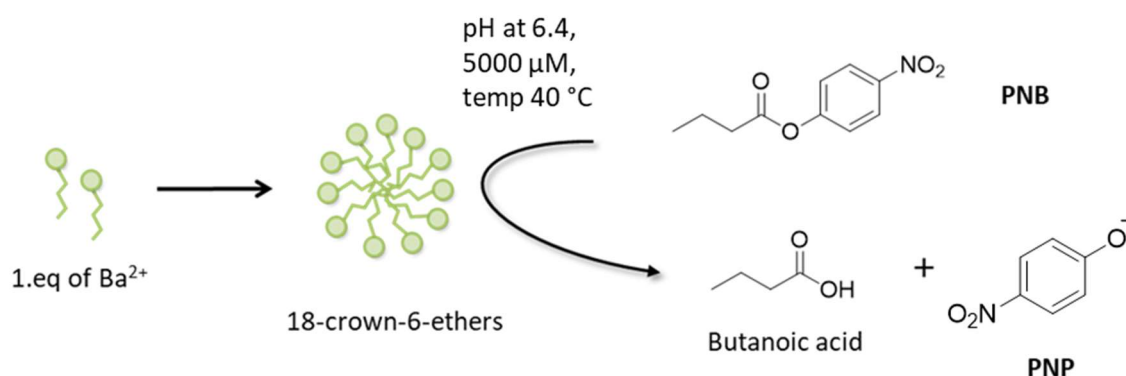


Figure 47. Cooperative catalysis induced by neighbouring C_{16} -18-crown-6-ether with Ba^{2+} complexes upon assembly

There is more work to do to fully demonstrate that cooperative effects are the cause of the rate acceleration mentioned above. Future work will focus on visualising the supramolecular structures formed using electron microscopy, and further investigation of the structure characteristics using dynamic light scattering. To unequivocally demonstrate cooperativity, we will also need to synthesise analogue of catalyst **32** with much shorter tails (e.g. C₂) and investigate its catalytic activity. This C₂ analogue will not be amphiphilic and would not be expected to give high catalytic activity as it would not be able to self-assemble. Further in the future, we will try to apply this design to explore other catalytic systems which have synthetic utility. The long-term goal is to demonstrate that by combining cooperative catalysis and self-assembly processes we can design new and efficient catalysts which can lead to greener and more sustainable chemical processes.

CHAPTER THREE: EXPERIMENTAL SECTION

5.1 General details

The organic molecules were synthesized and characterized by ^1H , ^{13}C NMR, HRMS and IR and this data compared to literature values where possible. All organic synthetic reactions were carried out in oven-dried glassware under inert gas. All reactions performed at 0 °C were cooled using a water-ice bath. Every reaction performed at high temperatures were heated in oil bath with digital thermometer to maintain the defined temperature.

Reagents including 4-nitrophenol, DCC, DMAP, Decanol, Decyl amine, Aza-18-crown-6 units and 18-crown-6-ethers and tetrahydrofuran (THF) were purchased from Sigma Aldrich and NMR solvents including deuterated methanol-d₄ and deuterated chloroform were purchased from EURISO-TOP. Acetone and hexane with analytical quality were purchased from ECP chemicals along with dichloromethane and ethyl acetate of laboratory quality. Hydrochloric acid 37% and methanol were purchased from Thermo Fisher Scientific. Celite[®] 545 was purchased from VELP Scientifica. Anhydrous magnesium sulfate was purchased from Scharlau. palladium on carbon (5 wt% loading, matrix activated carbon support) was purchased from Sigma-Aldrich.

Analytical thin layer chromatography (TLC) was performed using plates of DC Kieselgel 60 F 254, purchased from Merck. Compounds were visualized by UV light or by staining with methanolic solution of phosphomolybdic acid or ninhydrin. Flash column chromatography was carried out using Silica gel P60 (40-63 μm) purchased from SiliCycle Inc. solvents were removed by a BUCHI heating bath B-300 Base. Samples prepared for NMR were dried first under high vacuum.

NMR spectroscopy was conducted using a Bruker Ascend 400 NMR spectrometer operating at 400 MHz for ^1H nuclei and 101 MHz for ^{13}C nuclei and analyzed using MestReNova 6.0.2-5475. Chemical shifts are reported as parts per million (ppm) from tetramethylsilane ($\delta = 0$) and were measured relative to the solvent in which the sample was analyzed (CDCl_3 : δ 77.0

for ^{13}C NMR; CD_3OD : δ 33.31 for ^1H NMR, δ 49.0 for ^{13}C NMR) and coupling constants (J) are reported in hertz (Hz) to the nearest 0.1 ppm. ^1H NMR shift values are reported as chemical shift (δ H), relative integral, multiplicity (s, singlet; d, doublet; t: triplet; q: quartet; m: multiplet, dd: double of doublets; dt: doublet of triplets) and coupling constant (J Hz). The ^{13}C values were referenced to the residual chloroform peak at δ 77.0 ppm. ^{13}C values are reported as chemical shift (δ C).

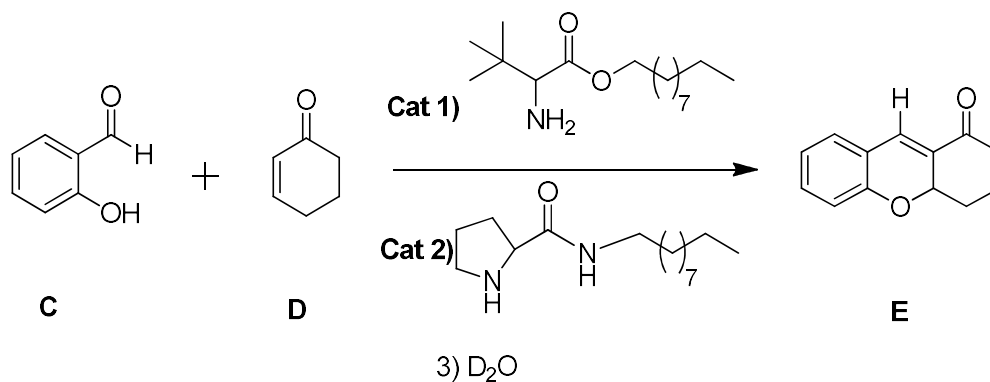
Infrared (IR) spectra were recorded using a Nicolet iS10 spectrometer (Thermo Fisher Scientific Inc.) with the absorption peaks expressed in wavenumbers (cm^{-1}) and recorded using a range of 450 to 4000 cm^{-1} . IR spectra were analyzed using OMNIC 9.2.86.

High resolution mass spectra (HRMS) were recorded using a VG-70SE spectrometer at a nominal resolution of 5000 to 10000 as appropriate. Major and significant fragments are quoted in the form x (y%), where x is the mass to charge ratio and y is the percentage abundance relative to the base peak.

Furthermore, the ability of these synthesized compounds to undergo micellar aggregation was determined using fluorescence studies, which was also used to determine the CMC. To determine the molecule's self-assembly properties, UV-Vis spectrometric and Fluorescence experiments were designed and carried out with and without irradiation. Finally, cooperative catalysis effects were determined by following the rate of production of PNP with a UV spectrophotometer.

5.2 Experimental Procedures

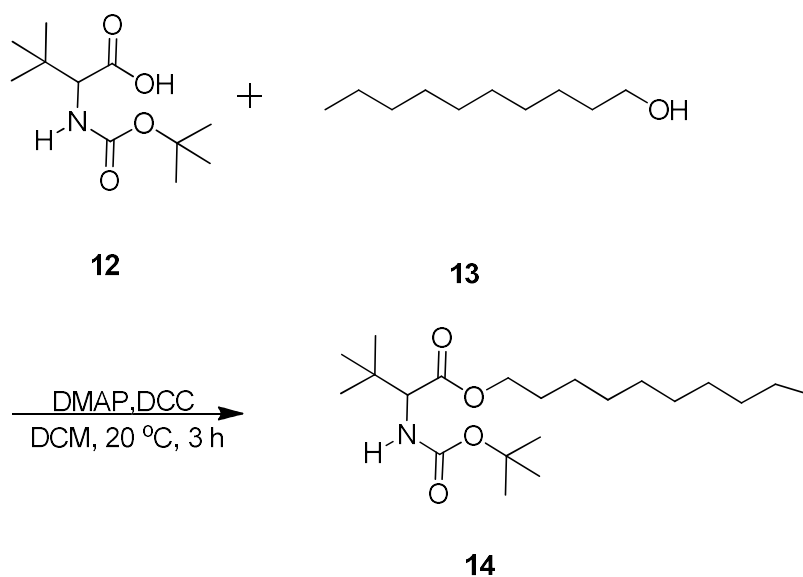
2,3,4,4a-Tetrahydro-1H-xanthen-1-one



2-Hydroxybenzaldehyde **C** (0.013 mL, 0.126 mmol, 1.0 eq.) and cyclohex-2-enone **D** (0.04 mL, 0.441 mmol, 3.5 eq.), **C** and **D** were added in D₂O. The reaction mixture was heated at reflux (50 °C) until completion of the reaction as monitored by TLC (usually between 3 and 4 days). Next, the reaction mixture was extracted thrice with ethyl acetate and the combined organic layers were washed two times with water, twice with brine and dried over anhydrous MgSO₄. Concentration in vacuo gave the crude material which was purified by flash chromatography (hexane/ethyl acetate 90:10) to yield **E** (0.010 g, 0.13 mmol, 40%)

¹H NMR (400 MHz, chloroform-*d*) δ 7.43 (d, *J* = 2.3 Hz, 1H), 7.38 – 7.15 (m, 3H), 7.09 – 6.61 (m, 2H), 5.01 (dd, *J* = 10.6, 2.4 Hz, 1H), 2.74 – 2.33 (m, 1H), 2.16 – 1.80 (m, 2H), 1.57 (s, 4H), 1.30 – 1.19 (m, 1H). ¹³C NMR (101 MHz, chloroform-*d*) δ 197.5, 155.9, 132.0, 131.5, 130.4, 129.8, 122.2, 122.1, 116.0, 74.7, 38.8, 29.7, 18.0.

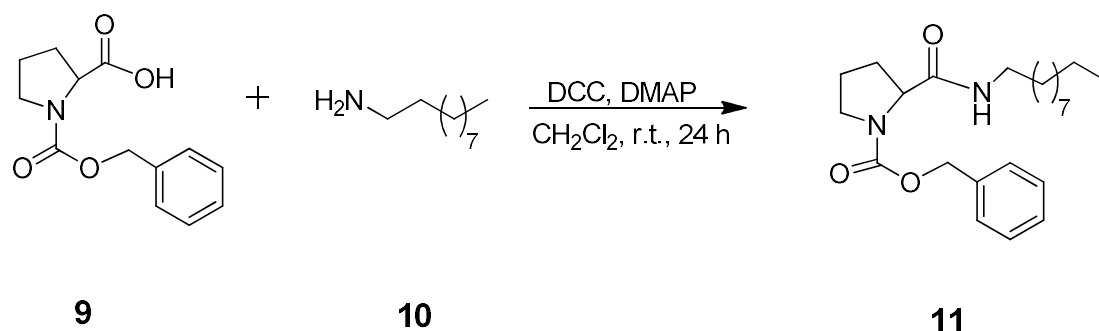
Decyl 2-((tert-butoxycarbonyl)amino)-3,3-dimethylbutanoate



To a solution of **12** (0.375 g, 1.62 mmol, 1.0 eq.) in DCM (1.50 mL) was added DCC (0.35 g, 1.68 mmol, 1.12 eq.) at room temperature under nitrogen gas. The reaction mixture was stirred for 3 hours then **13** (0.58 mL, 3.28 mmol, 2.0 eq.) was added followed by DMAP (0.20 g, 1.67 mmol, 1.1 eq.). The reaction mixture was stirred at room temperature overnight. The reaction mixture was filtered through Celite[®] and the solvent was removed under reduced pressure. The residue was dissolved up in DCM and filtered again through the Celite[®] and a saturated solution of ammonium chloride was added. The aqueous layer was extracted thrice with DCM and dried over MgSO₄ and concentrated in *vacuo* to give the crude product. The crude was purified by flash column chromatography on silica gel (hexane/ethyl acetate 95:5) to yield **14** (0.10 g, 1.6 mmol, 17%) as a colourless liquid.

¹H NMR (400 MHz, chloroform-*d*) δ 5.04 (d, *J* = 9.7 Hz, 1H), 4.03 (tt, *J* = 6.1, 3.1 Hz, 2H), 1.65 – 1.53 (m, 2H), 1.37 (s, 9H), 1.28 – 1.14 (m, 14H), 0.90 (s, 9H), 0.85 – 0.77 (t, 3H). ¹³C NMR (101 MHz, chloroform-*d*) δ 172.1, 155.5, 65.1, 61.7, 34.7, 31.9, 29.5, 29.5, 29.3, 29.2, 28.5, 28.3, 26.5, 25.9, 22.7, 14.1.

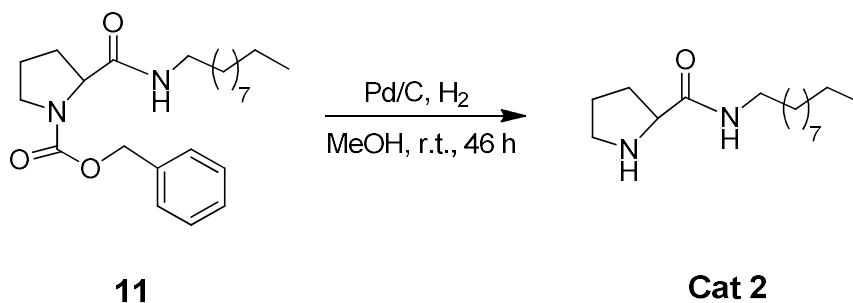
Benzyl 2-(decylcarbamoyl)pyrrolidine-1-carboxylate



To a solution of **9** (0.38 g, 1.5 mmol, 1.0 eq.) in DCM (1.50 mL) was added DCC (0.35 g, 1.65 mmol, 1.1 eq.) at room temperature under nitrogen gas. The reaction mixture was stirred for 2 h then **10** (0.51 g, 3.3 mmol, 2.2 eq.) was added followed by DMAP (0.20 g, 1.65 mmol, 1.1 eq.). The reaction mixture was stirred at room temperature overnight. The reaction mixture was filtered through Celite[®] and the solvent was removed under reduced pressure. The crude was purified by flash column chromatography on silica gel (hexane/ethyl acetate 60:40) to yield **11** (0.07 g, 1.5 mmol, 11%) as a colourless liquid.

¹H NMR (400 MHz, chloroform-*d*) δ 7.54 – 7.10 (m, 5H), 5.28 – 4.97 (s, 2H), 4.32 (t, *J* = 6.8 Hz, 1H), 3.63 – 3.38 (m, 2H), 3.19 (m, 2H), 2.36 – 1.71 (m, 4H), 1.54 – 1.11 (m, 16H), 1.07 – 0.67 (t, 3H). ¹³C NMR (101 MHz, chloroform-*d*) δ 128.5, 128.1, 127.9, 67.3, 39.5, 33.9, 31.8, 29.5, 29.5, 29.3, 29.3, 26.8, 24.9, 22.7, 14.1.

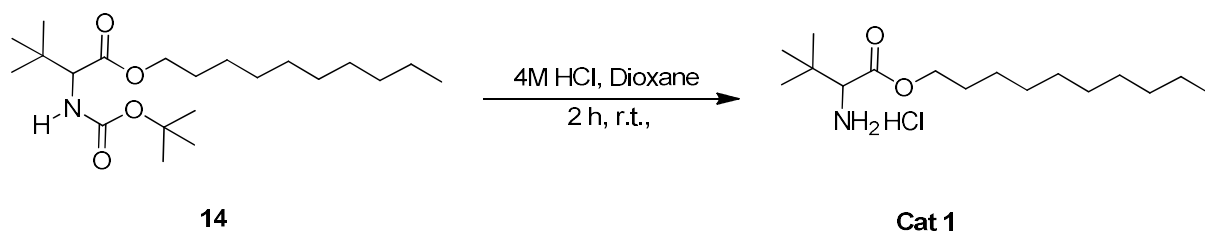
***N*-Decylpyrrolidine-2-carboxamide**



To a solution of **11** (0.060 g, 0.039 mmol, 1 eq.) in methanol (1.19 mL) was flushed with nitrogen to keep inert atmosphere, followed by adding palladium on carbon 5 wt% (0.002 g, 0.0004 mmol, 0.01 eq.). The reaction mixture was flushed with hydrogen to change the reactive atmosphere and was kept flushing under the surface for 48 h. The reaction mixture was filtered through Celite[®] and the solvent was removed under reduced pressure. The crude product was purified by flash column chromatography on silica gel (chloroform/methanol 88:12 + 0.05% TEA) to yield **Cat 2** (0.035 g, 0.16 mmol, 88%)

¹H NMR (400 MHz, chloroform-*d*) δ 3.65 (dd, $J = 9.1, 5.3$ Hz, 1H), 3.15 (td, $J = 7.3, 6.0$ Hz, 2H), 2.81 (dt, $J = 10.2, 6.3$ Hz, 2H), 2.28 (s, 1H), 1.93 – 1.74 (m, 2H), 1.64 (dd, $J = 13.8, 6.9, 5.0, 3.3$ Hz, 4H), 1.42 (t, $J = 7.1$ Hz, 2H), 1.21 (m, $J = 15.1$ Hz, 17H), 0.92 – 0.67 (t, 3H). **¹³C NMR** (101 MHz, chloroform-*d*) δ 60.6, 47.3, 38.9, 31.9, 30.8, 29.7, 29.5, 29.3, 26.9, 26.2, 22.7, 14.1. **IR** ν_{max} (film)/ cm^{-1} : 3426, 3403, 3311, 3210, 2922, 2852, 1650, 1530, 1462.

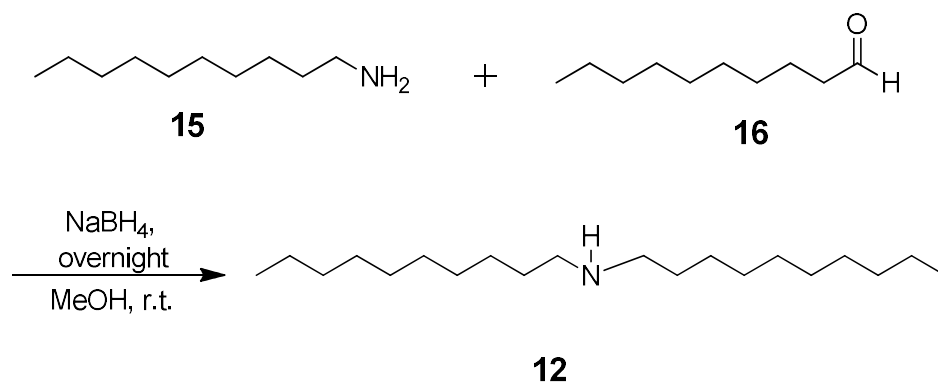
Decyl 2-amino-3,3-dimethylbutanoate hydrogen chloride



To a solution of **14** (0.098 g, 0.27 mmol, 1 eq.) was dissolved in dioxane (1.33 mL). The reaction mixture was heated (75 °C) at reflux overnight and dioxane was removed in vacuo. The crude product was purified by flash column chromatography on silica gel (chloroform/methanol 96:4 + 0.05% TEA) to yield **Cat 1** (0.043 g, 0.156 mmol, 60%).

¹H NMR (400 MHz, chloroform-*d*) δ 4.07 (t, *J* = 6.8 Hz, 3H), 3.58 (s, 1H), 1.62 – 1.55 (m, 2H), 1.35 (t, *J* = 7.3 Hz, 14H), 1.26 – 1.16 (s, 9H), 0.80 (t, *J* = 7.0 Hz, 3H). ¹³C NMR (101 MHz, chloroform-*d*) δ 65.5, 62.8, 45.8, 34.0, 31.8, 29.7, 29.5, 29.5, 29.3, 29.2, 28.5, 26.6, 25.9, 22.6, 14.1, 8.6.

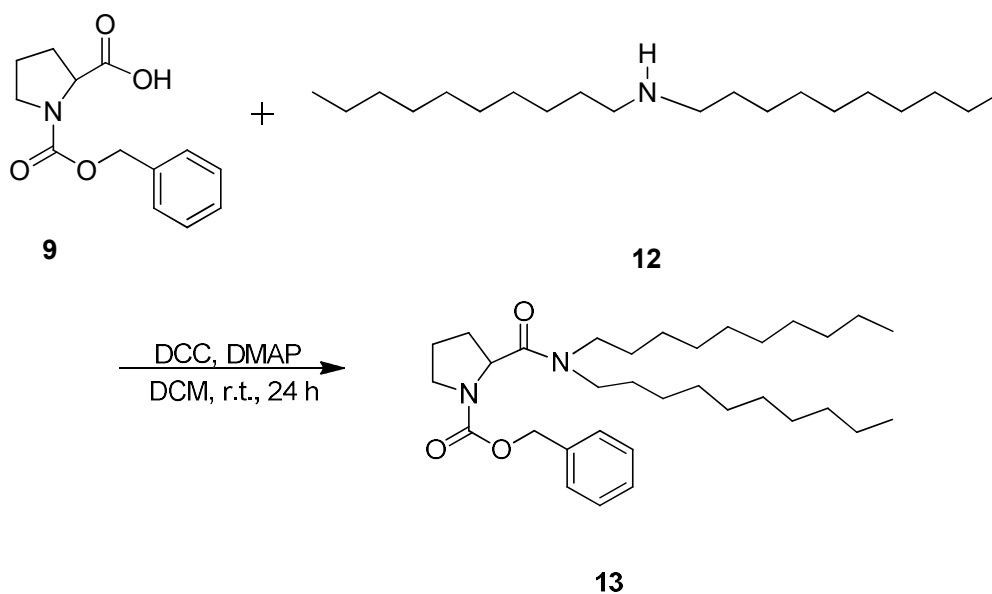
Didecylamine



Decylamine **15** (1.21 g, 3.87 mmol, 2.0 eq.) and decanal **16** (0.73 g, 4.65 mmol, 1.2 eq.) were dissolved in dry methanol (20 mL) and the reaction mixture was stirred at room temperature overnight before being cooled to 0 °C. Sodium borohydride (0.30 g, 7.74 mmol, 2.0 eq.) was added to the reaction mixture and allowed to room temperature overnight, followed by evaporation of the solvent under reduced pressure. To the residue was added in 2N NaOH (20 mL) and the aqueous and organic layers were separated. The organic layer was washed with water, twice with brine and dried over MgSO₄. After filtration and evaporation under reduced pressure, the residue was dissolved in methanol (2 mL) and 4N HCl (3 mL). The reaction mixture was filtered, and the solvent was removed under reduced pressure. The crude product was purified by flash column chromatography on silica gel (DCM/MeOH 97:3 + 0.05% TEA) to yield **12** (0.18 g, 14.8 mmol, 25.4%).

¹H NMR (400 MHz, chloroform-*d*) δ 2.62 – 2.52 (m, 4H), 1.48 (t, *J* = 7.3 Hz, 4H), 1.20 (d, *J* = 8.9 Hz, 28H), 0.85 – 0.76 (m, 6H). ¹³C NMR (101 MHz, chloroform-*d*) δ 49.7, 31.9, 29.6, 29.6, 29.5, 29.4, 29.3, 27.3, 22.6, 14.1.

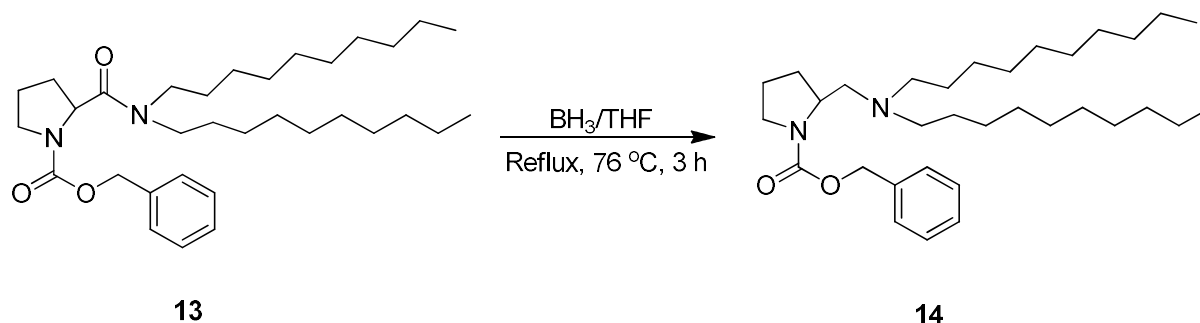
Benzyl 2-(didecylcarbamoyl)pyrrolidine-1-carboxylate



To a solution of **9** (0.13 g, 0.50 mmol, 0.5 eq.) in DCM (0.5 mL) was added DCC (0.11 g, 0.55 eq.) at room temperature under nitrogen gas. The reaction mixture was stirred for 2 h then **12** (dodecylamine) (0.12 g, 0.55 mmol, 0.55 eq.) was added followed by DMAP (0.06 g, 0.55 eq.). The reaction mixture was stirred at room temperature overnight. The reaction mixture was filtered through Celite[®] and the solvent was removed under reduced pressure. The crude was purified by flash column chromatography on silica gel (hexane/ethyl acetate 60:40) to yield **13** (0.083 g, 0.50 mmol, 32%) as a colourless liquid.

¹H NMR (400 MHz, chloroform-*d*) δ 7.63 – 6.97 (m, 5H), 5.05 (s, 2H), 4.12 (q, $J = 7.1$ Hz, 10H), 2.04 (s, 7H), 1.26 (m, $J = 7.2$ Hz, 25H), 1.04 – 0.63 (t, 6H). ¹³C NMR (101 MHz, chloroform-*d*) δ 171.0, 128.3, 128.2, 127.6, 67.1, 60.3, 56.8, 47.8, 47.6, 34.6, 31.9, 31.8, 31.5, 29.6, 29.5, 29.5, 29.4, 29.3, 29.2, 28.9, 27.6, 26.9, 25.2, 22.6, 22.6, 22.5, 20.9, 14.1, 14.0, 11.3.

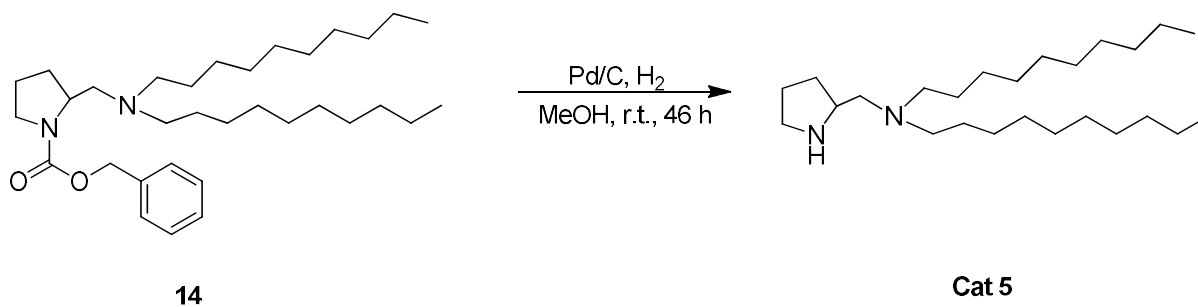
Benzyl 2-(dodecyl amino)methylpyrrolidine-1-carboxylate



To a solution of **13** (0.08 g, 0.14 mmol, 1.0 eq.) in THF was added BH_3/THF (3.11 mL, 1.38 mmol, 10.0 eq.) dropwise at room temperature under nitrogen gas. The reaction mixture was heated at reflux (76 °C) until completion of the reaction as monitored by TLC (usually between 3 to 4 hours). The solution of 10% HCl (0.03 mL) and 3N NaOH (0.12 mL) were added into the emulsion. Next, the reaction mixture was extracted with ether (1 mL) three times and dried over anhydrous MgSO_4 and the solvent was removed under reduced pressure to afford the desired product. The crude product was purified by using flash column chromatography to yield **14** (28%) as a colourless liquid.

$^1\text{H NMR}$ (400 MHz, chloroform-*d*) δ 7.85 – 7.23 (m, 5H), 5.38 – 4.97 (m, 2H), 3.75 – 3.62 (m, 4H), 3.57 – 3.27 (m, 4H), 2.03 – 1.77 (m, 4H), 1.62 – 1.45 (m, 4H), 1.49 – 1.04 (m, 24H), 0.90 (t, $J = 19.7, 7.6$ Hz, 6H). $^{13}\text{C NMR}$ (101 MHz, chloroform-*d*) δ 128.51, 127.77, 72.36, 70.58, 69.60, 62.75, 31.90, 29.57, 29.31, 22.68, 18.90, 14.12, 13.87.

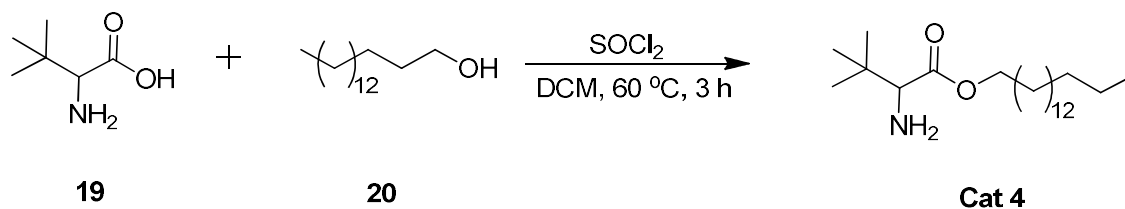
(*N*-Decyl-*N*-pyrrolidin-2-ylmethyl)decan-1-amine



To a solution of **14** (0.02 g, 0.04 mmol, 1.0 eq.) in methanol (0.39 mL) was flushed with nitrogen to keep inert atmosphere, followed by adding 5 wt% palladium on carbon (0.008 g, 0.0004 mmol, 0.01 eq.). The reaction mixture was flushed with hydrogen to change the reactive atmosphere and was kept flushing under the surface for 48 h. The reaction mixture was filtered through Celite[®] and the solvent was removed under reduced pressure. The crude product was purified by flash column chromatography on silica gel (chloroform/methanol 88:12 +0.05% TEA) to yield **Cat 5** (0.003 g, 0.04 mmol, 18%).

¹H NMR (400 MHz, chloroform-*d*) δ 3.11 (q, *J* = 7.3 Hz, 1H), 2.71 – 2.52 (m, 8H), 2.17 (s, 2H), 1.41 (t, *J* = 7.3 Hz, 2H), 1.26 (m, 24H), 0.96 – 0.78 (t, 6H). ¹³C NMR (101 MHz, chloroform-*d*) δ 59.1, 46.3, 45.7, 32.1, 29.6, 29.3, 24.0, 22.7, 8.6. IR ν_{max} (film)/cm⁻¹: 3396, 2977, 2924, 2855, 2601, 2496, 1475, 1396, 1258, 1301, 804.

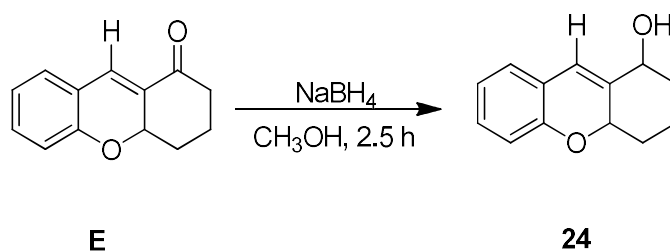
Pentadecyl 2-amino-3, 3-dimethylbutanoate



To a solution of **19** (0.25 g, 1.9 mmol, 1.00 eq.) in DCM was added palmityl alcohol **20** (4.6 g, 19 mmol, 10.0 eq.) dropwise at room temperature under nitrogen gas. The reaction mixture was heated at reflux (60 °C) and then added thionyl chloride (0.22 mL, 3.05 mmol, 1.6 eq.). The reaction mixture was stirred overnight and monitored by TLC. Once the reaction completed, cooled down to room temperature. The reaction mixture was dissolved in DCM and added 10% Na₂CO₃ in water, and then filtered through Celite[®] and the solvent was removed under reduced pressure. The crude product was dried over anhydrous MgSO₄ and the solvent was removed under reduced pressure to afford the desired product. The crude product was purified by flash column chromatography on silica gel (DCM/EtoAc) 80:20 to yield **Cat 4** (0.25 g, 1.9 mmol, 70%).

¹H NMR (400 MHz, chloroform-*d*) δ 4.02 (t, *J* = 6.7 Hz, 2H), 3.07 (s, 1H), 1.70 – 1.39 (m, 2H), 1.19 (m, 30H), 0.90 (s, 9H), 0.83 – 0.78 (t, 3H). ¹³C NMR (101 MHz, chloroform-*d*) δ 175.1, 64.6, 63.5, 34.3, 31.9, 29.7, 29.7, 29.6, 29.7, 29.5, 29.4, 29.2, 28.6, 26.3, 26.0, 22.7, 14.1. IR *v*_{max} (film)/cm⁻¹: 3710, 3617, 2927, 2855, 2361, 2028, 1868, 1521, 667.

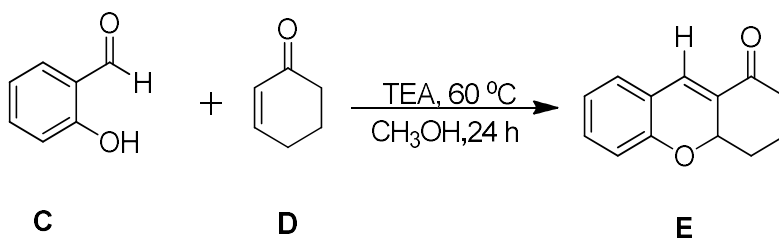
2,3,4,4a-Tetrahydro-1H-xanthen-1-ol



Sodium borohydride (0.009 g, 0.00024 mmol, 0.6 eq.) was added to a stirred solution of **E** (0.008 g, 0.00004 mmol, 0.51 eq.) in absolute methanol (2.5 mL). The reaction mixture was stirred at room temperature for 2-3 h (followed by TLC to see convergence of spots). This mixture was then concentrated in vacuo. The mixture was then extracted thrice with DCM (10 mL). The collected organic extracts were washed twice with water and thrice with brine, dried over MgSO₄ and the solvent was removed in vacuo to give the crude product to yield **24** (0.007 g, 0.00004 mmol, 90%). This product came from compound **Cat 5**.

¹H NMR (400 MHz, chloroform-*d*) δ 7.04 – 6.92 (m, 1H), 6.85 (dd, *J* = 7.4, 1.7 Hz, 1H), 6.72 (td, *J* = 7.4, 1.2 Hz, 1H), 6.61 (dt, *J* = 8.0, 1.0 Hz, 1H), 6.29 (t, *J* = 2.0 Hz, 1H), 4.86 (ddt, *J* = 11.3, 5.3, 1.6 Hz, 1H), 4.02 (dd, *J* = 11.1, 5.1 Hz, 1H), 2.09 (tq, *J* = 5.3, 3.9 Hz, 2H), 1.43 – 1.26 (m, 2H), 1.19 (s, 2H). ¹³C NMR (101 MHz, chloroform-*d*) δ 139.7, 128.7, 126.4, 120.9, 114.8, 113.5, 70.6, 36.3, 34.5, 19.9.

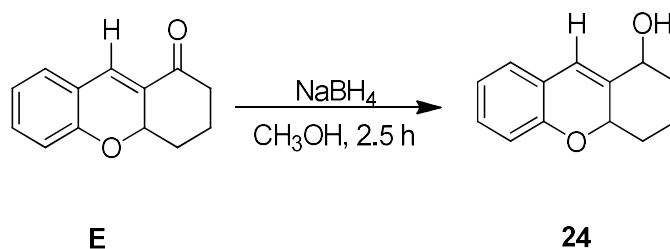
2,3,4,4a-Tetrahydro-1H-xanthen-1-one



2-Hydroxybenzaldehyde **C** (0.25 mL, 2.5 mmol, 1.0 eq.) and **TEA** (0.15 mL, 2.5 mmol and 1.0 eq.) were added in methanol and cyclohex-2-en-1-one **D** (0.7 mL, 7.5 mmol and 3.0 eq.) was added. The reaction mixture was heated at reflux (60 °C) until completion of the reaction as monitored by TLC (usually between 10 and 11 h). Next, the reaction mixture was extracted thrice with ethyl acetate (20 mL) and the combined organic layers were washed two times with water, twice with brine and dried over anhydrous MgSO₄. Concentration in vacuo gave the crude material which was purified by flash chromatography (hexane/ethyl acetate 90:10) to yield **E** (0.257 g, 2.5 mmol, 52%).

¹H NMR (400 MHz, chloroform-*d*) δ 7.29 – 7.18 (m, 2H), 7.07 – 6.80 (m, 2H), 5.00 (dd, *J* = 10.6, 2.4 Hz, 1H), 2.68 – 2.31 (m, 2H), 2.16 – 1.91 (m, 2H), 1.82 – 1.47 (m, 2H). ¹³C NMR (101 MHz, chloroform-*d*) δ 197.5, 155.9, 132.0, 131.5, 130.4, 129.8, 122.2, 122.1, 116.0, 74.7, 38.8, 29.7, 18.0.

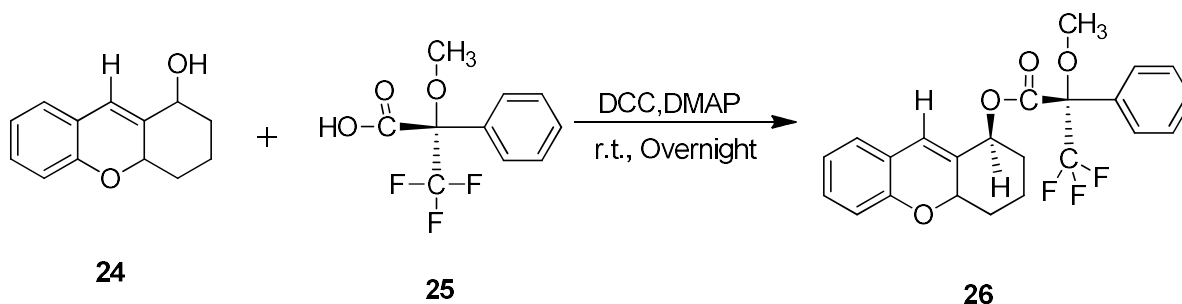
2,3,4,4a-Tetrahydro-1H-xanthen-1-ol



Sodium borohydride (0.01 g, 0.0005 mmol, 0.6 eq.) was added to a stirred solution of **E** (0.008 g, 0.00008 mmol, 0.51 eq.) in absolute methanol (5 mL). The reaction mixture was stirred at room temperature for 1 h (followed by TLC to see convergence of spots). This reaction mixture was then concentrated in vacuo. The mixture was then extracted thrice with DCM (20 mL). The collected organic extracts were washed twice with water and thrice with brine, dried over MgSO₄ and the solvent was removed in vacuo to give the crude product **24** (0.014 g, 0.00008 mmol, 88%). This product came from general procedure **TEA**.

¹H NMR (400 MHz, chloroform-*d*) δ 7.04 (td, *J* = 7.7, 1.7 Hz, 1H), 6.92 (dd, *J* = 7.4, 1.7 Hz, 1H), 6.79 (td, *J* = 7.4, 1.1 Hz, 1H), 6.68 (dt, *J* = 8.0, 1.0 Hz, 1H), 6.35 (t, *J* = 2.0 Hz, 1H), 4.92 (ddt, *J* = 11.4, 5.4, 1.6 Hz, 1H), 4.13 – 3.88 (m, 1H), 2.30 – 2.01 (m, 2H), 1.97 – 1.79 (m, 2H), 1.53 – 1.26 (m, 2H). ¹³C NMR (101 MHz, chloroform-*d*) δ 152.6, 139.7, 128.6, 126.4, 120.8, 120.7, 114.8, 113.5, 70.6, 36.3, 34.5, 29.7, 19.9.

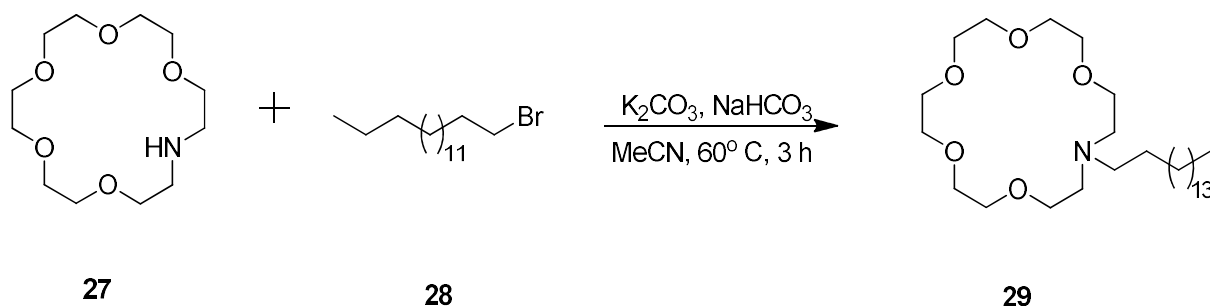
2,3,4,4a-Tetrahydro-1H-xanthen-1yl(2S)-3-fluoro-2-methoxy-3-methyl-2-phenylbutanoate



To a solution of **24** (0.013 g, 0.053 mmol, 1.0 eq.) in DCM (1.50 mL) was added DCC (0.032 g, 1.58 mmol, 2.98 eq.) at room temperature under nitrogen gas. The reaction mixture was stirred for 1 h then **25** (0.030 g, 0.13 mmol, 2.4 eq.) was added followed by DMAP (0.002 g, 0.04 mmol, 0.75 eq.). The reaction mixture was heated at reflux overnight. The reaction mixture was filtered through Celite[®] and the solvent was removed under reduced pressure. The residue was dissolved up in diethyl ether and filtered again through the Celite[®] and concentrated in *vacuo* to give the crude product **26** (0.021 g, 0.05 mmol, 94%) as a colourless liquid.

¹H NMR (400 MHz, chloroform-*d*) δ 8.25 (d, *J* = 6.2 Hz, 1H), 7.83 – 7.73 (m, 4H), 7.60 – 7.45 (m, 1H), 7.44 – 7.15 (m, 1H), 7.08 – 6.93 (m, 2H), 6.87 – 6.50 (m, 2H), 5.55 – 5.25 (m, 1H), 3.79 – 3.53 (m, 2H), 3.08 (s, 3H), 1.84 – 1.59 (m, 2H), 1.66 – 1.43 (m, 2H), 1.47 – 1.10 (m, 2H).

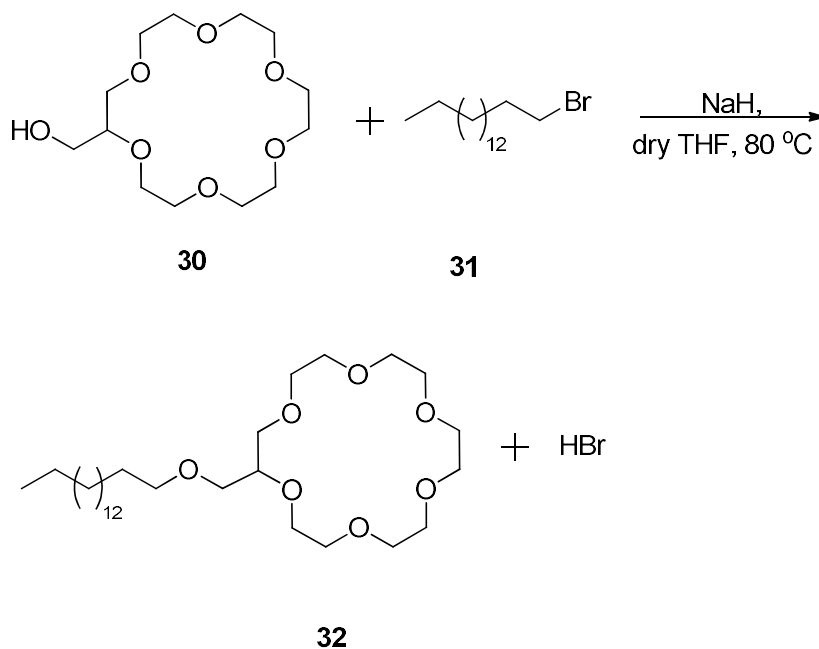
16-Hexadecyl-1,4,7,10,13-pentaoxa-16-azacyclooctadecane



The reaction was carried out by mixing aza-18-crown-6 units **27** (0.01 g, 0.398 mmol, 1.0 eq.) and 1-bromohexadecane **28** (146 μL , 0.478 mmol, 1.2 eq.) were added to a suspension of K_2CO_3 (0.16 g, 1.182 mmol, 2.97 eq.) and NaHCO_3 (0.1 g, 1.182 mmol, 2.97 eq.) in MeCN. The suspension was stirred for 3h at reflux (60°C). The suspension was filtered under a gouch filter and the solvent was removed under reduced pressure. The crude was purified by flash column chromatography on silica gel (DCM/methanol 90:10) to yield C_{16} -1-aza-18-crown-6-ether **29** (0.02 g, 0.398 mmol, 20%) as a colourless oil.

$^1\text{H NMR}$ (400 MHz, chloroform-*d*) δ 3.82 (t, $J = 4.6$ Hz, 1H), 3.65 – 3.46 (m, 5H), 3.16 (td, $J = 8.5, 3.9$ Hz, 1H), 2.69 (s, 1H), 1.36 – 1.11 (m, 7H), 0.81 (t, $J = 6.8$ Hz, 1H). $^{13}\text{C NMR}$ (101 MHz, chloroform-*d*) δ 70.17 (dd, $J = 43.6, 22.5$ Hz), 64.9, 53.9, 53.0, 31.9, 30.84 – 28.25, 26.8, 23.4, 23.0, 14.1.

2-((Hexadecyloxy)methyl)-1,4,7,10,13,16-hexaoxacyclooctadecane



The reaction was carried out by mixing sodium hydride (0.007 g, 0.17 mmol, 1.0 eq.) and added to a solution of **30** (0.05 g, 0.17 mmol, 1.0 eq.) in dry THF and heated at reflux (80 °C) for 30 min and added to a solution of **31** (0.05 g, 0.17 mmol, 1.0 eq.). The reaction mixture was heated at reflux (80 °C) overnight and THF was removed in vacuo. Next, the reaction mixture was then extracted thrice with chloroform and the reaction mixture was filtered through Celite[®] and the solvent was removed under reduced pressure. The crude was purified by flash column chromatography on silica gel (chloroform/methanol 90:10) to yield C₁₆-18-crown-6-ether **32** (0.011 g, 0.17 mmol and 13%).

¹H NMR (400 MHz, chloroform-*d*) δ 3.80 – 3.53 (m, 12H), 3.47 (d, *J* = 5.0 Hz, 6H), 3.36 (t, *J* = 6.7 Hz, 1H), 1.96 (d, *J* = 61.5 Hz, 4H), 1.47 (q, *J* = 6.8 Hz, 2H), 1.18 (s, 27H), 0.94 – 0.69 (t, 3H). **¹³C NMR** (101 MHz, chloroform-*d*) δ 77.34, 77.02, 76.70, 70.51, 31.93, 29.70, 29.36, 22.69, 14.12. **HRMS** found (ESI): MNa⁺, 541.4059, C₂₉H₅₈NaO₇, 541.4075.

REFERENCES

1. Belser, T.; Jacobsen, E. N., Cooperative Catalysis in the Hydrolytic Kinetic Resolution of Epoxides by Chiral [(salen)Co(III)] Complexes Immobilized on Gold Colloids. *Chem.Rev.* **2008**, *350* (7-8), 967-971.
2. Cacciapaglia, R.; Di Stefano, S.; Mandolini, L., The bis-barium complex of a butterfly crown ether as a phototunable supramolecular catalyst. *Chem.Rev.* **2003**, *125* (8), 2224-2227.
3. Mahadevi, A. S.; Sastry, G. N., Cooperativity in Noncovalent Interactions. *Chem.Rev.* **2016**, *116* (5), 2775-2825.
4. Roy, D.; Cambre, J. N.; Sumerlin, B. S., Future perspectives and recent advances in stimuli-responsive materials. *Progress in Polymer Science* **2010**, *35* (1), 278-301.
5. He, Y.; Li, Z.; Simone, P.; Lodge, T. P., Self-Assembly of Block Copolymer Micelles in an Ionic Liquid. *Chem.Rev.* **2006**, *128* (8), 2745-2750.
6. Biedermann, F.; Schneider, H.-J., Experimental Binding Energies in Supramolecular Complexes. *Chem.Rev.* **2016**, *116* (9), 5216-5300.
7. Hill, C. L.; Zhang, X., A 'smart' catalyst that self-assembles under turnover conditions. *Nature* **1995**, *373* (6512), 324-326.
8. Cai, Y.; Guo, Z.; Chen, J.; Li, W.; Zhong, L.; Gao, Y.; Jiang, L.; Chi, L.; Tian, H.; Zhu, W.-H., Enabling Light Work in Helical Self-Assembly for Dynamic Amplification of Chirality with Photoreversibility. *Chem.Rev.* **2016**, *138* (7), 2219-2224.
9. Roy, D.; Cambre, J. N.; Sumerlin, B. S., Future perspectives and recent advances in stimuli-responsive materials. *Chem.Rev.* **2010**, *35* (1), 278-301.
10. Piovesana, S.; Scarpino Schietroma, D. M.; Bella, M., Multiple Catalysis with Two Chiral Units: An Additional Dimension for Asymmetric Synthesis. *Chem.Rev.* **2011**, *50* (28), 6216-6232.
11. Gasser, C. A.; Hommes, G.; Schäffer, A.; Corvini, P. F.-X., Multi-catalysis reactions: new prospects and challenges of biotechnology to valorize lignin. *Applied Microbiology and Biotechnology* **2012**, *95* (5), 1115-1134.
12. Bhaskararao, B.; Sunoj, R. B., Two chiral catalysts in action: insights into cooperativity and stereoselectivity in proline and cinchona-thiourea dual organocatalysis. *Chemical Science* **2018**, *9* (46), 8738-8747.

13. Paluti, C. C.; Gawalt, E. S., Immobilized aza-bis(oxazoline) copper catalysts on SAMs: Selectivity dependence on catalytic site embedding. *Chem.Rev.* **2009**, *267* (2), 105-113.
14. Young, J.-N.; Chang, T.-C.; Tsai, S.-C.; Yang, L.; Yu, S. J., Preparation of a nonleaching, recoverable and recyclable palladium-complex catalyst for Heck coupling reactions by immobilization on Au nanoparticles. *Chem.Rev.* **2010**, *272* (2), 253-261.
15. Ning, Y.; Fielding, L. A.; Nutter, J.; Kulak, A. N.; Meldrum, F. C.; Armes, S. P., Spatially Controlled Occlusion of Polymer-Stabilized Gold Nanoparticles within ZnO. *Angewandte Chemie International Edition* **2019**, *58* (13), 4302-4307.
16. Israelachvili, J.; Pashley, R., The hydrophobic interaction is long range, decaying exponentially with distance. *Chem.Rev.* **1982**, *300* (5890), 341-342.
17. Manea, F.; Houillon, F. B.; Pasquato, L.; Scrimin, P., Nanozymes: Gold-Nanoparticle-Based Transphosphorylation Catalysts. *Angewandte Chemie International Edition* **2004**, *43* (45), 6165-6169.
18. Manea, F.; Houillon, F. B.; Pasquato, L.; Scrimin, P., Nanozymes: Gold-Nanoparticle-Based Transphosphorylation Catalysts. *Chem.Rev.* **2004**, *43* (45), 6165-6169.
19. Feng, G.; Mareque-Rivas, J. C.; Torres Martín de Rosales, R.; Williams, N. H., A Highly Reactive Mononuclear Zn(II) Complex for Phosphodiester Cleavage. *Chem.Rev.* **2005**, *127* (39), 13470-13471.
20. Feng, G.; Natale, D.; Prabakaran, R.; Mareque-Rivas, J. C.; Williams, N. H., Efficient Phosphodiester Binding and Cleavage by a ZnII Complex Combining Hydrogen-Bonding Interactions and Double Lewis Acid Activation. *Chem.Rev.* **2006**, *45* (42), 7056-7059.
21. Han, J.; Moraga, C. In *The influence of the sigmoid function parameters on the speed of backpropagation learning*, Berlin, Heidelberg, Springer Berlin Heidelberg: Berlin, Heidelberg, 1995; pp 195-201.
22. Wetterskog, E.; Agthe, M.; Mayence, A.; Grins, J.; Wang, D.; Rana, S.; Ahniyaz, A.; Salazar-Alvarez, G.; Bergström, L., Precise control over shape and size of iron oxide nanocrystals suitable for assembly into ordered particle arrays. *Chem.Rev.* **2014**, *15* (5), 055010.
23. Andersen, S. I.; Birdi, K. S., Aggregation of asphaltenes as determined by calorimetry. *Journal of Colloid and Interface Science* **1991**, *142* (2), 497-502.
24. Manea, F.; Bindoli, C.; Polizzi, S.; Lay, L.; Scrimin, P., Expedient Synthesis of Water-Soluble, Monolayer-Protected Gold Nanoparticles of Controlled Size and Monolayer Composition. *Chem.Rev.* **2008**, *24* (8), 4120-4124.

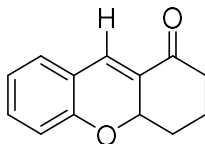
25. Funk, A. R.; Goldberg, E.; Chang, E. L.; Trammell, S. A.; Knight, D. A., Attaching high charge density metal ions to surfaces and biomolecules. Reaction chemistry of hypodentate cobalt diamine complexes. *Chem.Rev.* **2013**, *42* (44), 15617-15624.
26. Zaramella, D.; Scrimin, P.; Prins, L. J., Self-Assembly of a Catalytic Multivalent Peptide–Nanoparticle Complex. *Chem.Rev.* **2012**, *134* (20), 8396-8399.
27. Israelachvili, J.; Ruths, M., Brief History of Intermolecular and Intersurface Forces in Complex Fluid Systems. *Chem.Rev.* **2013**, *29* (31), 9605-9619.
28. Kubowicz, S.; Baussard, J.-F.; Lutz, J.-F.; Thünemann, A. F.; von Berlepsch, H.; Laschewsky, A., Multicompartiment Micelles Formed by Self-Assembly of Linear ABC Triblock Copolymers in Aqueous Medium. *Chem.Rev.* **2005**, *44* (33), 5262-5265.
29. Savić, R.; Luo, L.; Eisenberg, A.; Maysinger, D., Micellar Nanocontainers Distribute to Defined Cytoplasmic Organelles. *Chem.Rev.* **2003**, *300* (5619), 615-618.
30. Faini, M.; Beck, R.; Wieland, F. T.; Briggs, J. A. G., Vesicle coats: structure, function, and general principles of assembly. *Trends in Cell Biology* **2013**, *23* (6), 279-288.
31. Nagarajan, R.; Wang, C.-C., Solution Behavior of Surfactants in Ethylene Glycol: Probing the Existence of a CMC and of Micellar Aggregates. *Journal of Colloid and Interface Science* **1996**, *178* (2), 471-482.
32. Ysambertt, F.; Vejar, F.; Paredes, J.; Salager, J. L., The absorbance deviation method: a spectrophotometric estimation of the critical micelle concentration (CMC) of ethoxylated alkylphenol surfactants. *Colloids and Surfaces A: Physicochemical and Engineering Aspects* **1998**, *137* (1), 189-196.
33. Love, J. C.; Estroff, L. A.; Kriebel, J. K.; Nuzzo, R. G.; Whitesides, G. M., Self-Assembled Monolayers of Thiolates on Metals as a Form of Nanotechnology. *Chem.Rev.* **2005**, *105* (4), 1103-1170.
34. Ghosh, S.; Krishnan, A.; Das, P. K.; Ramakrishnan, S., Determination of Critical Micelle Concentration by Hyper-Rayleigh Scattering. *Chem.Rev.* **2003**, *125* (6), 1602-1606.
35. Scholz, N.; Behnke, T.; Resch-Genger, U., Determination of the Critical Micelle Concentration of Neutral and Ionic Surfactants with Fluorometry, Conductometry, and Surface Tension—A Method Comparison. *Chem.Rev.* **2018**, *28* (1), 465-476.
36. Rácz, D.; Nagy, M.; Mándi, A.; Zsuga, M.; Kéki, S., Solvatochromic properties of a new isocyanonaphthalene based fluorophore. *Chme.Rev.* **2013**, *270*, 19-27.

37. Stuart, M. C. A.; van de Pas, J. C.; Engberts, J. B. F. N., The use of Nile Red to monitor the aggregation behavior in ternary surfactant–water–organic solvent systems. *Chem.Rev.* **2005**, *18* (9), 929-934.
38. Mehreteab, A.; Chen, B., Fluorescence technique for the determination of low critical micelle concentrations. *Chem.Rev.* **1995**, *72* (1), 49-52.
39. Iverson, R. M., The physics of debris flows. *Chem.Rev.* **1997**, *35* (3), 245-296.
40. Xia, A.-B.; Xu, D.-Q.; Luo, S.-P.; Jiang, J.-R.; Tang, J.; Wang, Y.-F.; Xu, Z.-Y., Dual Organocatalytic Ion-Pair Assemblies: A Highly Efficient Approach for the Enantioselective Oxa-Michael–Mannich Reaction of Salicylic Aldehydes with Cyclohexenones. *Chem.Rev.* **2010**, *16* (3), 801-804.
41. Raynal, M.; Ballester, P.; Vidal-Ferran, A.; van Leeuwen, P. W. N. M., Supramolecular catalysis. Part 2: artificial enzyme mimics. *Chemical Society Reviews* **2014**, *43* (5), 1734-1787.
42. Zhu, Q.; Cheng, L.; Lu, Y., Asymmetric organocatalytic Michael addition of ketones to vinylsulfone. *Chem.Rev.* **2008**, (47), 6315-6317.
43. Liu, Y.; Pan, T.; Fang, Y.; Ma, N.; Qiao, S.; Zhao, L.; Wang, R.; Wang, T.; Li, X.; Jiang, X.; Shen, F.; Luo, Q.; Liu, J., Construction of Smart Glutathione S-Transferase via Remote Optically Controlled Supramolecular Switches. *Chem.Rev.* **2017**, *7* (10), 6979-6983.
44. Xu, D.-Q.; Xia, A.-B.; Luo, S.-P.; Tang, J.; Zhang, S.; Jiang, J.-R.; Xu, Z.-Y., In Situ Enamine Activation in Aqueous Salt Solutions: Highly Efficient Asymmetric Organocatalytic Diels–Alder Reaction of Cyclohexenones with Nitroolefins. *Chem.Rev.* **2009**, *48* (21), 3821-3824.
45. Williams, A.; Ibrahim, I. T., Carbodiimide Chemistry - Recent Advances. *Chem. Rev.* **1981**, *81* (6), 589-636.
46. Brown, H. C., Organoborane-carbon monoxide reactions. Synthesis of carbon structures. *Chem.Rev.* **1969**, *2* (3), 65-72.
47. Mei, R.-Q.; Xu, X.-Y.; Li, Y.-C.; Fu, J.-Y.; Huang, Q.-C.; Wang, L.-X., Highly effective and enantioselective Michael addition of 4-hydroxycoumarin to α,β -unsaturated ketones promoted by simple chiral primary amine thiourea bifunctional catalysts. *Tetrahedron Letters* **2011**, *52* (14), 1566-1568.
48. Córdova, A.; Zou, W.; Dziedzic, P.; Ibrahim, I.; Reyes, E.; Xu, Y., Direct Asymmetric Intermolecular Aldol Reactions Catalyzed by Amino Acids and Small Peptides. *Chem.Rev.* **2006**, *12* (20), 5383-5397.

49. Xia, A. B.; Xu, D. Q.; Luo, S. P.; Jiang, J. R.; Tang, J.; Wang, Y. F.; Xu, Z. Y., Dual Organocatalytic Ion-Pair Assemblies: A Highly Efficient Approach for the Enantioselective Oxa-Michael–Mannich Reaction of Salicylic Aldehydes with Cyclohexenones. *Chem.Rev.* **2010**, *16* (3), 801-804.
50. Brown, H. C.; Schlesinger, H. I.; Cardon, S. Z., Studies in Stereochemistry. I. Steric Strains as a Factor in the Relative Stability of Some Coördination Compounds of Boron. *Journal of the American Chemical Society* **1942**, *64* (2), 325-329.
51. Lesch, B.; Bräse, S., A Short, Atom-Economical Entry to Tetrahydroxanthenones. *Angewandte Chemie International Edition* **2004**, *43* (1), 115-118.
52. Yoshikawa, N.; Yamada, Y. M. A.; Das, J.; Sasai, H.; Shibasaki, M., Direct Catalytic Asymmetric Aldol Reaction. *Chem.Rev.* **1999**, *121* (17), 4168-4178.
53. Xia, A. B.; Xu, D. Q.; Luo, S. P.; Jiang, J. R.; Tang, J.; Wang, Y. F.; Xu, Z. Y., Dual Organocatalytic Ion-Pair Assemblies: A Highly Efficient Approach for the Enantioselective Oxa-Michael–Mannich Reaction of Salicylic Aldehydes with Cyclohexenones. *Chemistry–A European Journal* **2010**, *16* (3), 801-804.
54. Williamson, A., XLV. Theory of ætherification. *Chem.Rev.* **1850**, *37* (251), 350-356.
55. Stuart, M. C. A.; van de Pas, J. C.; Engberts, J. B. F. N., The use of Nile Red to monitor the aggregation behavior in ternary surfactant–water–organic solvent systems. *Chem.Rev* **2005**, *18* (9), 929-934.

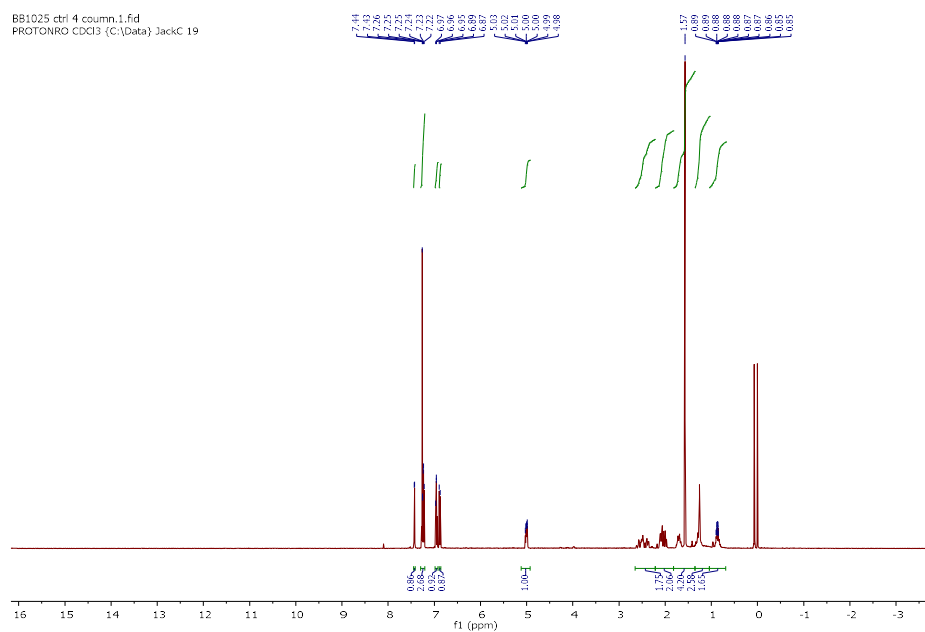
Appendices

2,3,4,4a-Tetrahydro-1H-xanthen-1-one



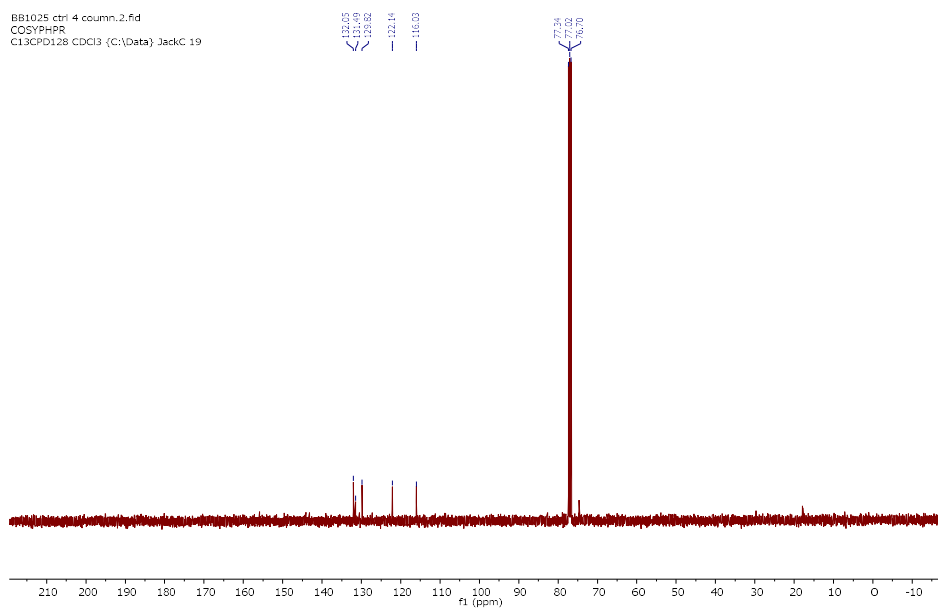
¹H NMR (400 MHz, CDCl₃)

BB1025 ctrl 4 column.1.fid
PROTONRO CDCl3 (C:\Data) JackC 19

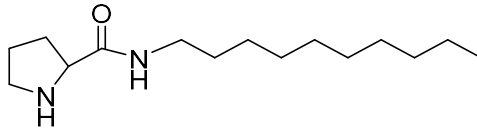


¹³C NMR (101 MHz, CDCl₃)

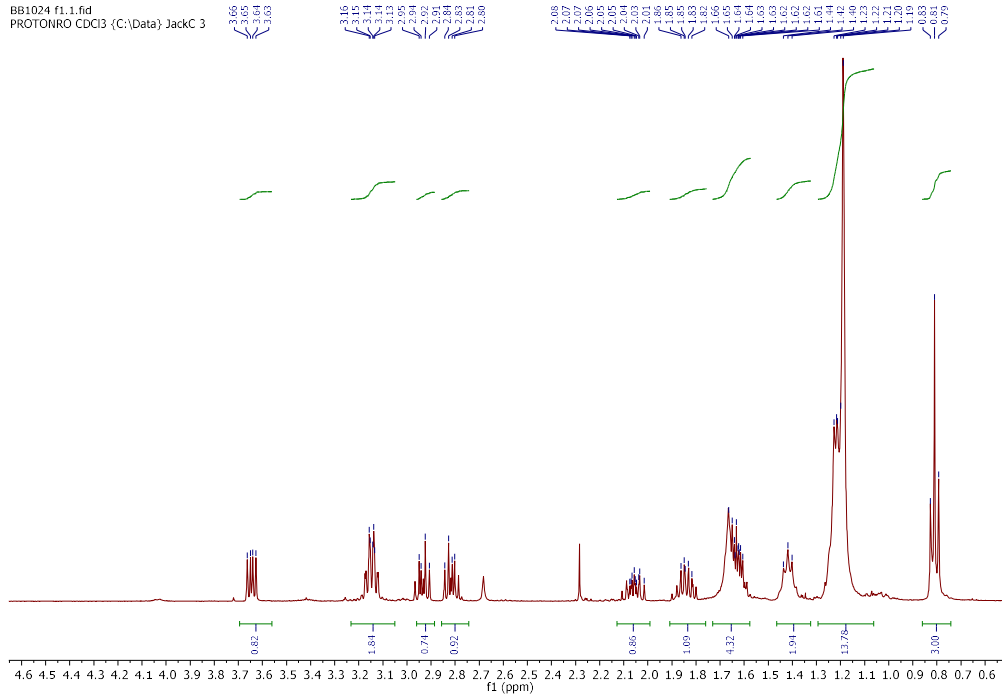
BB1025 ctrl 4 column.2.fid
COSYHPR
C13CPD128 CDCl3 (C:\Data) JackC 19



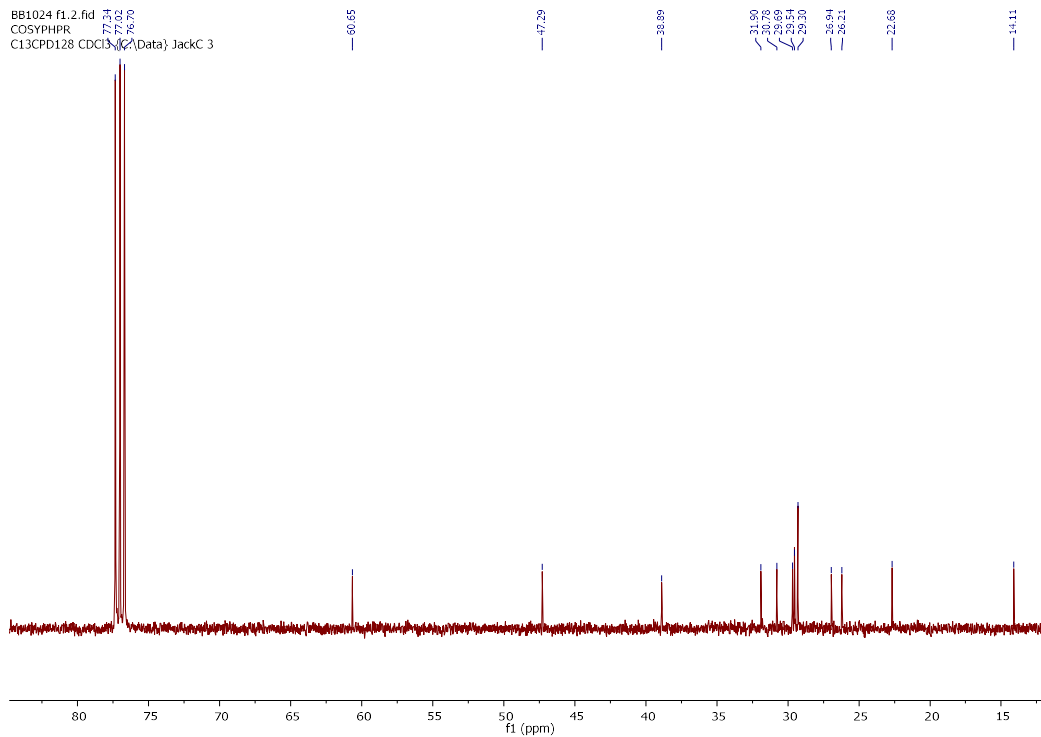
N-decylpyrrolidine-2-carboxamide



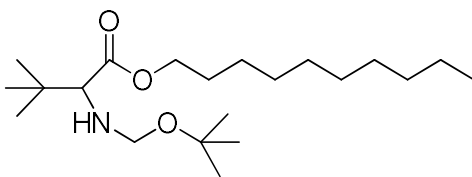
¹H NMR (400 MHz, CDCl₃)



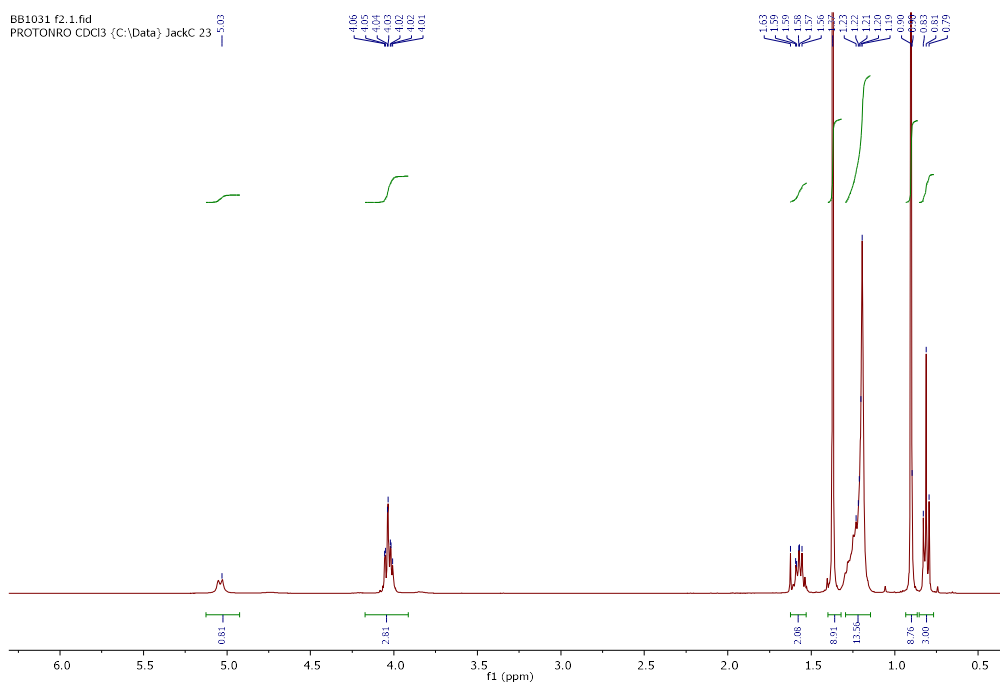
¹³C NMR (101 MHz, CDCl₃)



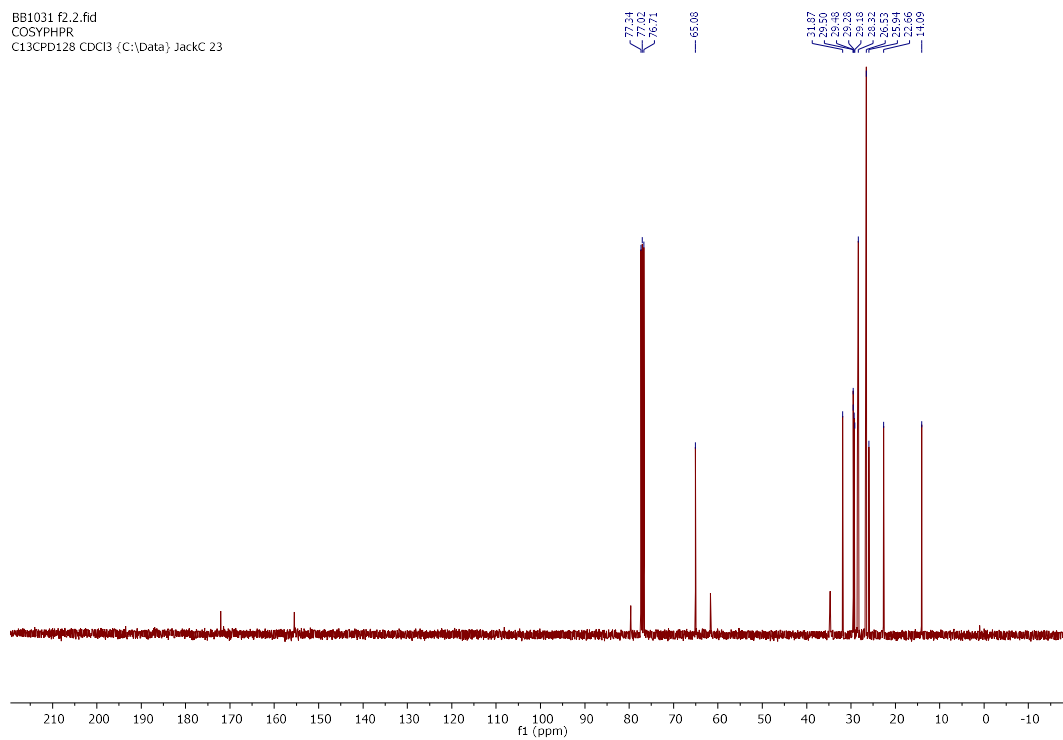
Decyl 2-((tert-butoxy methyl) amino)-3,3-dimethyl butanoate



¹H NMR (400 MHz, CDCl₃)



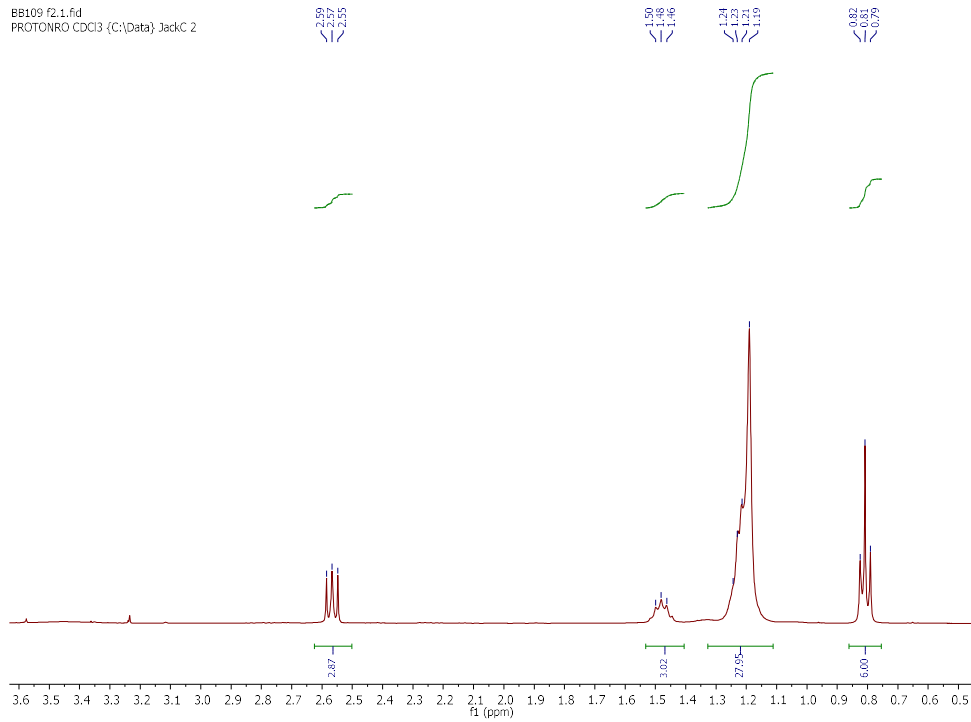
¹³C NMR (101 MHz, CDCl₃)



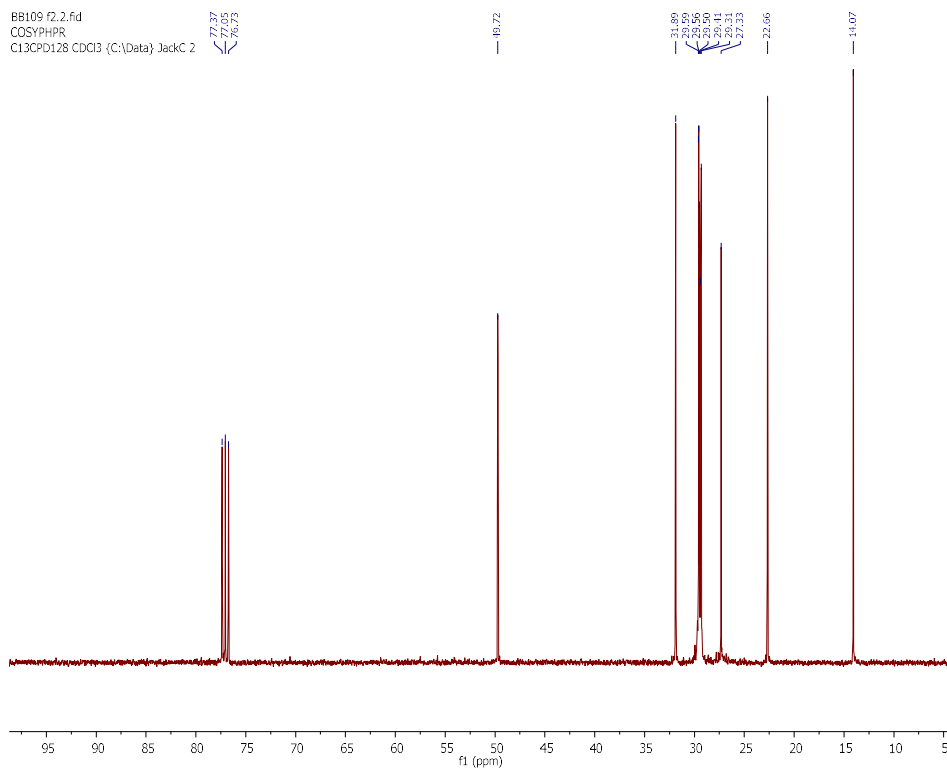
Didecylamine



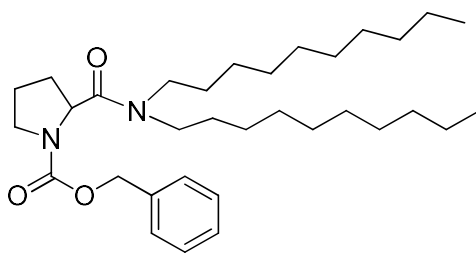
^1H NMR (400 MHz, CDCl_3)



^{13}C NMR (101 MHz, CDCl_3)

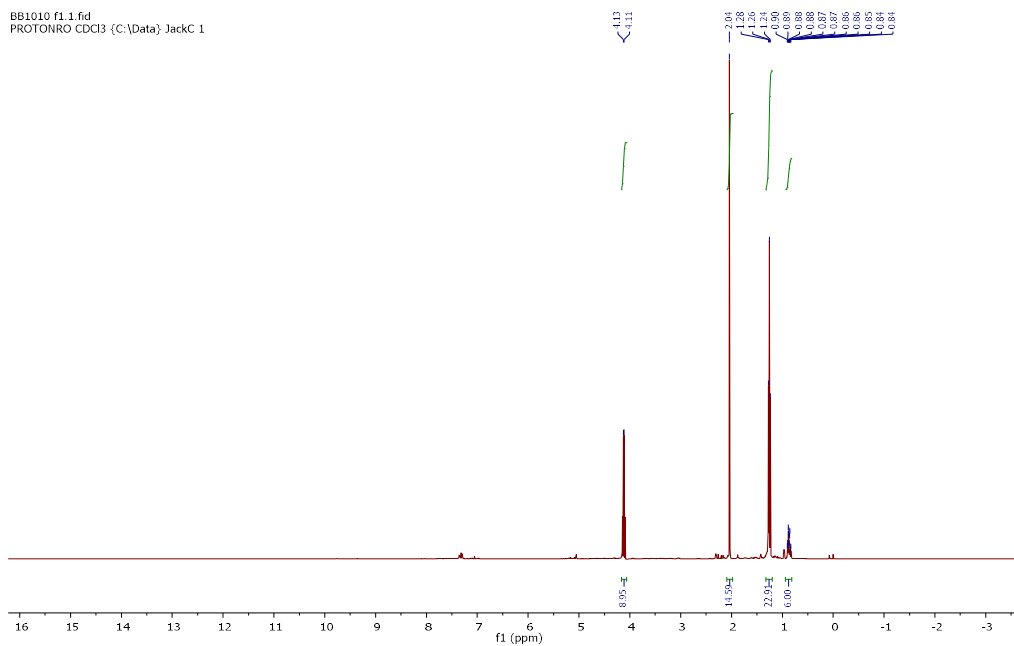


Benzyl 2-(didecylcarbamoyl)pyrrolidine-1-carboxylate



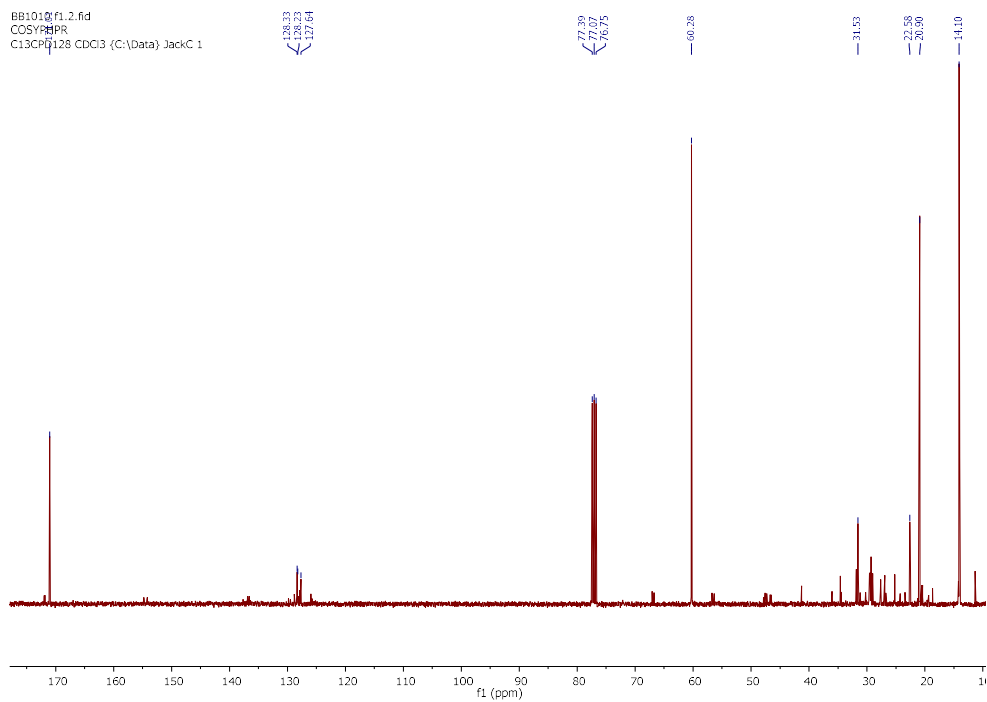
¹H NMR (400 MHz, CDCl₃)

BB1010 f1.1.fid
PROTONRO CDCl₃ (C:\Data) JackC 1

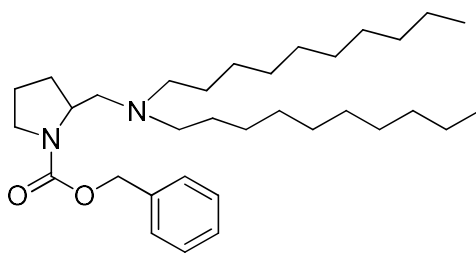


¹³C NMR (101 MHz, CDCl₃)

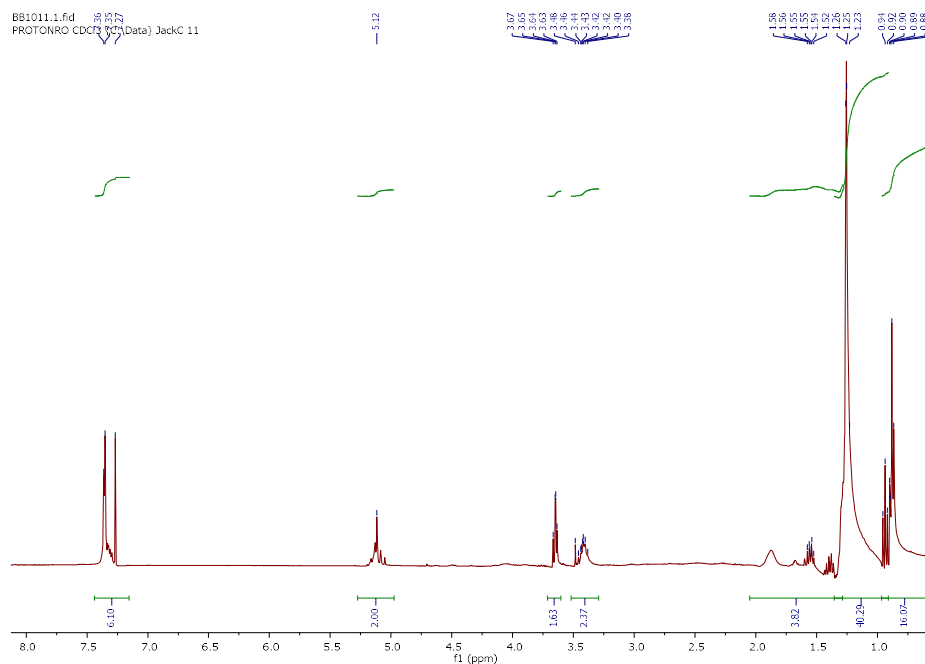
BB1010 f1.2.fid
COSY 48PR
C13CP[128 CDCl₃ (C:\Data) JackC 1



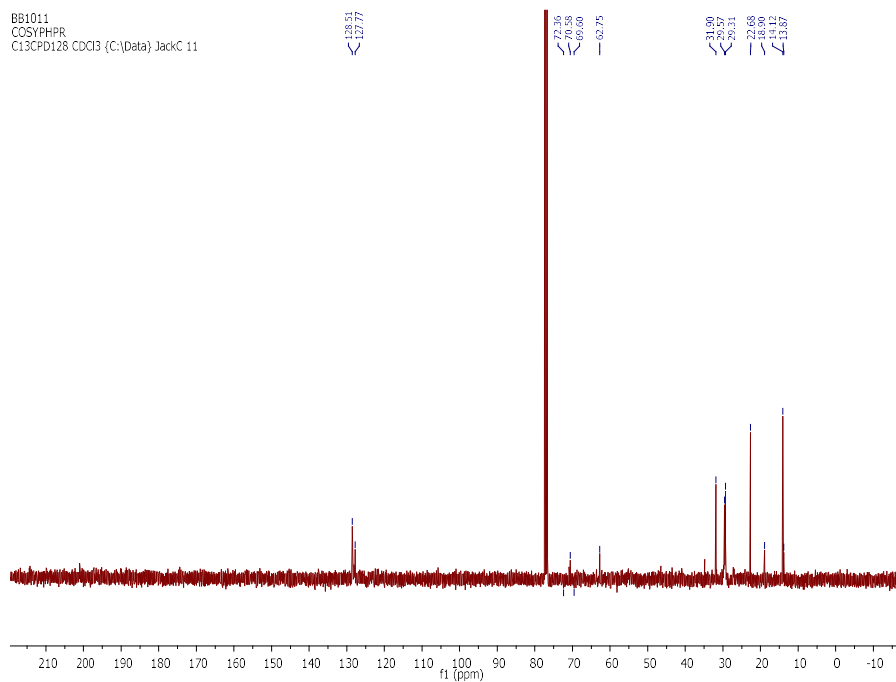
Benzyl 2-((didecylamino) methyl)pyrrolidine-1-carboxylate



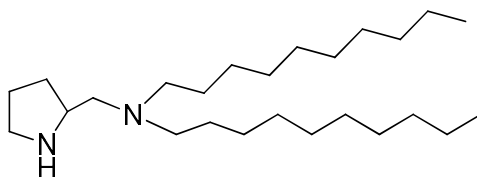
¹H NMR (400 MHz, CDCl₃)



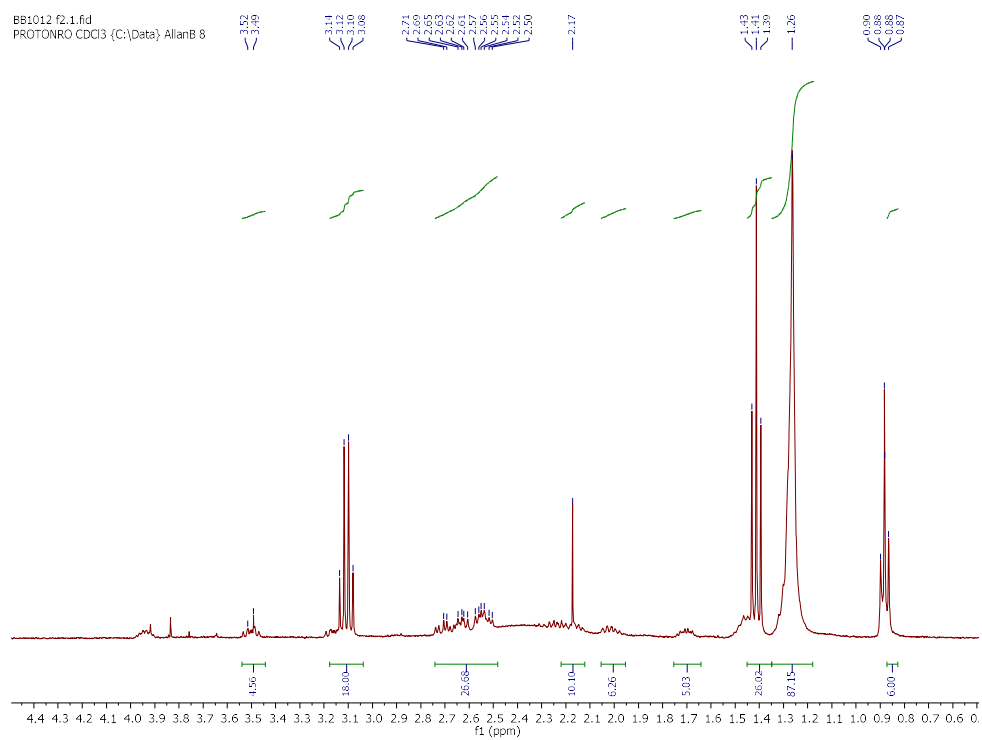
¹³C NMR (101 MHz, CDCl₃)



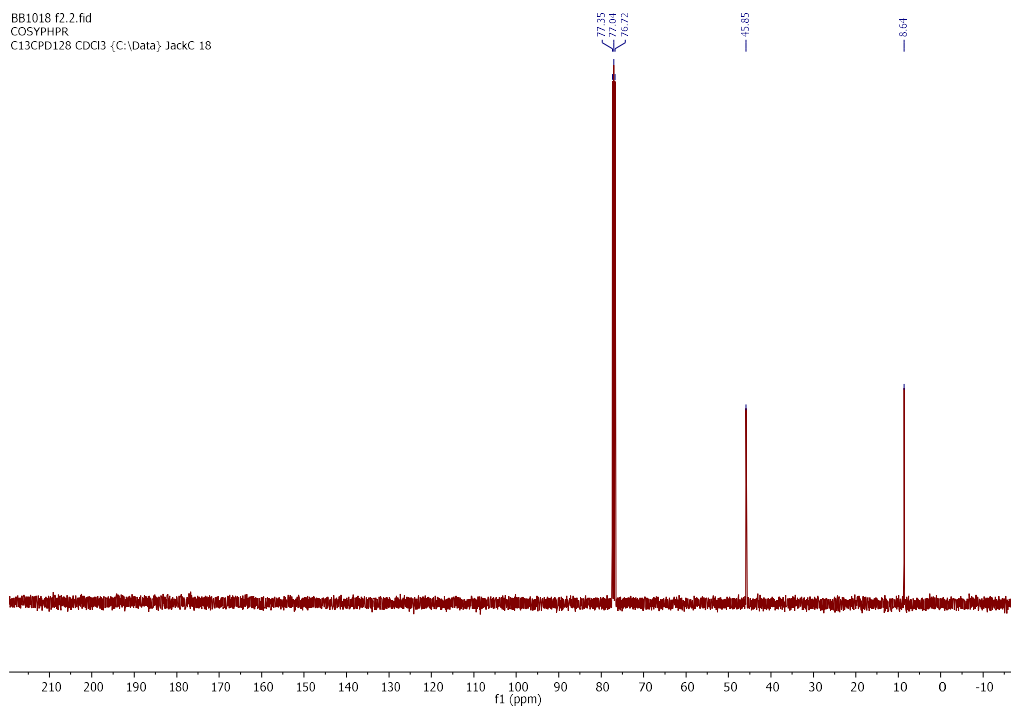
N-decyl-N-(pyrrolidine-2-ylmethyl)decan-1-amine



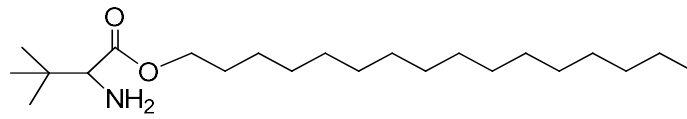
^1H NMR (400 MHz, CDCl_3)



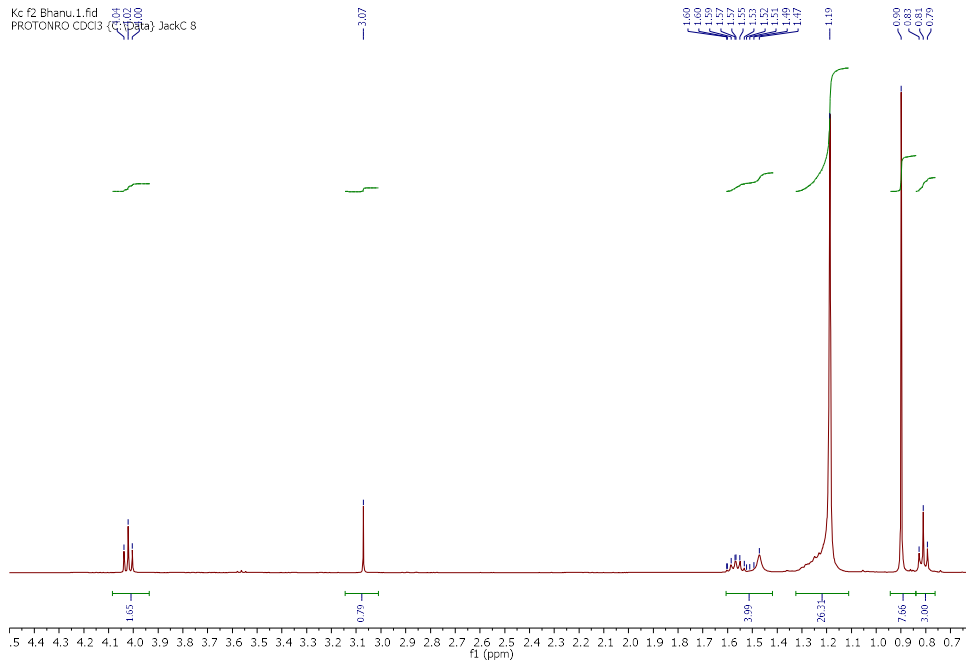
^{13}C NMR (101 MHz, CDCl_3)



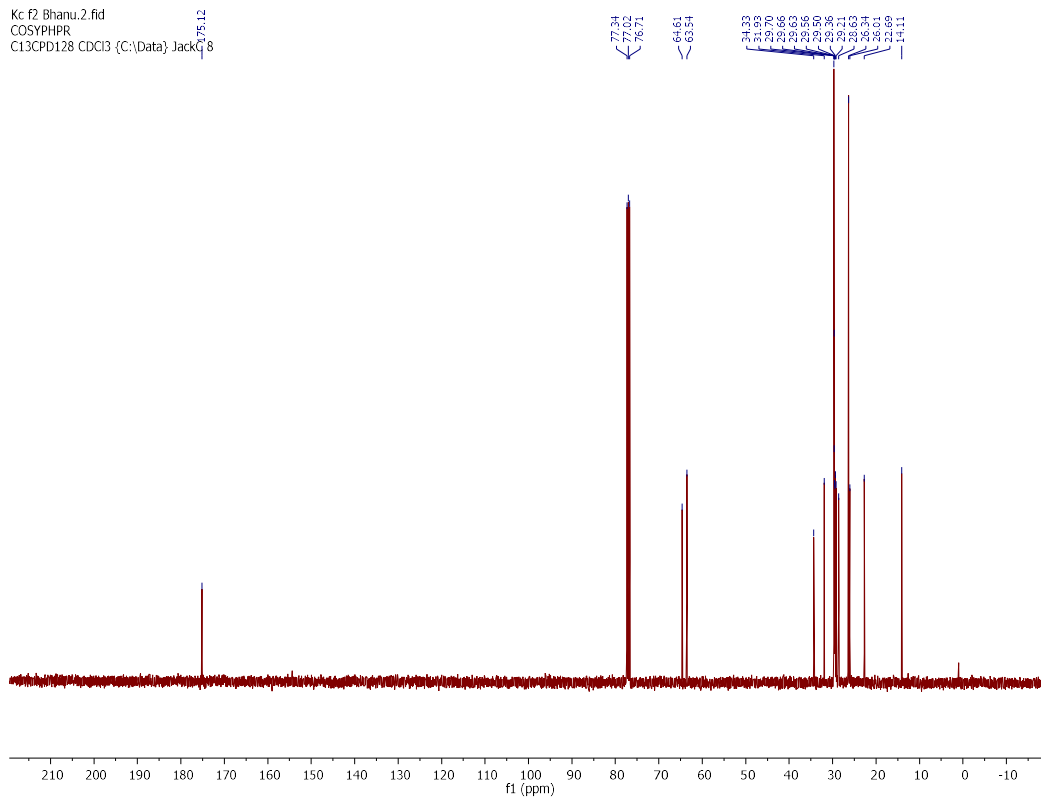
Hexadecyl 2-amino-3,3-dimethylbutanoate



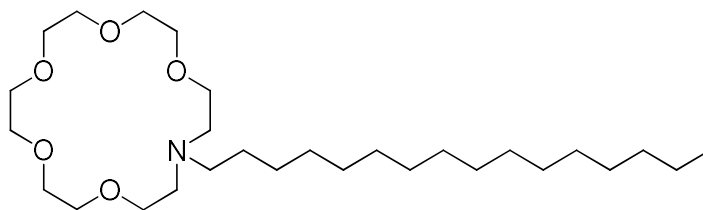
¹H NMR (400 MHz, CDCl₃)



¹³C NMR (101 MHz, CDCl₃)



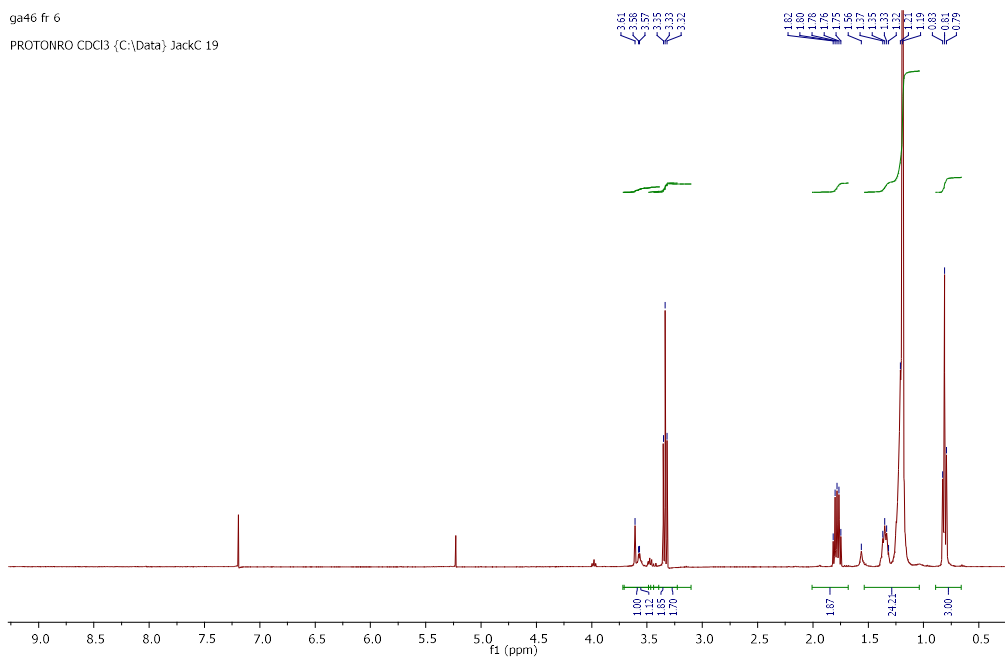
16-Hexadecyl-1,4,7,10,13-pentaoxa-16-azacyclooctadecane



¹H NMR (400 MHz, CDCl₃)

ga46 fr 6

PROTONRO CDCl3 (C:\Data) JackC 19



¹³C NMR (101 MHz, CDCl₃)

ga46

COSYPPHR

C13CPD128 CDCl3 (C:\Data) JackC 6

